

The Role of Sex Hormones in SARS-CoV-2 Pathogenesis

Dissertation zur Erlangung des Doktorgrades
der Naturwissenschaften (Dr. rer. nat.)

des Fachbereiches Chemie
der Fakultät Mathematik, Informatik und Naturwissenschaften
der Universität Hamburg

Vorgelegt von
Berfin Schaumburg (geb. Tuku)
aus Köln

Hamburg, 2021

Reviewer: Prof. Dr. Gülşah Gabriel

Second Reviewer: Prof. Dr. Michael Kolbe

Date of Thesis Defense: August 27, 2021

Publications related to this study (as of June 2021):

Berfin Tuku*, Stephanie Stanelle-Bertram*, Julie Sellau, Sebastian Beck, Tian Bai, Nancy Mounogou Kouassi, Annette Preuß, Stefan Hoenow, Thomas Renné, Hanna Lotter, Gülşah Gabriel. Testosterone Protects Against Severe Influenza by Reducing the Pro-Inflammatory Cytokine Response in the Murine Lung. *Frontiers in Immunology* 11:697 (2020).

Maria Schröder*, **Berfin Schaumburg***, Zacharias Müller, Ann Parplys, Dominik Jarczak, Kevin Roedl, Axel Nierhaus, Geraldine de Heer, Jörn Grensemann, Bettina Schneider, Fabian Stoll, Tian Bai, Henning Jacobsen, Martin Zickler, Stephanie Stanelle-Bertram, Kristin Klaetschke, Thomas Renné, Andreas Meinhardt, Jens Aberle, Jens Hiller, Sven Peine, Lothar Kreienbrock, Karin Klingel, Stefan Kluge, Gülşah Gabriel. High estradiol and low testosterone levels are associated with critical illness in male COVID-19 patients. *Emerging Microbes & Infections* (2021, in review).

Stephanie Stanelle-Bertram*, **Berfin Schaumburg***, Nancy Mounogou Kouassi*, Sebastian Beck*, Martin Zickler, Fabian Stoll, Georg Beythien, Kathrin Becker, Fabian Heinrich, Martina Sauter, Susanne Krasemann, Philine Lange, Axel Heinemann, Debby von Riel, Lonneke Leitjen, Lisa Bauer, Thierry van den Bosch, Boaz Lopuhaä, Tian Bai, Hanna Jania, Zacharias Müller, Vinicius Pinho dos Reis, Vanessa Krupp-Buzumkic, Maria Schröder, Dominik Jarczak, Axel Nierhaus, Stefan Kluge, Jan von der Thusen, Benjamin Ondruschka, Wolfgang Baumgärtner, Karin Klingel, Gülşah Gabriel. SARS-CoV-2 infection induces transcriptional dysregulation of the sex hormone metabolizing CYP19A1 enzyme in the lung of golden hamsters. (2021, in preparation).

Other publications (as of June 2021):

Patricia Resa-Infante, Jaume Bonet, Swantje Thiele, Malik Alawi, Stephanie Stanelle-Bertram, **Berfin Tuku**, Sebastian Beck, Baldo Oliva, Gülşah Gabriel. Alternative Interaction Sites in the Influenza A Virus Nucleoprotein Mediate Viral Escape from the Importin- α 7 Mediated Nuclear Import Pathway. *The FEBS Journal* 286(17):3374-3388 (2019).

Swantje Thiele, Stephanie Stanelle-Bertram, Sebastian Beck, Nancy Mounogou Kouassi, Martin Zickler, Martin Müller, **Berfin Tuku**, Patricia Resa-Infante, Debby van Riel, Malik Alawi, Thomas Günther, Franziska Rother, Stefanie Hügel, Susanne Reimering, Alice McHardy, Adam Grundhoff, Wolfram Brune, Albert Osterhaus, Michael Bader, Enno Hartmann, Gülşah Gabriel. Cellular Importin- α 3 Expression Dynamics in the Lung Regulate Antiviral Response Pathways against Influenza A Virus Infection. *Cell Reports* 31(3):107549 (2020).

Kathrin Becker*, Georg Beythien*, Nicole de Buhr*, Stephanie Stanelle-Bertram, **Berfin Tuku**, Nancy Mounogou-Kouassi, Sebastian Beck, Martin Zickler, Lisa Allnoch, Gülşah Gabriel, Maren von Köckritz-Blickwede, Wolfgang Baumgärtner. Vasculitis and neutrophil extracellular traps in lungs of golden Syrian hamsters with SARS-CoV-2. *Frontiers in Immunology* 12(12):640842 (2021).

Lisa Allnoch, Georg Beythien, Eva Leitzen, Kathrin Becker, Franz-Josef Kaup, Stephanie Stanelle-Bertram, **Berfin Schaumburg**, Nancy Mounogou-Kouassi, Sebastian Beck, Martin Zickler, Vanessa Herder, Gülşah Gabriel, Wolfgang Baumgärtner. Vascular Inflammation Is Associated with Loss of Aquaporin 1 Expression on Endothelial Cells and Increased Fluid Leakage in SARS-CoV-2 Infected Golden Syrian Hamsters. *Viruses* 13(4):639 (2021).

Martin Zickler*, Stephanie Stanelle-Bertram*, Sandra Ehret*, Fabian Heinrich, Philine Lange, Klaus Püschel, **Berfin Schaumburg**, Nancy Mounogou Kouassi, Sebastian Beck, Benjamin Ondruschka, Ludger Scheja, Jörg Heeren, Gülşah Gabriel. Adipose tissue acts as a reservoir for SARS-CoV-2 replication. (2021, in preparation).

*shared first authorships

Table of contents

1	Zusammenfassung.....	1
2	Abstract	2
3	Introduction.....	3
3.1	Coronaviruses.....	3
3.1.1	Taxonomy	3
3.1.2	Virion structure and genome organization	3
3.1.3	Coronavirus replication cycle (SARS-CoV-2).....	6
3.1.3.1	Virus entry	6
3.1.3.2	Viral gene expression and RNA synthesis.....	6
3.1.3.3	Viral particle assembly and viral release	7
3.1.4	Ecology and host spectrum	8
3.1.5	Epidemiology	11
3.1.5.1	Endemic coronaviruses.....	11
3.1.5.2	Severe acute respiratory syndrome coronavirus	11
	(SARS-CoV).....	11
3.1.5.3	Severe acute respiratory syndrome coronavirus 2	14
	(SARS-CoV-2)	14
3.1.6	Prevention and treatment.....	16
3.1.6.1	Vaccine development.....	16
3.1.6.2	Therapeutics.....	17
3.1.7	Sex hormone biosynthesis and metabolism.....	20
3.1.8	Sex differences and the role of hormones in infections	22
3.1.8.1	Sex differences in respiratory viral infections	23
4	Aim.....	25
5	Results	26
5.1	Sex hormones and metabolic dysregulations in critically ill COVID-19 patients.....	26
5.1.1	Higher mortality in male COVID-19 patients.....	26
5.1.2	Characteristics and demographics of COVID-19 patients	27
5.1.3	Male COVID-19 patients present reduced androgen and increased estrogen levels ...	28
5.1.4	Cytokine and chemokine levels are increased in severely ill COVID-19 patients.....	32
5.1.5	IFN- γ levels correlate with estradiol levels in COVID-19 patients	34
5.1.6	Estradiol levels are associated with disease severity in COVID-19 patients	36
5.2	SARS-CoV-2 infection mediates dysregulation of sex hormones in the Syrian golden hamster model	39

5.2.1	SARS-CoV-2 infection induces weight loss and a systemic infection in Syrian golden hamsters	39
5.2.2	SARS-CoV-2 infected hamsters present elevated cytokine and chemokine levels	42
5.2.3	SARS-CoV-2 infection leads to hormone dysregulation in male and female hamsters	44
5.2.4	SARS-CoV infected hamsters present elevated aromatase mRNA levels in the lungs	46
5.2.5	SARS-CoV-2 infected male golden hamsters present abundantly high aromatase protein expression levels in perivascular and peribronchiolar infiltrates	48
6	Discussion and outlook	51
6.1	Sex differences in SARS-CoV-2 pathology	51
6.2	The role of testosterone in SARS-CoV-2 infection	52
6.3	The role of estradiol in SARS-CoV-2 infection	55
6.4	Aromatase CYP19A1 dysregulation upon SARS-CoV-2 infection	58
7	Materials and methods	60
7.1	Materials	60
7.1.1	Chemicals	60
7.1.2	Buffers and solutions	61
7.1.3	Kits	62
7.1.4	Antibodies	62
7.1.5	Animals	62
7.1.6	DNA oligonucleotides	63
7.1.7	Narcotics and supplements	63
7.1.8	Eukaryotic cell lines	64
7.1.9	Media and supplements for eukaryotic cell culture	64
7.1.10	Virus strains	65
7.1.11	Consumables	65
7.1.12	Safety gear	66
7.1.13	Laboratory equipment	66
7.1.14	Software	67
7.2	Methods	68
7.2.1	Ethics statement	68
7.2.2	Collection of human samples	68
7.2.2.1	Collection of COVID-19 and non-COVID-19 patient cohort samples	68
7.2.2.2	Collection of coronary heart disease cohort patient samples	69
7.2.2.3	Collection of healthy cohort samples	69
7.2.3	Animal experiments	69
7.2.3.1	<i>In vivo</i> experiments in mice	70
7.2.3.2	<i>In vivo</i> experiments in golden hamsters	71

7.2.4	Cell culture techniques	72
7.2.4.1	Cultivation of eukaryotic cells	72
7.2.4.2	Freezing and thawing of eukaryotic cells	73
7.2.4.3	Mycoplasma sp PCR.....	73
7.2.5	Nucleic acid techniques.....	73
7.2.5.1	Isolation of total RNA from murine PBMCs.....	73
7.2.5.2	Isolation of total RNA from hamster tissues	74
7.2.5.3	Isolation of viral RNA from patient and hamster samples	74
7.2.5.4	Reverse transcription PCR (RT-PCR)	74
7.2.5.5	Real-time reverse transcription PCR (RT-PCR)	75
7.2.5.6	Qualitative real-time reverse transcription PCR	76
7.2.6	Protein biochemical methods	76
7.2.6.1	Cytokine/chemokine and hormone quantification by Multiplex-Immunoassay	76
7.2.6.2	Hormone quantification by external institutes/companies	77
7.2.6.3	Enzyme-linked immunosorbent assay (ELISA).....	78
7.2.7	Virological techniques	78
7.2.7.1	Isolation of SARS-CoV-2.....	78
7.2.7.2	Propagation of SARS-CoV-2 on VeroE6 cells	79
7.2.7.3	Propagation of influenza A viruses on MDCK II cells.....	79
7.2.7.4	Determination of virus titers by plaque assay.....	80
7.2.8	Histological techniques.....	80
7.2.8.1	Preparation of murine and hamster organ tissues for histology	81
7.2.8.2	Deparaffining and rehydration of FFPE- tissue sections	81
7.2.8.3	Hematoxylin and eosin (H&E)- staining of murine and hamster organ tissue.....	82
7.2.8.4	Immunohistochemical staining (ICH-P)	83
7.2.9	Statistical evaluations.....	84
7.2.10	Collaborations	85
7.2.10.1	Providing of patient materials.....	85
7.2.10.2	Measurement of hormone in levels in serum/plasma of COVID-19 patients and healthy cohort	85
7.2.10.3	Measurement of murine plasma testosterone levels	85
7.2.10.4	Immunohistology and histopathology.....	86
7.2.10.5	Statistical evaluation of COVID-19 patient cohort data analyzes.....	86
8	Literature.....	87
9	Eidesstattliche Erklärung	106
I.	Supplements - Hazardous materials.....	107
II.	Supplements – Figures	109

III.	Supplements - List of tables and figures	116
IV.	Danksagung	118

List of abbreviations

The abbreviations of chemical elements/compounds and SI units are considered to be known according to the common literature.

°C	degree celsius
µg	microgram
µl	microliter
ACE2	Angiotensin-converting enzyme 2
AR	androgen receptor
ARDS	acute respiratory distress syndrome
bp	base pair
BSA	bovine serum albumin
BSL	biosafety level
cDNA	complementary DNA
CHD	coronary heart disease
CO ₂	carbon dioxide
CoV	corona viruses
COVID-19	corona virus disease
CYP19A1	cytochrome P450 family 19 subfamily a member 1
DAB	3,3'-diaminobenzidin
d p.i.	days post infection
ddH ₂ O	double distilled H ₂ O
DHY-TT	dihydrotestosterone
DMEM	Dulbecco's Modified Eagle's Medium
DMSO	dimethylsulfoxide
DNA	deoxyribonucleic acid
dNTP	2'-deoxynucleotide-5'-triphosphate
DPP4	Dipeptidyl-peptidase 4
E ₂	17-β estradiol
e.g.	example given
EDTA	ethylenediamine tetraacetate
EL	endothelial lipase
ESR	estrogen receptor
FBS	fetal bovine serum
FFPE	formalin-fixed paraffin-embedded
FGF	Fibroblast growth factor
FSH	follicle-stimulating hormone
fwd	forward
g	gram
GAPDH	glycerinealdehyde 3'-phosphate dehydrogenase
G-CSF	granulocyte colony-stimulating factor
ECLIA	electro-chemiluminescence immunoassay
ELISA	enzyme-linked immunosorbent assay
h	hour

H&E	haematoxylin and eosin
h p.i.	hours post infection
HPRT1	Hypoxanthine-Guanine Phosphoribosyltransferase 1
H ₂ O	water
HPI	Heinrich Pette Institute
HRP	horse radish peroxidase
i.p.	intraperitoneal
IP-10	interferon gamma-induced protein <i>10</i>
IAV	influenza A virus
ICU	intensive care unit
IFN	interferon
IL	interleukin
L	litre
LC-MS/MS	liquid chromatography–mass spectrometry
LH	luteinizing hormone
LRT	lower respiratory tract
M	molar
MCP-1	monocyte chemoattractant protein-1
MEM	Minimum Essential Medium
mg	milligram
min	minute
ml	millilitre
mM	millimolar
mRNA	messenger RNA
NF-κB	nuclear factor κB
NP	nucleoprotein
P/S	penicillin – streptomycin
PBS	phosphate buffered saline
PCR	polymerase chain reaction
PDGF	platelet-derived growth factor
PFA	paraformaldehyde
PFU	plaque-forming units
Poly(I:C)	Polyinosinic:polycytidylic acid
PT	plaque test
qRT-PCR	quantitative reverse transcription PCR
rev	reverse
RIA	radioimmunoassay
RNA	ribonucleid acid
rpm	rounds per minute
RT	reverse transcriptase
RT	room temperature
RT-PCR	reverse transcription PCR
SD	standard deviation
sec	second
SHBG	sex hormone-binding globulin

SOP	standard operating procedure
T3	free triiodothyronine
T4	free thyroxine
TMPRSS2	Transmembrane protease serine 2
TPCK	L-(tosylamido-2-phenyl) ethyl chloromethyl ketone
Tris	tris(hydroxymethyl)aminomethane
TSH	thyroid-stimulating hormone
TT	testosterone
U	unit (enzymatic activity)
URT	upper respiratory tract
VEGF	vascular endothelial growth factor
vRNA	viral RNA
x g	gravity
ZIP9	Zinc transporter 9

1 Zusammenfassung

Das *severe acute respiratory virus 2* (SARS-CoV-2) wurde erstmals Ende 2019 in Wuhan identifiziert. Zum jetzigen Zeitpunkt wurden weltweit über 170 Millionen SARS-CoV-2 Infektionen und mehr als 3 Millionen Todesfälle durch das Virus gemeldet (08.06.2021)¹. Insbesondere ältere Menschen mit zugrundeliegenden Komorbiditäten haben ein größeres Risiko einen schwerwiegenden Krankheitsverlauf zu entwickeln. Zudem kam zum Vorschein, dass Männer ebenfalls schlechtere Prognosen für den Ausgang der Erkrankung haben. Dies impliziert, dass neben sozialen Umgebungsfaktoren, auch biologische Faktoren dafür verantwortlich sein könnten, dass Männer ein höheres Risiko für einen schweren *coronavirus disease 2019* (COVID-19) - Krankheitsverlauf haben. Daher ist es von großer Bedeutung die biologischen Geschlechtsunterschiede während der Infektion zu untersuchen, um Einblick auf den Einfluss der biologischen Faktoren auf die Immunantwort zu erhalten. In dieser Studie wurden COVID-19 Patientenproben auf Hormonlevel und Zytokin- und Chemokinexpressionslevel untersucht. Um zu untersuchen, ob die Ergebnisse in COVID-19 Patienten durch die Infektion oder durch zugrundeliegende Komorbiditäten verursacht wurden, wurde ein Tiermodell für die SARS-CoV-2 Infektion etabliert. Dafür wurden männliche und weibliche syrische Goldhamster mit SARS-CoV-2 infiziert und für Organentnahmen an verschiedenen Zeitpunkten der Infektion euthanisiert.

Unsere Analysen haben gezeigt, dass Testosteronlevel nach SARS-CoV-2 Infektion in männlichen Patienten stark reduziert sind. Im Gegensatz dazu, zeigen männliche sowie weibliche Patienten erhöhte Estradiollevel nach Infektion auf. Erhöhte Estradiollevel konnten mit einem schwereren Krankheitsverlauf korreliert werden. Auch in männlichen Goldhamstern wurden nach Infektion niedrige Testosteronlevel und erhöhte Estradiollevel beobachtet. Hinweise deuten darauf hin, dass eine höhere Expression der Aromatase CYP19A1 in den Lungen an dem hormonellen Ungleichgewicht beteiligt sein könnte. Weitere Analysen haben gezeigt, dass CYP19A1 im Endothelium und Makrophagen in den Lungen SARS-CoV-2 infizierter Hamster exprimiert wird. Diese Ergebnisse heben die Bedeutung der Sexualhormone und deren Einfluss auf das Immunsystem während der Infektion hervor. Zudem bieten die Daten eine Grundlage für weitere Forschungen an, um zu untersuchen wie Sexualhormone zelluläre und molekulare Signalwege in der SARS-CoV-2 Immunantwort beeinflussen. Außerdem konnten neue Biomarker identifiziert werden, die das klinische Management von COVID-19 Patienten verbessern könnten.

2 Abstract

Since the emergence of the severe acute respiratory virus 2 (SARS-CoV-2) in Wuhan in 2019, the virus has been posing great threats to the world. The SARS-CoV-2 pandemic has caused over 170 million cases and more than 3 million related deaths worldwide (8th June 2021)¹. Especially elderly persons with underlying comorbidities have a greater risk to develop severe disease. In addition, in the majority of datasets all over the world, male sex has been identified as a risk factor for worse outcome and increased mortality. These findings implicate that besides social and environmental factors, also biological factors could be involved in the male sex bias in coronavirus disease 2019 (COVID-19). However, there is a need for studying biological sex differences to elucidate how sex modifies immunological responses to improve the clinical management of COVID-19 patients.

In this study, COVID-19 patient material has been analysed to establish a large profile of sexual hormone levels and cytokine expression levels. To further confirm the results in a model without underlying comorbidities influencing the results, we established an animal model for SARS-CoV-2 infection. Therefore, young male and female Syrian golden hamsters were infected with SARS-CoV-2 and euthanized at different time points after infection for analysis compared to control groups.

We could show that upon SARS-CoV-2 infection testosterone levels in male patients are tremendously downregulated. In contrast, estradiol levels are elevated in male and female COVID-19 patients. Elevated estradiol levels could be correlated with severe disease outcome. In the Syrian golden hamster model, we could observe a downregulation of testosterone levels and high levels of estradiol. Furthermore, we could find evidence, that a higher expression of the aromatase CYP19A1 in the lungs could be involved in the hormonal dysregulation. Subsequent analysis showed that CYP19A1 was expressed in the endothelium and macrophages in the lungs of SARS-CoV-2 infected Syrian golden hamsters.

These results emphasise the importance of sex hormones and influence on the immune system during the infection. Furthermore, these findings allow more precise further research to elucidate how sex hormones modify cellular and molecular pathways in the immune response associated with SARS-CoV-2 and improve interpretation of biomarkers and clinical management of COVID-19 patients.

3 Introduction

3.1 Coronaviruses

3.1.1 Taxonomy

Coronaviruses belong to the family *Coronaviridae* in the order of *Nidovirales*. The family of *Coronaviridae* can be subdivided into two families, *Coronavirinae* and *Torovirinae*. Coronaviruses are further sorted into four genera: *Alpha-*, *Beta-*, *Gamma-*, and *Deltacoronavirus*. Originally, they were classified according to their serological relationships, but now the classification is based on a threshold level of sequence identity of a the pp1ab polyprotein and the ORF1ab gene². So far, six human-pathogenic coronaviruses are known, of which HCoV-229 and HCoV-NL63 belong to the genera of *Alphacoronaviruses* and HCoV-HKU1, SARS-CoV, MERS-CoV as well as SARS-CoV-2 belong to the genera of *Betacoronaviruses*. In contrast to *Gamma-*, and *Deltacoronaviruses*, which are largely associated with avian hosts and marine mammal species, almost all *Alpha-*, and *Betacoronaviruses* have mammalian hosts^{3,4}.

3.1.2 Virion structure and genome organization

Coronaviruses are membrane-enveloped, non-segmented 26-32 kb positive strand RNA viruses. The virions are roughly spherical and differ from 100 to 160 nm⁵. The spike proteins are predominantly presented at the surface of the virion, described as club-like or pedal-shaped, prompting the name coronavirus. Enclosed within the virion is a helically symmetric nucleocapsid (**Figure 1**).

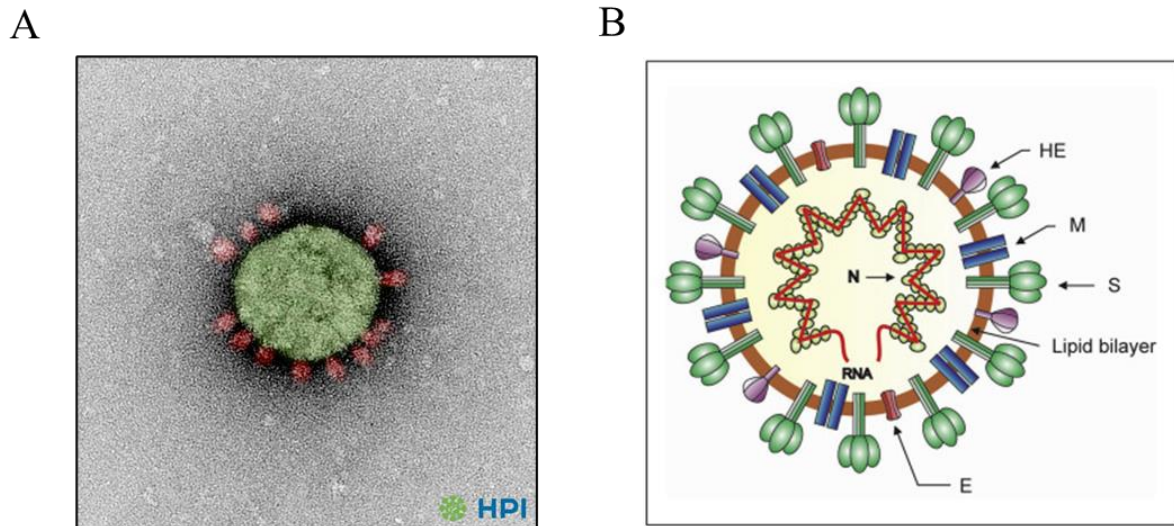


Figure 1: Coronavirus virion structure.

Negative stain electron microscopy image of SARS-CoV-2 (A, kindly provided by Carola Schneider and Dr. Rudolph Reimer, HPI, Hamburg) and a schematic diagram of a coronavirus particle: S; spike protein; M: membrane protein, E: envelope protein, N: nucleocapsid protein, HE: haemagglutinin esterase (B, adapted from Artika *et al.*⁶)

The coronavirus genome comprises four main structural proteins: the spike (S), membrane (M), envelope (E) and nucleocapsid (N) protein. On the virions surface trimers of S molecules form the spike protein^{7,8} and mediate virus entry into the host cell. The S protein acts as a class I viral fusion protein⁹. In many coronaviruses the S protein is cleaved by a furin-like host cell protease into S1 and S2, two polypeptides equal in size, whereas S1 is important for viral attachment and S2 for fusion of virus und host membranes^{10,11}. In contrast to the S1 domain, which is extremely variable, the S2 domain is highly conserved¹². The most abundant structural protein, the M protein, is embedded in the envelope and is about 25-30 kDa in size¹³. It is conserved within each coronavirus genus and has three transmembrane domains¹⁴. The M protein is important for promoting membrane curvature and binding to the nucleocapsid¹⁵. The E protein is found in limited amount in the virion envelope and is critical for viral infectivity. It is about 8-12 kDa in size and highly divergent in coronaviruses but shares a common architecture¹⁶.

Inside of the helically symmetric nucleocapsid the N protein can be found¹⁷. Composed of an N-terminal domain (NTD) and a C-terminal domain (CTD) it binds along the RNA genome in a beads-on-a-string configuration. Optimal binding requires contributions from both domains^{18,19}, although the N protein does not offer protection against ribonucleases.

Introduction

Only present in a subset of *Betacoronaviruses*, such as HCoV-HKU1 and HCoV-OC43, the haemagglutinin esterase (HE) protein is located beneath the canopy of S proteins acting as a cofactor by assisting attachment to host cells virus spread through the mucosa²⁰.

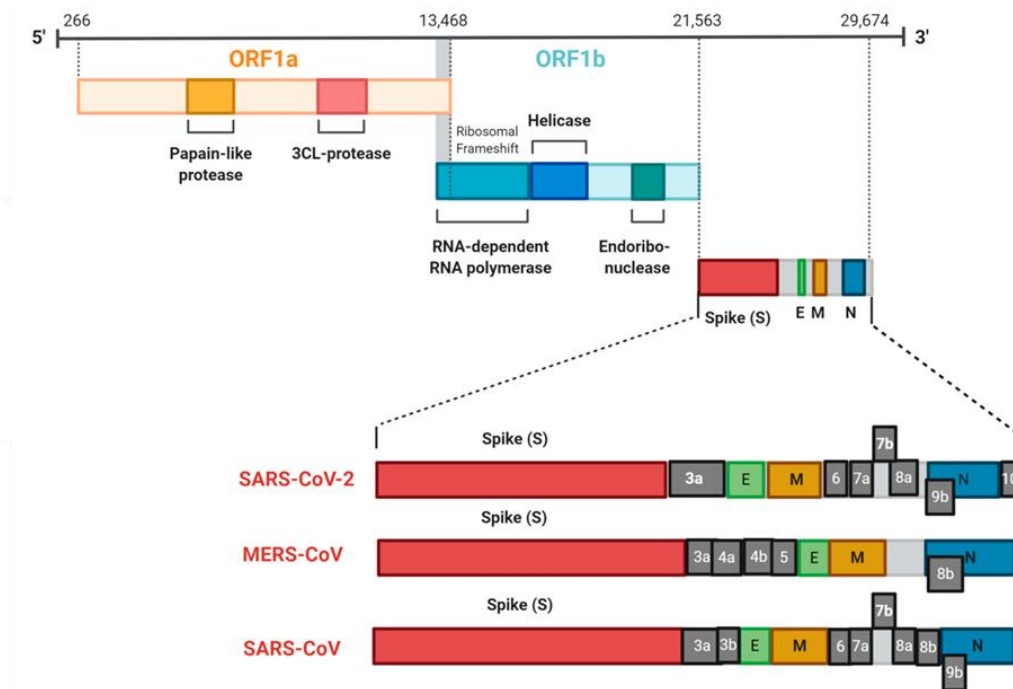


Figure 2: Coronavirus genomic organization.

The replicase gene constitutes of open reading frame 1 (ORF1)a/b, and encodes a polyprotein. The four main structural proteins and several accessory proteins are encoded by additional ORFs. (adapted from Zhand and Jazi *et al.*²¹)

The coronavirus genome has a standard eukaryotic 5'-terminal cap structure and a 3'-polyadenylate tail (**Figure 2**). The overlapping ORF1a and ORF1b, which are located at the 5' end, are expressed by ribosomal frameshifting and yield polyproteins (pp), which are cleaved into non-structural proteins (nsps) by viral proteases. At the 3' end of the genome the structural as well as additional ORFs, which are designated accessory genes are encoded. The accessory genes are numbered according to their transcript's length. For example, the SARS-CoV-2 genome encodes for 27 proteins. ORF1a/b encodes for pp1ab and pp1a polyproteins, which are cleaved into 15 nsps (nsp1-10 and nsp12-16). At the 3' end the structural proteins S, E, M and N are encoded as well as eight accessory proteins (3a, 3b, p6, 7a, 7b, 8a, 9b and ORF10).

3.1.3 Coronavirus replication cycle (SARS-CoV-2)

The coronavirus replication cycle can be subdivided into six parts: the virus entry, the RNA replication and transcription in the cytoplasm, translation of the mRNAs, the viral particle assembly and the viral release (exocytosis). In the following, the life cycle will be described using SARS-CoV-2 as an example (**Figure 3**).

3.1.3.1 Virus entry

The virus entry takes place via binding of the receptor-binding domain (RBD) of the S1 to ACE2, which was identified as the functional host cell receptor for SARS-CoV-2 and SARS-CoV-1²²⁻²⁵. In addition, a second entry receptor neuropilin-1 has been identified to facilitate SARS-CoV-2 entry and infectivity^{26,27}. The S2 domain of the S protein is responsible for the fusion of viral and cellular membranes upon conformational rearrangements^{22,28,29}.

During the entry process, the S protein has to be separated into the receptor-binding and fusion components and expose its fusion peptide. The SARS-CoV-2 S protein has a polybasic cleavage site (PRRAR) at the S1-S2 boundary. The proprotein convertase furin is responsible for efficient cleavage of the S protein. The cleavage enables subsequent exposure of the S2 site for binding to ACE2 and a second cleavage step by TMPRSS2^{23,30}, a cell surface serine protease^{31,32}. This adaptation to cellular proteases for efficient human cell entry is proposed to be required for a successful infection and is a main determinant in overcoming species barriers^{22,23,28,29}.

3.1.3.2 Viral gene expression and RNA synthesis

After the coronavirus genome is released into the cytoplasm, the ORF1a and ORF1ab are translated by a ribosomal frameshift at the overlapping ORFs³³ and the polyproteins pp1a and pp1ab are produced, with a ratio of 1.4-2.2/1.0, respectively³⁴. Following the translation of pp1a and pp1ab the cysteine proteases papain-like protease (PL_{pro}) within the nsp3 and the chymotrypsin-like protease within nsp5 cleave the polyproteins into 16 non-structural proteins. Nsp12-16 are responsible for RNA synthesis, RNA proofreading and RNA modification^{33,35}. Thereby, the RNA-dependent RNA polymerase (RdRP) nsp12 acts with its two cofactors nsp7

and nsp8. The RNA proofreading is performed by nsp14³⁶. Nsp13 (RNA 5'-triphosphate activity), nsp14 (N7-methyltransferase), nsp16 (2'O-methyltransferase) and nsp10 (cofactor) perform the RNA capping. The proteins involved in transcription form replication complexes and associate with double-membrane vesicles derived from the ER³⁷.

Characteristically for coronaviruses is the discontinuous viral negative strand RNA synthesis, generating a set of nested 3' and 5' co-terminal positive-sense subgenomic mRNAs (sgRNAs)³⁸, that are translated into structural and accessory proteins.

3.1.3.3 Viral particle assembly and viral release

For virus assembly and budding, coronavirus genomic RNA is transported to the ER-Golgi intermediate compartment and encapsulated in N proteins before assembling to particles with the S, M and E proteins that are suggested to exit the infected cell by exocytosis^{39,40}. In recent studies, however, it could be shown that SARS-CoV-2 egresses infected cells via the lysosomal trafficking pathway⁴¹.

Introduction

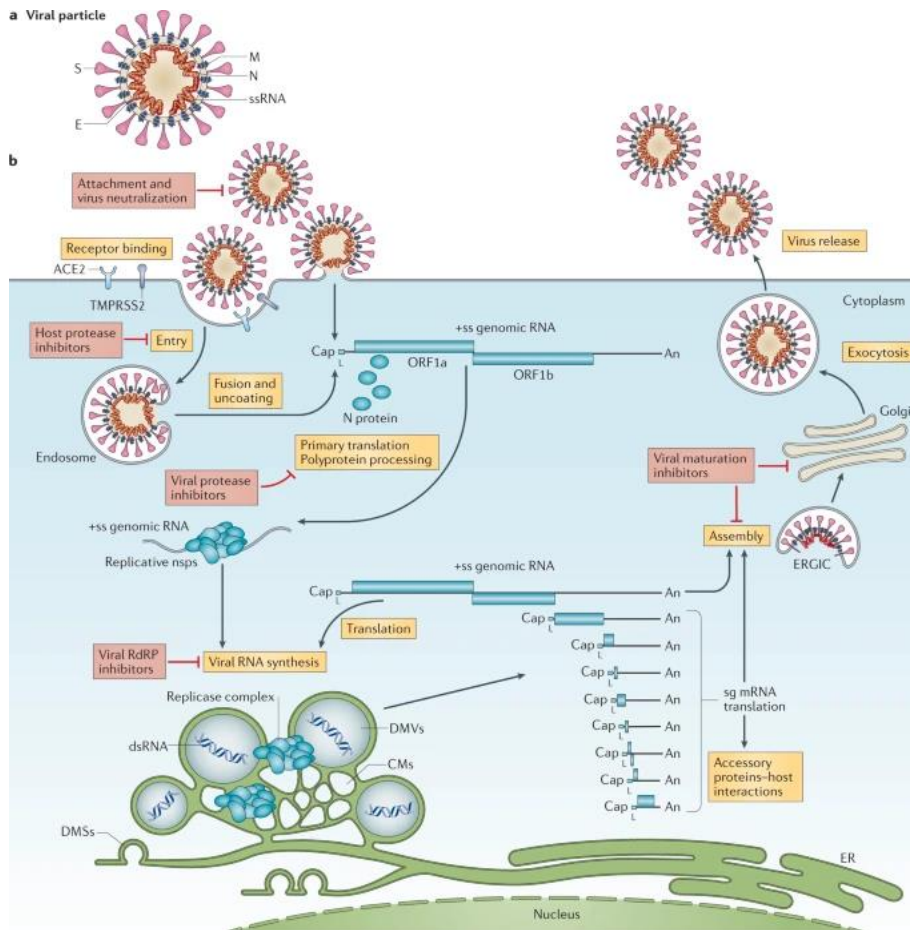


Figure 3: SARS-CoV-2 replication cycle.

The cell entry of SARS-CoV into the host cell occurs via interaction of the S protein with cellular receptors and host factors (ACE2, TMPRSS2). After virus entry the genomic RNA is released into the cytoplasm and transcription replication takes place. After the new virion assembly process the virus is transported out of the cell. (adapted from V'kovski *et al.*⁴²)

3.1.4 Ecology and host spectrum

The emergence of new epidemic diseases often resulted from interspecies transmission of zoonotic RNA viruses. For the control and intervention of zoonotic outbreaks it is important to identify closely related viruses in animal hosts to reconstruct evolutionary pathways⁴³. The recent coronavirus outbreaks demonstrated the ability of coronaviruses to cross species barriers from the natural reservoir to new hosts.

Due to their error-prone RNA replication⁴⁴ and frequent recombination, coronaviruses can rapidly adapt to new hosts. Bats, rodents and birds act as the natural reservoir for many coronaviruses⁴⁵⁻⁴⁷. Almost all known human coronaviruses originate from bat hosts^{48,49}, except HCoV-OC43 and HCoV-HKU1 are proposed to have rodent origin⁵⁰ (**Figure 4**). For example,

Introduction

SARS-CoV, which emerged in 2002 was identified to have most likely horseshoe bats as a natural reservoir^{45,51–53} but adapted to infect the intermediate host palm civet and later humans. The closely related SARS-CoV-2 also appears to have originated from horseshoe bats^{25,54}, although the intermediate host still remains unknown. Pangolins were discussed to be a candidate for an intermediate host as strains of SARS-CoV-2 have been shown to have relatively high similarity to pangolin coronaviruses⁵⁵ but phylogenetic analyses and a special amino acid sequence in the S gene of SARS-CoV-2 did not support the hypothesis of SARS-CoV-2 arising directly from the pangolin-CoV-2020⁵⁶.

Among all mammalian species bats harbour the largest diversity of coronaviruses. Furthermore, the highest diversity can be found in areas with the most diverse bat species appearance^{57–59}. Especially China with its two zoogeographic regions harbours a rich bat diversity⁶⁰. Bats can harbour many viruses without developing disease. Host-switching is an important driver for the evolution of bat-coronaviruses, however the cross species transmission dynamics remain poorly understood^{61,62}. In recent studies it has been shown that the host receptor is a determinant of host range expansion and can act as a screen to identify viruses that have the potential to jump into the human population⁶³.

SARS-CoV-2 naturally acquired a polybasic cleavage site at the junction of subunits S1 and S2 of the S protein^{54,64}, which is discussed to be a reason of higher transmissibility of SARS-CoV-2 compared to SARS-CoV. The polybasic cleavage site enables effective cleavage by furin and can reduce the S protein stability and facilitate conformational adaption required for binding to the entry receptor^{65,66}.

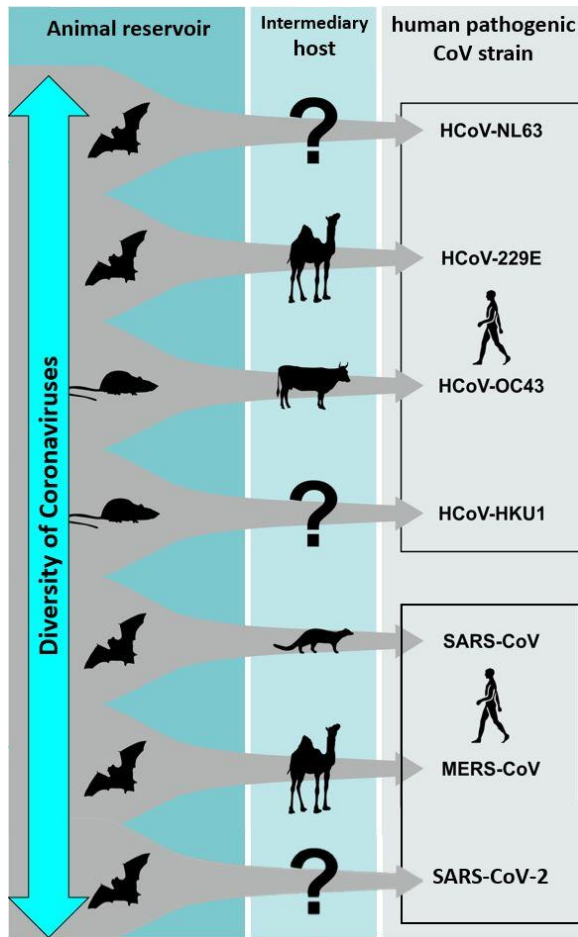


Figure 4: Interspecies transmission of coronaviruses.

The virus reservoirs and potential intermediate hosts of human coronaviruses (endemic and epidemic coronaviruses). All human coronaviruses emerge from bats as a natural reservoir except HCoV-OC43 and HCoV-HKU1 originating from rodents. After adapting to an intermediate host, which is still unknown for HCoV-NL63, HCoV-HKU1 and SARS-CoV-2, spill-overs into the human population were enabled (adapted from Corman *et al.*⁶⁷).

3.1.5 Epidemiology

In the last two decades, three new coronaviruses emerged from an animal reservoir and spread worldwide causing devastating human diseases.

3.1.5.1 Endemic coronaviruses

The four endemic coronaviruses HCoV-HKU1, HCoV-OC43, HCoV-229E and HCoV-NL63 are circulating usually in winter or early spring and typically cause common colds. HCoV-OC43 and HCoV-229E were first discovered in the 1960s⁵ and studies have shown that they cause up to 30% of all upper respiratory tract infections^{5,68,69}. Although they usually cause mild disease, they can also lead to severe pneumonia in risk groups as neonates and aged populations with underlying illnesses⁶⁹⁻⁷¹. After the emergence of SARS-CoV the coronaviruses HCoV-HKU1 and HCoV-NL63 were isolated and are known to typically cause mild respiratory disease and are responsible for up to 10% of respiratory tract infections^{72,73}. In addition HCoV-NL63 is also causing acute laryngotracheitis in children under the age of three⁷². Typically, first infections with endemic coronavirus strains occur in young children and then repeatedly throughout life^{74,75}.

3.1.5.2 Severe acute respiratory syndrome coronavirus (SARS-CoV)

Severe acute respiratory syndrome coronavirus (SARS-CoV) was the first known coronavirus causing a major epidemic. In November 2002 SARS-CoV emerged, and the first case, a 46-year-old man was detected in Foshan, Guangdong Province, China⁷⁶. From November 2002 until February 2003 retrospective surveillance revealed severe cases of the disease, described as acute community-acquired atypical pneumonia syndrome, in Guangdong Province⁷⁶. Usually the illness started with fever and mild respiratory symptoms but then rapidly progressed to pneumonia. On the 9th February 2003, a total of 305 cases were reported in mainland China from independent clusters of cases. The cases included patients, who had contact to wild game animals, close family members and healthcare workers, suggesting a zoonotic origin. The first known spread of SARS-CoV to Hong Kong occurred in February 2003, involving a physician

acquiring the disease from his patients, who travelled from Guangdong Province to Hong Kong. His stay at the Metropole Hotel in Hong Kong before hospitalisation led to transmission of the virus to 16 hotel guests within one day. These secondary cases led directly to tertiary cases in two Hong Kong hospitals and outbreaks in other countries and continents including Singapore, Canada, the United Kingdom, the United States, the Philippines and Vietnam and back to China⁷⁷. The first isolate was discovered in a lung biopsy of one of the secondary case patients in Hong Kong⁷⁸ and the novel coronavirus was named SARS-CoV⁷⁹⁻⁸¹. On March 13, 2003 the World Health Organisation (WHO) issued a global alert.

To identify the source of human infections, soon wild life animals on markets in the Guangdong Province were screened and SARS-CoV-like viruses were found in palm civets and horseshoe bats^{51,82}. Due to serological evidence in persons working on wild animal markets, the virus may have circulated for a few years before the outbreak in wild animals^{83,84}. However, the primary mode of global spread occurred via person-to-person-spread by indirect contact of the mucosae with infectious respiratory droplets or fomites⁸⁵. The attack rate among health care workers was very high as the risk of nosocomial transmission was elevated by the use of treatments generating large numbers of infectious droplets⁸⁶⁻⁸⁸. High viral loads could be also detected in feces^{89,90}, suggesting possible faecal-oral transmission. Transmission occurred via close contact and only after onset of symptoms, which resulted in household contact and nosocomial transmission but were infrequently in other settings.

All in all, 8437 cases and 813 related deaths were reported by the end of the outbreak in July 2003. Until June 2004, 17 additional cases of SARS were reported resulting from exclusively laboratory exposures^{91,92}.

3.1.5.2.1 Middle East respiratory syndrome coronavirus (MERS-CoV)

The first case of Middle East respiratory syndrome coronavirus (MERS-CoV) was reported in a private hospital in Jeddah, Saudi Arabia in June 2012. The patient was admitted to the hospital with acute pneumonia and renal failure. The novel coronavirus was identified as the etiological agent and could be isolated from the patient's sputum at the Erasmus Medical Center in Rotterdam, Netherlands. After naming it Human Coronavirus Erasmus Medical Center/2012 (HCoV-EMC/2012)⁹³, the virus was renamed MERS-CoV after global consensus⁹⁴. In the

Introduction

following, a patient in the United Kingdom was identified, who was transferred from a hospital in Qatar⁹⁵. The number of cases increased dramatically, with a peak in 2014 (Figure 5), including several clusters of healthcare workers and family members in hospital settings, resulting in over 300 infections and 40 deaths. MERS-CoV cases have been observed worldwide but were always linked to travel histories from the Middle East.

In the following, an outbreak was reported in South Korea in 2015. It has been the biggest outbreak to occur outside of Saudi Arabia. The first confirmed case of a MERS-CoV infected patient developed symptoms after returning from the Middle East at May 4, 2015 and was reported on 20 May 2015⁹⁶. After treatment in several hospitals, additional nosocomial infections in two hospitals were reported⁹⁷. Subsequently, multiple secondary clusters of infections in other medical facilities were reported, caused by the patients from the nosocomial infection clusters in the first two hospitals⁹⁸. Immediately, after laboratory confirmation of the first cluster of infections, increased surveillance for MERS-CoV and improved infection-control measures in hospitals were introduced leading to a containment of the outbreak. All in all, during the South Korea outbreak, 186 MERS-CoV cases and 36 deaths were reported⁹⁹.

Studies have shown prevalence of the MERS-CoV in dromedary camels¹⁰⁰⁻¹⁰², suggesting dromedary camels functioning as intermediate host. Furthermore, serological evidence could prove circulation of MERS-CoV in the Arabian Peninsula, Africa and on the Canary islands for at least 2-3 decades in dromedary camels¹⁰³ suggesting camel farms as potential source of MERS-CoV infections. MERS-CoV similar viruses have been detected in bats¹⁰⁴, which are most likely the original reservoir, although there is no epidemiologic evidence of their role in transmission.

Primary zoonotic transmission from dromedaries to humans were reported in 54.9% among cases¹⁰⁵ and resulted in limited human-to-human transmission chains, which included healthcare and household settings¹⁰⁶⁻¹¹¹. For dromedaries to humans transmission of MERS-CoV contact with nasal secretions, saliva and respiratory droplets is suggested to be a route of infection¹¹². Transmission by camel urine or meat have not been reported, however consumption of raw milk is discussed as a risk factor^{113,114}.

Secondary transmission is typically restricted to healthcare or household settings, however from 2015-2018, 14% of reported cases had unknown exposure¹⁰⁵. MERS-CoV symptoms are typically fever, cough and shortness of breath and can result in a broad range from asymptomatic and mild respiratory symptoms to severe acute respiratory disease to death.

Since April 2012, the WHO reported 2468 laboratory-confirmed cases and 851 related deaths (25th November 2020).

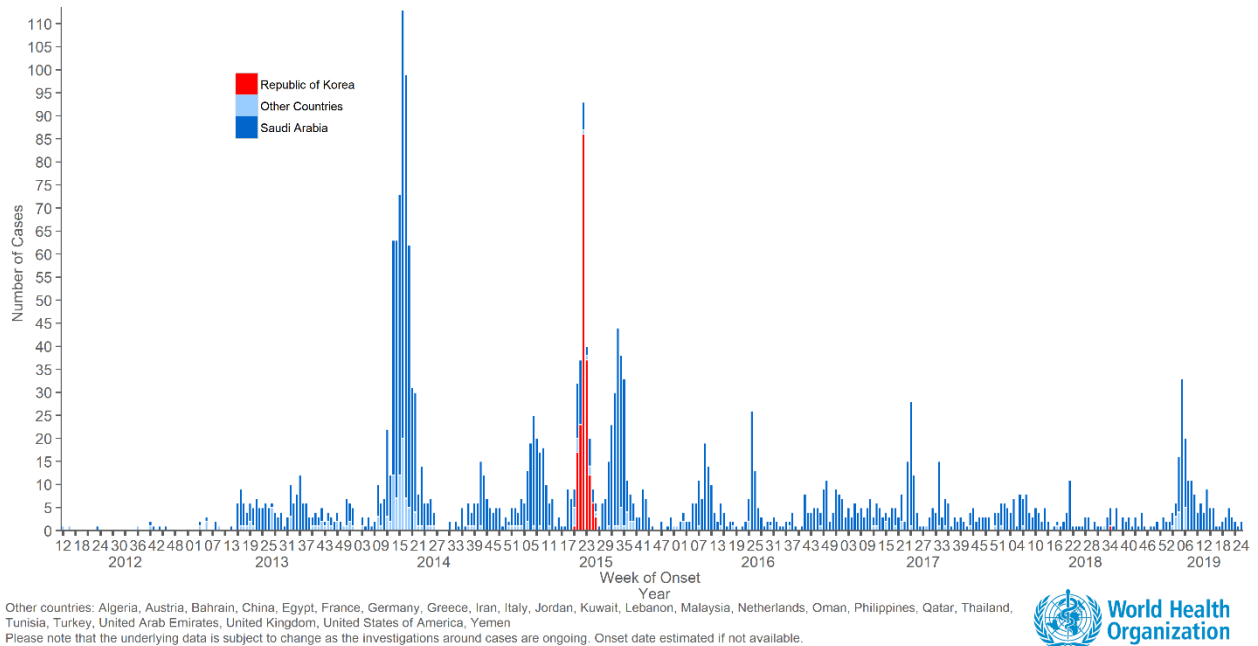


Figure 5: Global map of countries with confirmed cases of MERS-CoV.

MERS-CoV emerged in Saudi-Arabia and number of cases increased dramatically in 2014 including transmission to other countries. The second largest outbreak in 2015 appeared in the South Korea outbreak. There are still ongoing outbreaks in hospital settings in Saudi-Arabia¹¹⁵.

3.1.5.3 Severe acute respiratory syndrome coronavirus 2 (SARS-CoV-2)

In December 2019, the first outbreak of a novel coronavirus, named 2019-nCoV by Chinese authorities¹¹⁶, was reported in Wuhan City, Hubei Province, China¹¹⁷, after being alerted about a cluster of pneumonia of unknown etiology^{118,119}. Most of the patients visited an animal market in Wuhan, suggesting that the outbreak started from a single or multiple zoonotic events at the Huanan Seafood Wholesale wet market¹²⁰. The symptoms included pneumonia, fever, cough, chest discomfort as well as dyspnoea and lung infiltration^{121,122}. Human-to-human transmission of the virus was proven by following cases with no link to the wet market in addition to several family clusters and nosocomial infections^{123,124}. The virus spread massively to other parts of

Introduction

China most likely due to facilitated virus transmission because of travellers during the Chinese New Year festival. Until end of January, the number of cases increased dramatically in China with an epidemic peak in February and the WHO declared the novel coronavirus outbreak as public health emergency of international concern¹²⁵. The International Committee on Taxonomy of Viruses named the novel coronavirus SARS-CoV-2 and the WHO named the disease coronavirus disease 2019 (COVID-19). Chinese authorities introduced unprecedentedly strict public health measures to contain the virus outbreak, such as shutting down the city of Wuhan and restricting public gatherings and activities as well as blocking travel and transportation¹²⁶. In the following, new cases in China decreased¹²⁷. On the other hand, an increasing number of countries reported large cluster of infection due to international travel and the high transmission efficiency of SARS-CoV-2. The WHO declared the outbreak as a pandemic on 11th March 2020¹²⁸. Since March 2020, the case numbers and COVID-19-related deaths (Figure 6) increased dramatically in Europe, the USA and other parts of the world.

For COVID-19 disease several risk groups are defined, which have a higher probability of developing severe and even fatal disease courses. Demographic factors increasing the risk for severe disease include higher age, defined as >64 or >65 years¹²⁹⁻¹³⁷, male gender^{131,132,138} and menopausal women¹³⁸. Furthermore, pre-existing comorbidities, such as hypertension, diabetes and cardiovascular diseases are known to influence COVID-19 mortality. In addition, further risk factors were identified, such as obesity and type II diabetes^{129,131,132,138}.

On 25th November 2020, SARS-CoV-2 was reported in 191 countries, 59,9 Mio. cases were reported including 1,4 Mio. deaths worldwide¹³⁹. The USA, followed by India and Brazil, has reported the largest number of cases and deaths.

Introduction

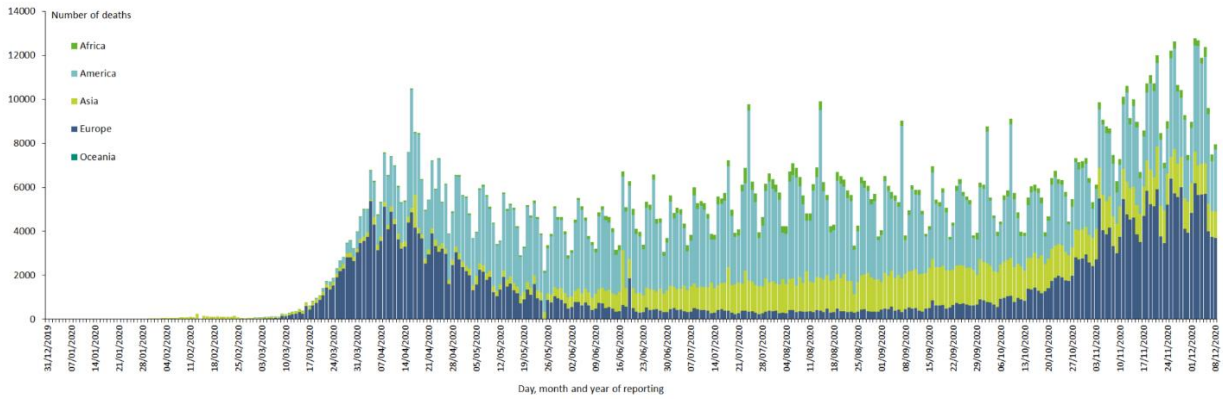


Figure 6: Distribution of COVID-19 related deaths worldwide by continent (as of 9th December 2020).

The first cases of SARS-CoV-2 were reported in Wuhan, China. Since March 2020 case numbers and COVID-19 related deaths increased globally. Most cases and deaths appear in USA, Asia and Europe¹⁴⁰.

3.1.6 Prevention and treatment

As of December 8th 2020 no proven effective antivirals or therapeutics against SARS-CoV-2 or other human coronavirus infections are available, although some treatments have been shown to have beneficial effects (chapter 3.1.6.2 Therapeutics)¹⁴¹. Currently, infection prevention measures as well as oxygen supplementation and mechanical ventilation are implemented in clinical management. Due to the absence of effective vaccines and therapeutics, SARS-CoV-2 infections are controlled by an active public health surveillance system and infection control practices. Therefore, the WHO implies physical distancing, avoiding closed environments (restaurants, bars) and crowded places, wearing face masks, maintaining basic hygiene (washing hands), isolation of infected persons and contact tracking. These recommendations have been implemented by the governments of many countries worldwide. Nonetheless, 184 vaccines and 449 therapeutic drugs are in development (9th December 2020)¹⁴².

3.1.6.1 Vaccine development

At the moment, no vaccines are available that protect against endemic human coronavirus infections. On the other hand, vaccines to prevent infections against domestic animal coronaviruses are routinely used in young animals. For SARS-CoV and MERS-CoV specific

Introduction

vaccines are under development and several neutralizing antibodies have been detected for passive immunisation^{143,144}.

Due to the urgency of the ongoing SARS-CoV-2 pandemic, 59 vaccine candidates are presently in human trials including phase III trials. The vaccine strategies include recombinant protein vaccines (based on the spike protein, the receptor-binding domain (RBD) or on virus-like particles), replication-incompetent and competent vectors, DNA, mRNA in lipid nanoparticles, inactivated viruses, and live attenuated viruses^{145–147}. Usually, vaccine development can take up to 15 years. In the discovery phase of vaccine development, exploratory preclinical experiments are performed following further, more formal, preclinical experiments and toxicology studies. Upon completion of the preclinical trials, the vaccine candidate can enter phase I, II and III clinical trials and be licensed afterwards. Due to the previous information from the development of SARS-CoV and MERS-CoV vaccines, the vaccine development for SARS-CoV-2 was able to follow an accelerated timeline by omitting the discovery phase and directly entering the phase I and II trials, allowing development in an unprecedented speed. In addition, clinical trials were running in parallel and the large-scale production was started before licensing¹⁴⁸.

Inactivated virus, recombinant spike-protein-based, replication-incompetent and RNA vaccine candidates are in phase III trials. Two replication-incompetent vector vaccines were licensed in Russia and in China for the Chinese Military without a phase III trial. Currently, 17 vaccines are authorized globally and 34 vaccine candidates are in phase III trials (08th June 2021).

3.1.6.2 Therapeutics

At present, 362 therapeutic drugs against SARS-CoV-2 are in human trials. Further clinical trials have to be assessed to prove efficacy of antiviral drugs and therapies (Figure 7).

To prevent virus entry arbidol (umifenovir) inhibits membrane fusion by targeting the interaction of the S protein with ACE2. Clinical trials have not shown improvement of virus clearance in patients with mild or moderate outcome, however arbidol proved to be more effective than liponavir and ritonavir^{149–152}. In addition, camostat mesylate is known to inhibit TMPRSS2 activity and blocking virus entry into human lung cells²³. Chloroquine or hydroxychloroquine have been previously used in the treatment of malaria and autoimmune diseases and inhibit the glycosylation of cellular receptors as well as prevent membrane fusion

Introduction

by increasing the endosomal pH. In vitro studies showed SARS-CoV-2 inhibition^{153,154}, but clinical studies showed no improvement of death rates and even suggested a higher risk of cardiac attack^{155,156}. Furthermore, soluble recombinant ACE2, specific monoclonal antibodies and fusion inhibitors targeting the S protein have been investigated but require further clinical trials^{157–159}.

To inhibit virus replication, antivirals such as remdesivir (GS-5734), favilavir (T-705), ribavirin, lopinavir and ritonavir are assessed in clinical trials. Remdesivir has been shown to shorten the recovery time in hospitalized adults and lower the need for oxygen support, however further clinical trials are continued to prove safety and efficacy^{160,161}. Most of the Favilavir trials were conducted in small cohorts in China and Japan but have been shown to reduce signs of disease and shortened the time for virus clearance¹⁶². Lopinavir and ritonavir were already conducted in in vitro analyses for SARS-CoV and MERS-CoV infection but randomized trials have shown no beneficial effects^{163,164}.

Severe COVID-19 outcome is characterized by a cytokine storm^{118,165}. Therefore, immunomodulatory agents have been implemented in treatment of COVID-19 patients. Dexamethasone is a corticosteroid, found to be reducing mortality in patients requiring mechanical ventilation and oxygen supplementation¹⁶⁶. Furthermore, IL-6 receptor-specific antibodies, such as tocilizumab and sarilumab, were shown to be effective against the cytokine storm in a small uncontrolled cohort¹⁶⁷. In addition, SARS-CoV-2 is sensitive against interferon treatment and clinical trials are conducted in China by vapor inhalation of IFN- α ¹⁶⁸.

Preliminary findings have shown that convalescent plasma treatment improved clinical outcome^{169,170}, however the treatment may have adverse effects such as antibody mediated enhancement of infection, transfusion-associated acute lung injury and allergic reactions. On the other hand, therapy with convalescent plasma is discussed controversial and requires further high-quality, multicentred, randomized, controlled trials. Monoclonal antibody therapy on the other hand has also been shown to neutralize SARS-CoV-2 infection in vitro and in vivo^{171–174} but therapy is restricted by high costs and limited capacity of manufacturing.

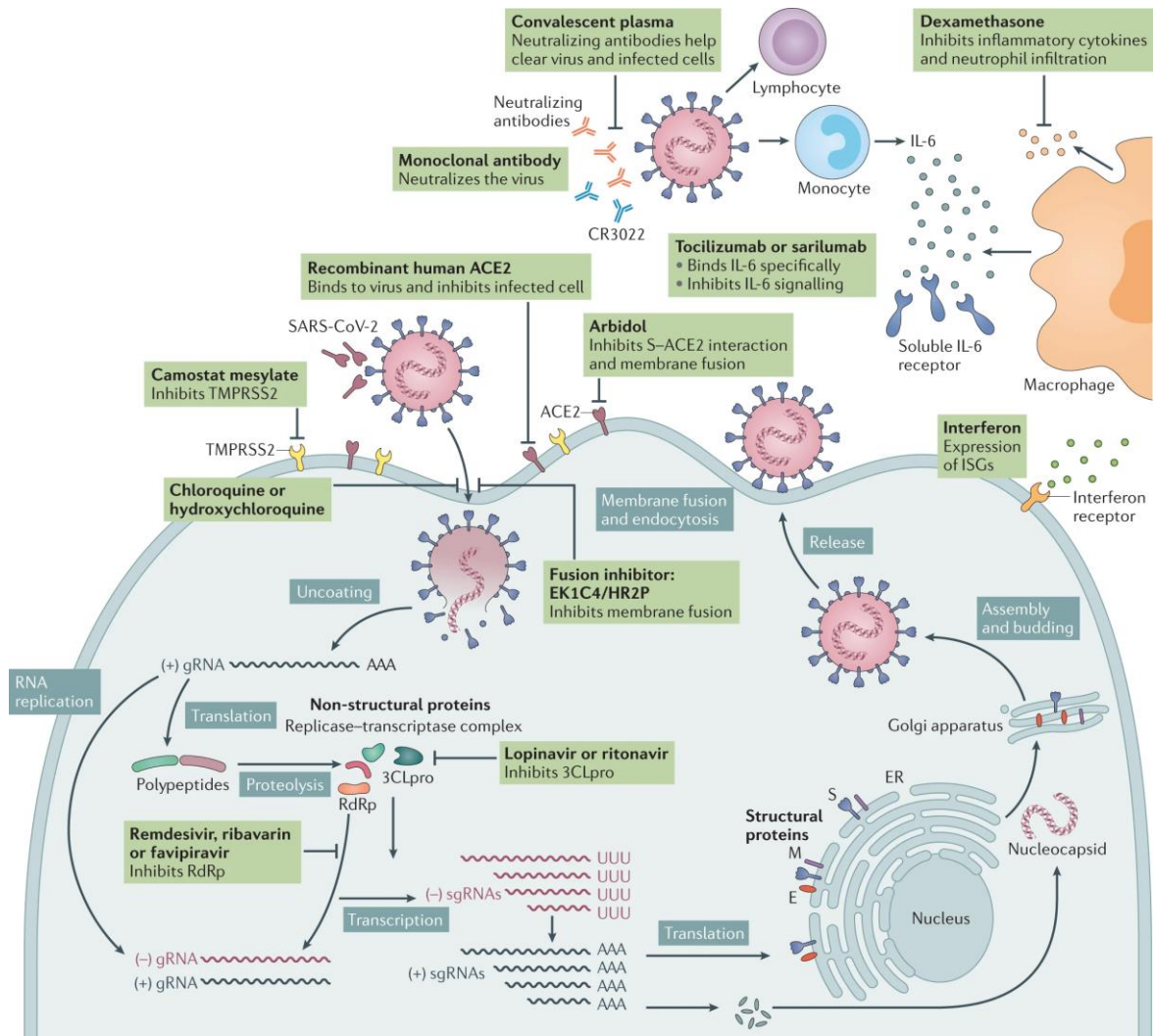


Figure 7: Potential therapeutic targets in SARS-CoV-2 replication.

The SARS-CoV-2 replication cycle is targeted by antivirals at different steps, such as receptor binding, entry and fusion. Currently, there are no clinical efficacy data on treatments with antivirals (adapted from Hu *et al.*¹⁴¹).

3.1.7 Sex hormone biosynthesis and metabolism

The synthesis of sex steroids takes place in the primary steroidogenic organs (gonads, adrenal cortex, placenta) and peripheral tissues (liver, fat, kidney)^{175,176}. Steroids are composed of four fused rings. Cholesterol is the precursor for all steroid hormones and can be obtained from de novo biosynthesis from acetate in the primary steroidogenic organs (Figure 8)¹⁷⁷⁻¹⁷⁹.

All steroid hormones are synthesized with the help of either the heme-containing cytochrome p450 (CYP) enzymes, utilizing NADPH as an electron donor, or hydroxysteroid dehydrogenase (HSD) enzymes, which are dependent on NAD(P)H and NAD(P)⁺ co-factors. There are two types of CYP enzymes. Type I CYP enzymes are found in mitochondrial membranes, whereas type II CYP enzymes are located in the endoplasmic reticulum (ER). Furthermore, CYP enzymes are divided based on their mode of electron transfer as type I CYP enzymes are dependent on ferredoxin and type II CYP enzymes are dependent on the donor enzyme cytochrome P450 oxidoreductase (POR) for the delivery of their electrons. There are two HSD enzyme superfamilies, which are regulating the activity of the steroid at specific steroid receptors¹⁸⁰.

In the gonads, steroidogenic enzymes are expressed cell-specific patterns determining the production of androgens and estrogens. The steroidogenesis in the gonads is initiated by pulsatile secretion of gonadotropin-releasing hormone (GnRH), which is produced in the hypothalamus. In the following, GnRH secretion is stimulating the production of luteinizing hormone (LH) from the pituitary gland. LH stimulates the Leydig cells to produce androgens. In the Leydig cells of the testes either dehydroepiandrosterone (DHEA) is converted in testosterone via androstenedione (A4) or androstenediol (5-Adiol). In the following, testosterone is released into circulation. In the theca cells, located in the ovaries, androgens are produced in a similar way.

Testosterone is mostly bound to the sex hormone-binding globulin (SHBG), which is regulating the amount of unbound testosterone circulating in the blood stream before entering the target cells. Only less than 3% of testosterone is circulating as a free bioavailable form¹⁸¹. In the target cells, testosterone is converted to DHT by 5 α -reductase primarily in the male reproductive organs or is metabolized into estradiol by aromatase (CYP19A1). In the female reproductive tract, A4 and testosterone are transported into the granulosa cells resulting in estradiol biosynthesis by CYP19A1. The aromatase is found in several tissues and cells, including ovarian granulosa cells, adipose and skin fibroblasts, bone and the brain¹⁸². Thus, regulating the

balance between androgen and estrogen production is being determined by the expression levels of local enzymes in target tissues and cells.

Testicular Leydig cells / Ovarian Theca cells

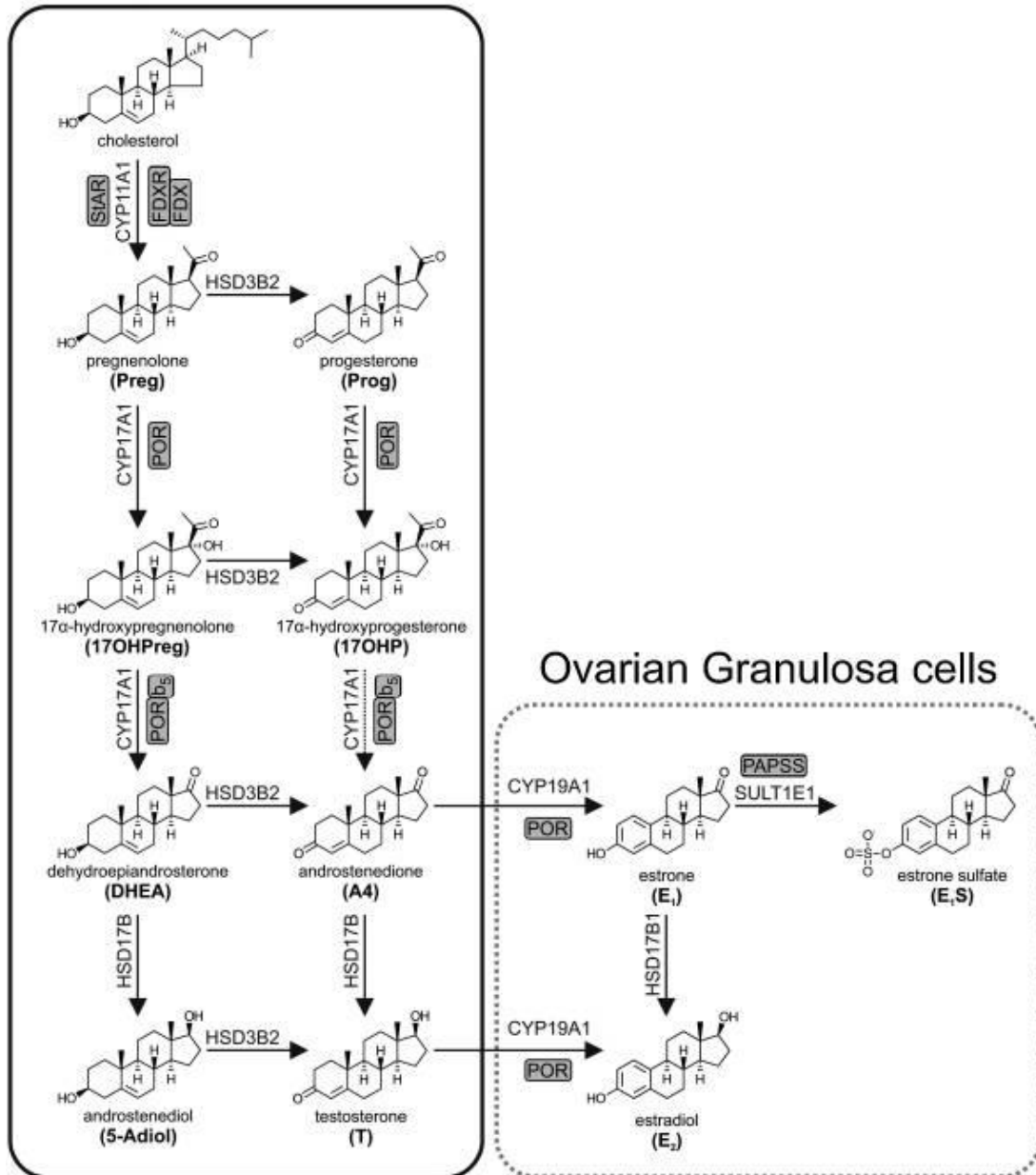


Figure 8: Biosynthesis of sex hormones in the gonads.

The precursor of steroid hormones cholesterol is metabolized into androgens in testicular Leydig cells or ovarian theca cells. In the female reproductive tract, androstenedione (A4) and testosterone enter the ovarian granulosa cells and are metabolized to estrogens (adapted from Schiffer *et al.*¹⁸³).

3.1.8 Sex differences and the role of hormones in infections

The prevalence and outcome of infections, including diverse viruses (human immunodeficiency virus (HIV), herpes simplex virus, hantavirus, hepatitis B virus, influenza virus, measles virus, West Nile virus¹⁸⁴) are suggested to be dependent on sex differences among mammalian species. Males and females differ in their response to a variety of different pathogens and autoimmune diseases. The mechanisms can result from differences in hormone levels or from environmental and genetic factors. In general, females before menopause are more resistant to bacterial, viral and parasitic infections and have higher innate and adaptive immune responses, which can for example lead to accelerated virus clearance and reduced virus load compared to men^{185–188}. In addition, females have a better response to vaccination programs^{189,190}. On the other hand, females have a higher prevalence of autoimmune diseases and can suffer from immunopathology. For example, females have a more rapid progression to acquired immunodeficiency syndrome (AIDS) despite similar viral loads¹⁹¹. In addition, studies show, that females in their reproductive age suffer from more severe influenza than males due to more severe inflammation^{192,193}. Conversely, accumulating data indicate that intensity and prevalence of viral infections are typically higher in males¹⁹⁴.

As sex differences are mainly observed from puberty to menopause, sex steroid hormones may play a role in differential immune responses. For example, higher 17 β -estradiol levels are reported in rheumatoid arthritis patients than in healthy controls¹⁹⁵. Estrogen influences physiological functions via estrogen receptors (ER). Estrogen receptors have three subtypes including ER- α , ER- β and G protein-coupled estrogen receptor 1 (GPER1). ER- α and ER- β are nuclear receptors and are translocated to the nucleus after estrogen binding, where the complex can bind estrogen-responsive elements in DNA to regulate gene transcription¹⁹⁶. ER expression is tissue specific. ER- α is expressed mainly in female sex organs and ER- β is expressed in different types of tissues and cells with higher levels in females compared to males¹⁹⁷. Among expression in the female reproductive tract, ER- α is expressed in several immune cells, such as B- and T-lymphocytes, neutrophils, macrophages, NK cells, thymic stromal cells, bone marrow and endothelial cells^{198–200} to varying degrees, whereas ER- β is infrequently expressed. GPER1 is a membrane receptor mediating estrogen-dependent rapid signalling events, independent of ER- α and ER- β ²⁰¹.

Conversely, androgens influence the immune response by decreasing antibody production, T-cell proliferation, NK cytotoxicity, and stimulating the production of anti-inflammatory

cytokines²⁰². Androgens, mainly testosterone and dihydrotestosterone (DHT), are mediated through the androgen receptor (AR), a ligand-dependent nuclear transcription factor²⁰³. AR are expressed and can act on immune cells, such as neutrophils, macrophages, mast cells, monocytes, T- and B-cells by controlling the transcription of immune-regulatory genes^{204–212}. In addition to the nuclear androgen receptors a membrane-bound androgen receptor zinc transporter SLC39A9 (ZIP9) was identified^{213,214}. It has been shown to mediate testosterone regulation of tight junction formation in Sertoli cells²¹⁵.

3.1.8.1 Sex differences in respiratory viral infections

Interferons (IFNs) can be subdivided into three types of cytokines (I, II and III) in mammals and are important components of innate immune response activating the transcription of the JAK-STAT signalling pathway. Type I IFNs consist of 13 subtypes of IFN- α , IFN- β , IFN- ϵ and IFN- ω , whereas type II IFN only comprise of IFN- γ . There are four known type III IFNs; IFN- λ 1- IFN- λ 4²¹⁶.

Respiratory viral infections trigger a strong type I immune response by activation of pathogen pattern recognition receptors (PRRs), which involves production of type I and III interferons and proinflammatory mediators. Type I immune responses are important for virus clearance. Studies have shown, that ER- α signalling is promoting type I IFN synthesis. Furthermore, female plasmacytoid dendritic cells produce more type I IFN than male plasmacytoid dendritic cells^{217–220}.

Testosterone decreases the production of proinflammatory cytokines, such as IFN- γ and TNF- α , in contrast to lower physiological levels of estrogen²²¹. Type II immune responses are important for tissue repair and resolution of the immune response upon influenza and respiratory syncytial virus infection^{222–224}. In murine models of allergic asthma, ER- α signalling contributes to macrophage polarization promoting type II response of alveolar macrophages²²⁵.

The majority of studies on sex differences during influenza infections showed that the incidence of infection is often higher in males, while the hospitalisation rates and mortality was higher in females during their reproductive age^{193,226–229}. Conversely, the mortality in males younger than 20 years or older than 80 years, was higher compared to females leading to the suggestion that low levels of testosterone are associated with disease severity²²⁸. On the other hand, pregnant women are at high risk to be hospitalized during an 2009 pH1N1 infection, which may be due

Introduction

to elevated estrogen and progesterone levels during pregnancy²³⁰⁻²³². Murine models of IAV infection suggest that the increased mortality in females is due to the proinflammatory response leading to tissue damage. Female mice treated with testosterone as well as ovariectomized mice supplemented with estrogen or progesterone were protected from mortality. In contrast, male mice treated with testosterone or estradiol did not show enhanced disease outcome^{233,234}.

Conversely, infection by respiratory syncytial virus (RSV), SARS-CoV, MERS-CoV and SARS-CoV-2 led to increased disease severity in males^{132,235,244,245,236-243}. In C57BL/6 and BALB/c mice it could be observed that male mice were more susceptible to SARS-CoV infection, while ER signalling in females seemed to be protective²⁴⁶. Interestingly, studies have shown that lower testosterone levels in COVID-19 patients present a poor prognostic marker for disease outcome^{247,248}. The mechanisms behind the observed sex differences remain unclear and require further investigation.

4 Aim

Males experience higher mortality upon SARS-CoV-2 infection than females. However, it is yet unclear whether sex hormones are associated with a severe COVID-19 disease outcome. The aim of this study was to investigate, whether the sex bias is caused by SARS-CoV-2 infection itself or by additional confounding factors.

We analysed a large profile of hormones and cytokines of critically ill COVID-19 patients in comparison to critically ill non-COVID-19 patients, as well as healthy controls and patients with coronary heart disease, representing one of the most abundant COVID-19 comorbidities. Additionally, a golden hamster animal model for SARS-CoV-2 infection was established to further investigate the dysregulation of sex hormones during the SARS-CoV-2 infection course independently of other confounding factors. This work focuses on the analysis of the sex hormones testosterone and estradiol and their converting enzyme aromatase CYP19A1 in the reproductive organs and the lung.

Findings of this study shall provide a basis for in-depth molecular analysis as well as the development of new antiviral strategies.

5 Results

5.1 Sex hormones and metabolic dysregulations in critically ill COVID-19 patients

5.1.1 Higher mortality in male COVID-19 patients

During the current SARS-CoV-2 pandemic, most countries report a higher case fatality of male patients compared to female patients, indicating male sex as a risk factor for fatal outcome.

To assess the case fatalities in men and women, COVID-19 patient data from the intensive care unit at the University Medical Centre Hamburg-Eppendorf were analysed retrospectively. From 9th March to 9th December 2020, 136 PCR confirmed COVID-19 patients were admitted to the intensive care unit, of which 88 patients (65%) were male and 48 patients (35%) were female. Overall, 41 COVID-19 patients (30%) at the intensive care unit died. Of these, 25 (61%) were male and 16 (39%) were female (Figure 9).

All in all, the disease severity as well as the mortality at the intensive care unit at the University Medical Centre Hamburg-Eppendorf was higher in male patients and is thereby confirming the higher case fatality rate of male patients observed worldwide.

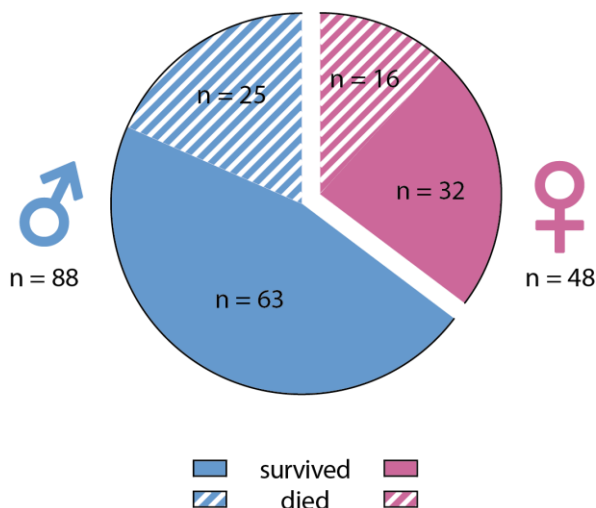


Figure 9: Mortality of male and female COVID-19 patients at the intensive care unit.

Pie chart visualizing COVID-19 patient numbers at the Clinic for Intensive Care Medicine at the University Medical Centre Hamburg-Eppendorf within the period of 9th March-to 9th December 2020. Shown are surviving (males, $n=63$; females, $n=32$) and deceased (males, $n=25$; females, $n=16$) patient numbers.

5.1.2 Characteristics and demographics of COVID-19 patients

We observed a higher mortality of male COVID-19 patients compared to female patients. In the following, we collected COVID-19 patient plasma from the intensive care unit to further investigate potential disease severity markers contributing to the higher mortality in male patients. From 09th March to 27th April 2020, 39 male and 11 female patients were admitted to the intensive care unit. The majority of these patients presented several comorbidities. Among the comorbidities, coronary heart disease (CHD), diabetes type II and obesity were the most frequent observed diseases (Table 1), which are already known to influence COVID-19 mortality. Both male and female patients, presented the same frequencies for diabetes type II and obesity (male, 30.8%; female, 27.3%, $P=1$). On the other hand, a tendency could be observed regarding a higher frequency of CHD in male patients (male, 20.5%; female, 9.1%, $P=0.6$).

Table 1: COVID-19 patient comorbidities

Characteristics	Males (<i>n</i> =39)	Females (<i>n</i> =11)	<i>P</i> value
Comorbidities (%)			
Coronary Heart Diseases (CHD)	8 (20.5)	1 (9.1)	0.6
Diabetes mellitus type II	12 (30.8)	3 (27.3)	1.0
Obesity (BMI>30)	12 (30.8)	3 (27.3)	1.0

In previous studies, we could observe a testosterone depletion in male mice upon infection with pH1N1 (Supplemental Figure 1). Due to the observed sex-dependent disease outcome, we measured the major sex hormone levels in COVID-19 patients. As a control group, we recruited age- and sex-matched SARS-CoV-2 negative male and female blood donors as a healthy control (HC; male, *n*=30; female, *n*=20). In addition, as age- and sex-matched SARS-CoV-2 negative male and female CHD patients were recruited (male, *n*=25; female, *n*=14), as we observed a higher frequency of CHD in male COVID-19 patients, to exclude an influence of their comorbidity on hormone levels. Furthermore, a control cohort was recruited including SARS-

Results

CoV-2 PCR negative intensive care unit patients (ICU non-COVID-19; male, n=27; female, n=15) (Table 2).

Table 2: Healthy control, coronary heart disease, non-COVID-19 and COVID-19 critically ill patient demographics

Characteristics	HC (n=50)	CHD (n=39)	Non- COVID-19 (n=42)	COVID-19 (n=50)
Sex, No (%)				
Male	30 (60)	25 (64)	27 (64)	39 (78)
Female	20 (40)	14 (36)	15 (36)	11 (22)
Age, mean, y				
Male	58.5	65.7	67.0	63.0
Female	55.7	64.6	71.0	65.8

5.1.3 Male COVID-19 patients present reduced androgen and increased estrogen levels

In the following, estradiol, estrone, testosterone and dihydrotestosterone levels were measured in the plasma of healthy donors, CHD patients, critically ill non-COVID-19 patients and COVID-19 patients (Figure 10 and Supplemental Figure 2).

Estradiol levels in COVID-19 patients were significantly enhanced compared to HC, CHD patients and critically ill non-COVID-19 patients (Figure 10a). Interestingly, estradiol levels in female COVID-19 patients were also increased compared to HC, CHD patients and critically ill non-COVID-19 patients (Figure 10c). As we observed high estradiol levels in both male and female COVID-19 patients, we measured plasma estrone levels as in addition to aromatization of androstenedione, estrone is also metabolized from estradiol. In line with increased estradiol levels, estrone levels were also significantly enhanced in male and female COVID-19 patients compared to HC (Supplemental Figure 2).

Reduced testosterone levels in men are suggested to increase the risk of developing coronary heart disease and are associated with increased mortality²⁴⁹. In COVID-19 male patients, the plasma testosterone levels were significantly reduced compared to HC, CHD patients and also severely reduced compared to critically ill non-COVID-19 patients (Figure 10b). In contrast, in female COVID-19 patients testosterone levels were not significantly altered (Figure 10d).

Results

As we observed a significant reduction of testosterone levels in male patients, we further analysed the dihydrotestosterone levels. In the target organs, testosterone is metabolized into its active form dihydrotestosterone by 5- α reductase. In line with the reduced testosterone levels the dihydrotestosterone levels were also significantly reduced in male COVID-19 patients compared to HC (Supplemental Figure 2). Dihydrotestosterone levels in female COVID-19 patients and HC were within the reference ranges and did not show significant changes (Supplemental Figure 2).

Overall, we could observe severely reduced androgen levels in male COVID-19 patients and in addition increased estrogen levels in male and female COVID-19 patients.

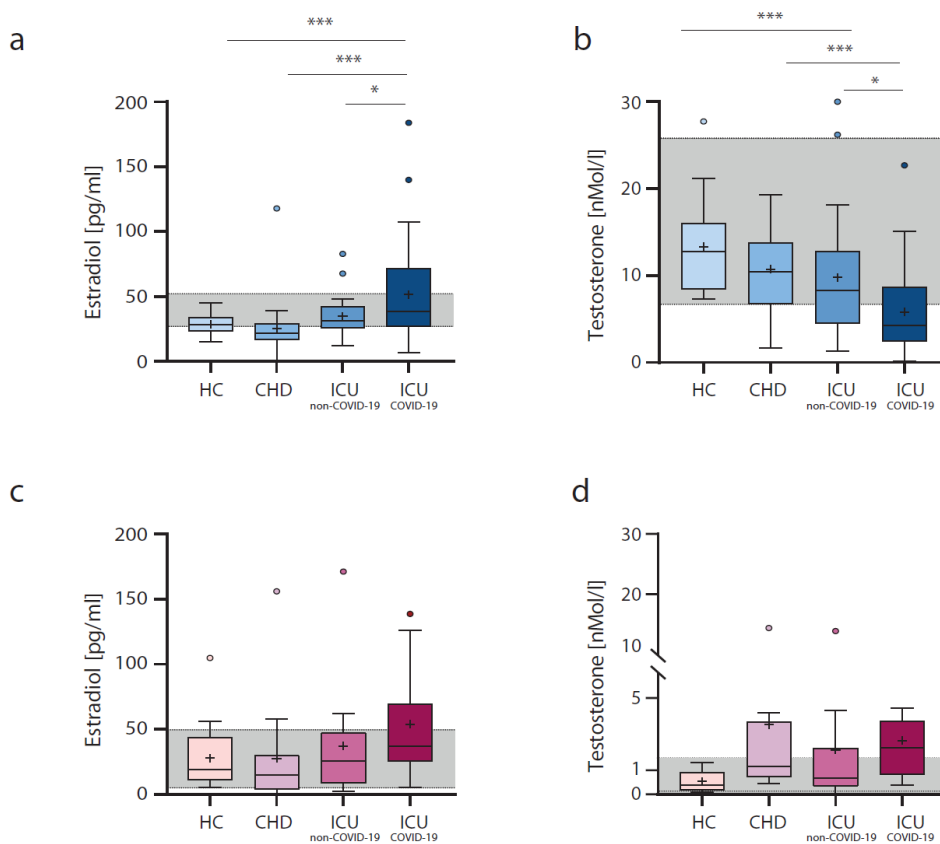


Figure 10: Sex hormone levels in COVID-19 patients, critically-ill non-COVID-19 patients, healthy controls and patients with coronary heart disease.

Estradiol (a,c) and testosterone (b,d) levels were measured in plasma obtained from COVID-19 patients, aged-matched critically-ill SARS-CoV-2 negative patients (ICU_{non-COVID-19}), healthy donors (HC) and coronary heart disease patients (CHD). Blue graphs represent males (HC, $n=30$; CHD, $n=25$; ICU_{non-COVID-19}, $n=27$; COVID-19, $n=30$) and pink graphs represent females (HC, $n=20$; CHD, $n=14$; ICU_{non-COVID-19}, $n=15$; COVID-19, $n=11$). Percentile boxplots represent 25-75% of values with the median value indicated by a crossline, and mean values by a plus icon. The laboratory assessed hormone reference ranges are indicated in grey. Statistical significance was assessed via One-Way-ANOVA. Statistical significance was defined as $P < 0.05$ (* $P < 0.05$, *** $P < 0.001$).

Results

To further analyze the endocrine status in severely ill COVID-19 patients, we measured additional hormones (Table 3). The reference values were assessed by the clinical laboratory performing the hormone measurements. As we observed low total testosterone levels in male COVID-19 patients, we analyzed free testosterone levels. The majority of testosterone is bound by the sex hormone-binding globulin (SHBG). SHBG is transporting testosterone from Leydig cells to the target organs. 66.7% of male COVID-19 patients presented reduced free testosterone levels, confirming the androgen deficiency in male COVID-19 patients. Interestingly, 54.5 % of female COVID-19 patients presented elevated free testosterone levels. In most of the male and female COVID-19 patients SHBG levels were in a normal range (69.2%, 63.6%), although in 28.2% of male COVID-19 patients SHBG levels were elevated. Consequently, high SHBG levels lead to decreased free testosterone levels, which could contribute to androgen deficiency in 28.2% of male COVID-19 patients.

Luteinizing hormone (LH) as well as the follicle stimulating hormone (FSH) are important for the production of testosterone in the testicles in men and for the menstrual cycle in women. In the majority of male COVID-19 patients (69.2%), LH levels were in a normal range; however, 30.8% presented elevated LH levels. Dysregulation in LH levels can impair the steroidogenesis in the testis. However, only 25% of male COVID-19 patients with low testosterone levels also presented elevated LH levels. 12.8% of male COVID-19 patients had elevated FSH levels accompanied by high LH levels. Most likely, due to the menopausal state of the female COVID-19 patients, 45.5% of female patients had reduced FSH levels.

Thyroid hormones (TSH) and T4 are known to affect SHBG levels and were within the reference values in the majority of male and female COVID-19 patients. Interestingly, 56.4% of male and 81.8% of female COVID-19 patients presented elevated cortisol levels, which could be due to increased stress because of mechanical ventilation.

In conclusion, we could confirm the androgen depletion in male COVID-19 patients with low free testosterone levels, which could be explained with impaired steroidogenesis as a consequence of primary hypogonadism in only 25% of male patients, whereas in 75% of male patients with testosterone deficiency the mechanisms require further investigations.

Table 3: Hormone levels in COVID-19 patients

Hormone Levels	COVID-19 Males (n=39)	COVID-19 Females (n=11)
Free testosterone		
Normal males: 20-39 yr: 7-22.7 pg/ml 40-60 yr: 6.3-17.8 pg/ml ≥61 yr: 2.5-17.8 nMol/l	13 (33.3%)	
Low (all age groups, below reference)	26 (66.7%)	
Normal females 40-60 yr: ≤2.3 pg/ml ≥61 yr: ≤2.1 pg/ml		5 (45.5%)
High (all age groups, above reference)		6 (54.5%)
Sex hormone-binding globulin		
Normal males: 10-40 nMol/l	27 (69.2%)	
Low: <10 nMol/l	1 (2.6%)	
High: 41-100 nMol/l	7 (17.9%)	
Very High: ≥101 nMol/l	4 (10.3%)	
Normal females: 26-110 nMol/l		7 (63.6%)
High: ≥110 nMol/l		1 (9.1%)
Low: <26 nMol/l		3 (27.3%)
Luteinizing hormone		
Normal males: 0-8.6 mIU/ml	27 (69.2%)	
High: ≥8.7 mIU/ml	12 (30.8%)	
Normal females: <58.5 mIU/ml		11 (100%)
Follicle stimulating hormone		
Normal males: 1.5-12.4 mIU/ml	32 (82.1%)	
High: 12.5-25 mIU/ml	5 (12.8%)	
Low: <1.5 mIU/ml	2 (5.1%)	
Normal females: 25.8-134.8 mIU/ml		6 (54.5%)
Low: 10-25.7 mIU/ml		5 (45.5%)
Thyroid stimulating hormone		
Normal: 0.27-4.2 μU/ml	30 (76.9%)	7 (63.6%)
High: >4.2 μU/ml	2 (5.1%)	1 (9.1%)
Low: <0.27 μU/ml	7 (18.0%)	3 (27.3%)
Free T4		
Normal: 8-17 ng/dl	38 (97.4%)	11 (100%)
High: >17 ng/dl	1 (2.6%)	
Cortisol		
Normal: 2.5-19.5 μg/dl	16 (40.0 %)	2 (18.2%)
High: 23-30 μg/dl	22 (56.4%)	9 (81.8%)
Low: <23 μg/dl	1 (2.6%)	

5.1.4 Cytokine and chemokine levels are increased in severely ill COVID-19 patients

Next, major pro-inflammatory cytokines and chemokines were assessed in male and female COVID-19 patient plasma to analyse the association with disease severity. Therefore, a panel of 27 cytokines and chemokines was analysed. The patients were subdivided in groups according to their Sequential Organ Failure Assessment Score (SOFA scores). In male COVID-19 patients IFN- γ , IL-1RA, IL-6, MCP-1 and MIP-1 α levels were significantly increased with progressive disease severity (Figure 11a-e). IL-10 levels were elevated by trend in male patients with higher SOFA scores, whereas in patients with lower SOFA score IL-12 was elevated by trend (Supplemental Figure 3).

In female COVID-19 patients TNF- α levels were elevated significantly in female patients with higher SOFA scores (Figure 11f). IFN- γ , IL-1RA and IL-6 levels were also elevated by trend with progressive disease severity (Figure 11g, Supplemental Figure 3), whereas MCP-1, MIP-1 α , IL-10 and IL-12 were comparable among female patients (Supplemental Figure 3).

Taken together, these data demonstrate that in COVID-19 patients pro-inflammatory cytokine and chemokine levels (IFN- γ , IL-1RA, IL-6, MCP-1, MIP-1 α) are elevated with progressive disease severity and may contribute to the excessive inflammatory response known as “cytokine storm” causing acute respiratory distress syndrome (ARDS) and multiple organ failure.

Results

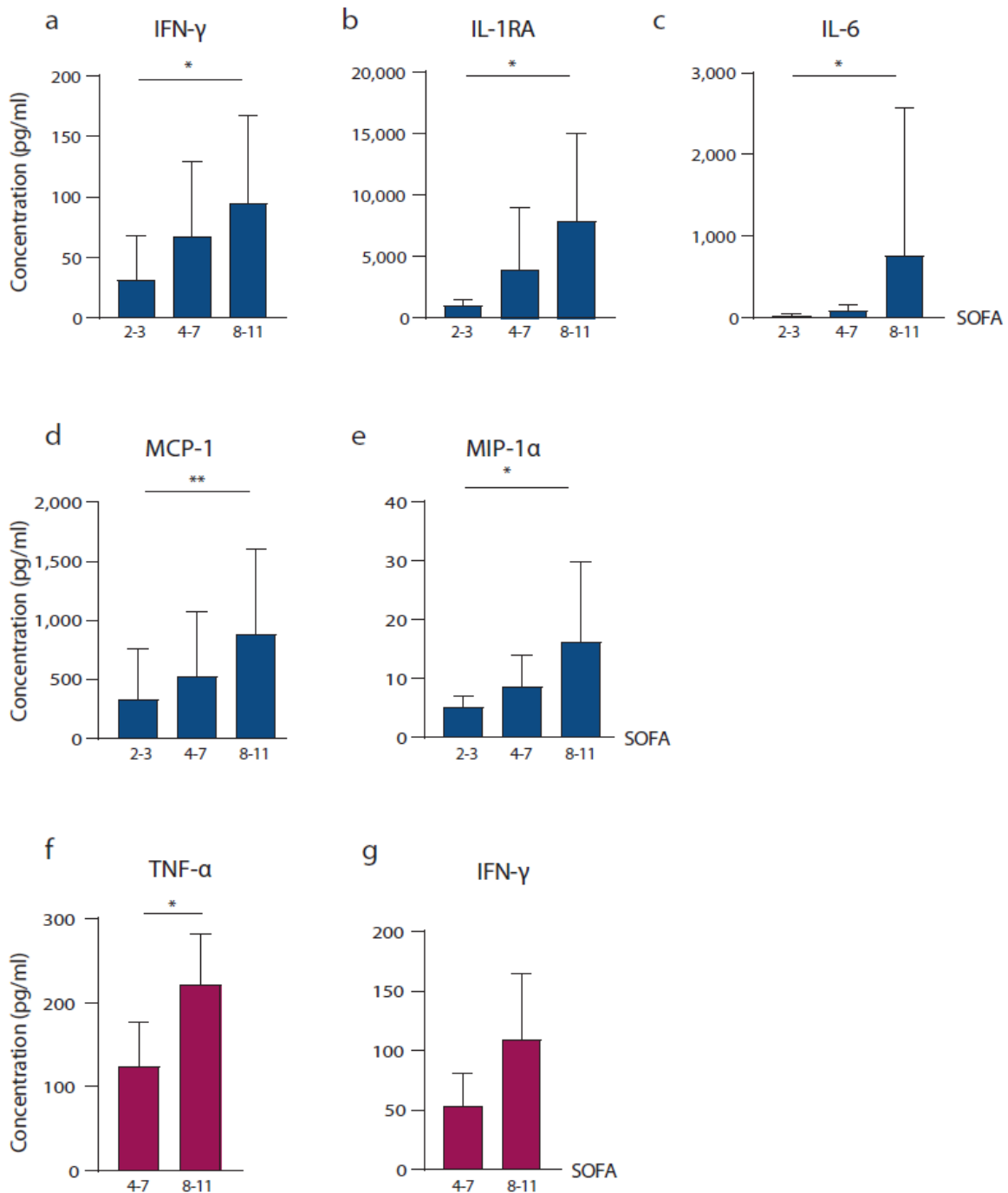


Figure 11: Chemokine and cytokine responses in male COVID-19 patients.

Shown are cytokine and chemokine levels of male COVID-19 patients in dependency of disease severity as assessed by Sequential Organ Failure Assessment Score (SOFA scores) (2-3; 4-7; 8-11). Cytokine and chemokines were measured in plasma obtained from COVID-19 patients (SOFA 2-3, $n=7$; SOFA 4-7, male: $n=15$, female: $n=6$; SOFA 8-11, male: $n=16$, female: $n=4$) by using a 27-plex immunoassay. Blue bar graphs represent male and pink bar graphs represent female COVID-19 patients. Here, those with significant differences are shown: IFN- γ (a,g), IL-1RA (b), IL-6 (c), MCP-1 (d), MIP-1 α (e) and TNF- α (f). Values are shown as mean. Statistical significance in males was assessed by non-parametric tests (Kruskal-Wallis test and Dunn's test for multiple comparisons). Statistical significance was defined as $P < 0.05$ (* $P < 0.05$, ** $P < 0.01$).

5.1.5 IFN- γ levels correlate with estradiol levels in COVID-19 patients

We could observe significant androgen depletion in male patients as well as increased estrogen levels in both male and female COVID-19 patients. To assess whether the hormone levels of COVID-19 patients correlate with pro-inflammatory immune responses, we plotted hormone levels of the two major sex hormones testosterone and estradiol and 27 assessed cytokine and chemokine levels of male and female COVID-19 patients. Of all 27 assessed cytokine and chemokines, only IFN- γ showed a significant correlation with estradiol in both male and female patients, suggesting that COVID-19 patients with high estradiol levels presented enhanced IFN- γ levels (Figure 12a). In contrast, no correlation of IFN- γ levels with testosterone could be observed (Figure 12b) in male or female patients.

IFN- γ has been previously reported to be associated with mortality in COVID-19 patients²⁵⁰ and is proposed to be a key driver for the abundant inflammatory macrophage phenotype in severe COVID-19²⁵¹. Our findings hereby confirm elevated IFN- γ expression as a risk factor in COVID-19 patients, that is promoted by estradiol²⁵².

Results

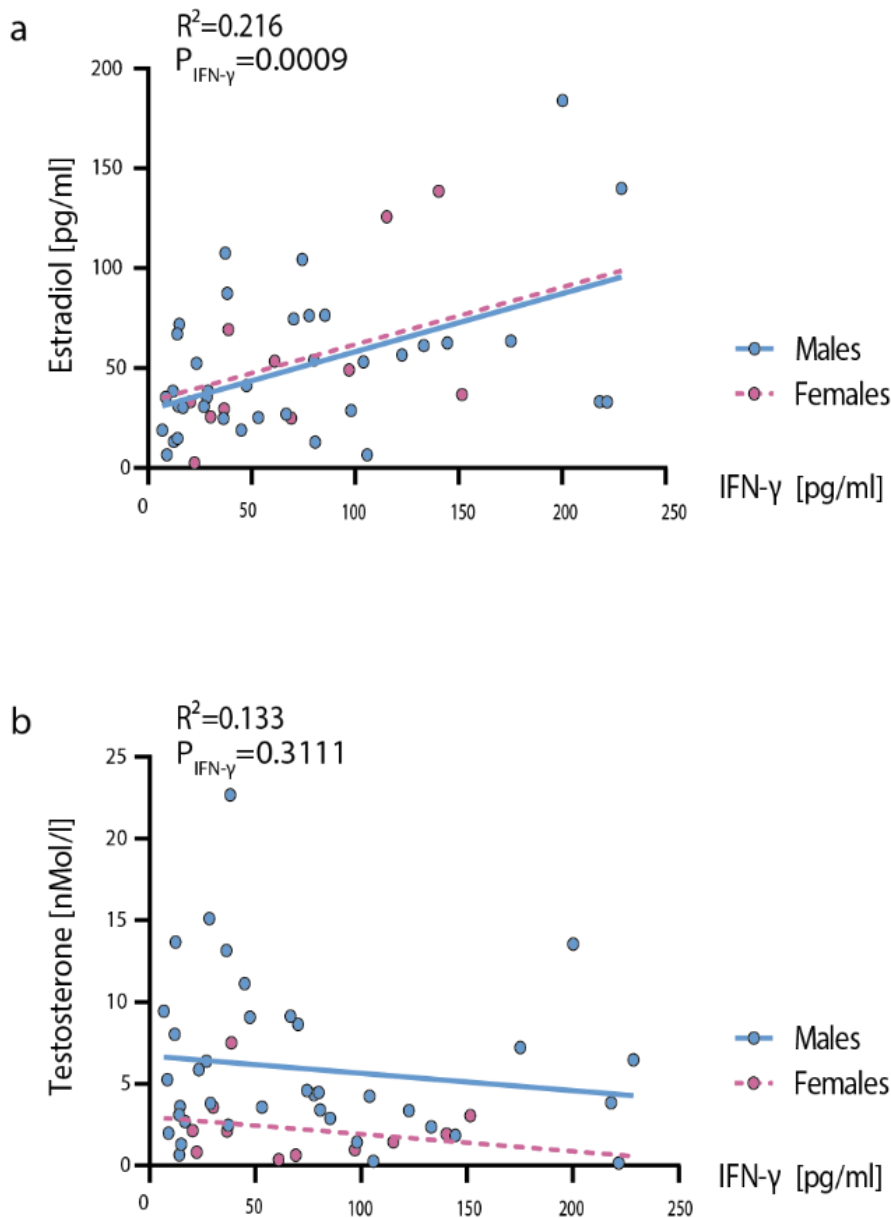


Figure 12: Correlation analysis of plasma IFN- γ levels to testosterone and estradiol levels of COVID-19 patients.

Estradiol (a) and testosterone (b) levels as well as cytokine and chemokine levels obtained from male (n=39; blue dots) and female (n=11; pink dots) patients were plotted and fit by linear regression. A correlation analysis was conducted to compute R-squared value (R^2) and level of significance (P). Shown is IFN- γ as the only cytokine among the 27 assessed cytokines and chemokines correlating significantly with estradiol levels.

5.1.6 Estradiol levels are associated with disease severity in COVID-19 patients

As we could observe a correlation of estradiol with pro-inflammatory cytokines known to be a risk factor for severe COVID-19, we further assessed if we could associate the sex hormone levels with disease severity. Therefore, we subdivided the COVID-19 patients into three groups according to the assessed SOFA scores (2-3, 3-7 and 8-11) and into patients that required ECMO as well patients that did not require ECMO during their hospital stay. As a control, critically ill male non-COVID-19 patients were also subdivided into three groups according to the assessed SOFA scores (1-3, 3-7 and 8-11), accordingly. Female COVID-19 patients were only divided into two groups according to their SOFA scores (4-7, 8-11) as only one female patient required connection to an ECMO not allowing statistical analyzes. Furthermore, critically-ill non-COVID-19 female patients could not be subdivided according to assessed SOFA scores, due to small patient numbers. We could observe significantly enhanced estradiol levels in male COVID-19 patients with a SOFA score of 8-11 compared to lower SOFA scores (Figure 13a), in contrast to male non-COVID-19 patients (Figure 13b). In addition, we could also observe significant higher estradiol levels in male COVID-19 patients requiring ECMO compared to male COVID-19 patients not requiring ECMO (Figure 13d). In female COVID-19 patients estradiol levels were elevated by trend in patients with a SOFA score of 8-11 compared to patients with a SOFA score of 4-7 (Figure 13c), albeit not statistically significant, most likely due to the small sample size. In contrast, no significant differences in testosterone levels according to disease severity could be observed in neither male nor female COVID-19 patients (Supplemental Figure 3).

To sum it up, we could observe an association of high estradiol levels in dependency of disease severity in COVID-19 patients.

Results

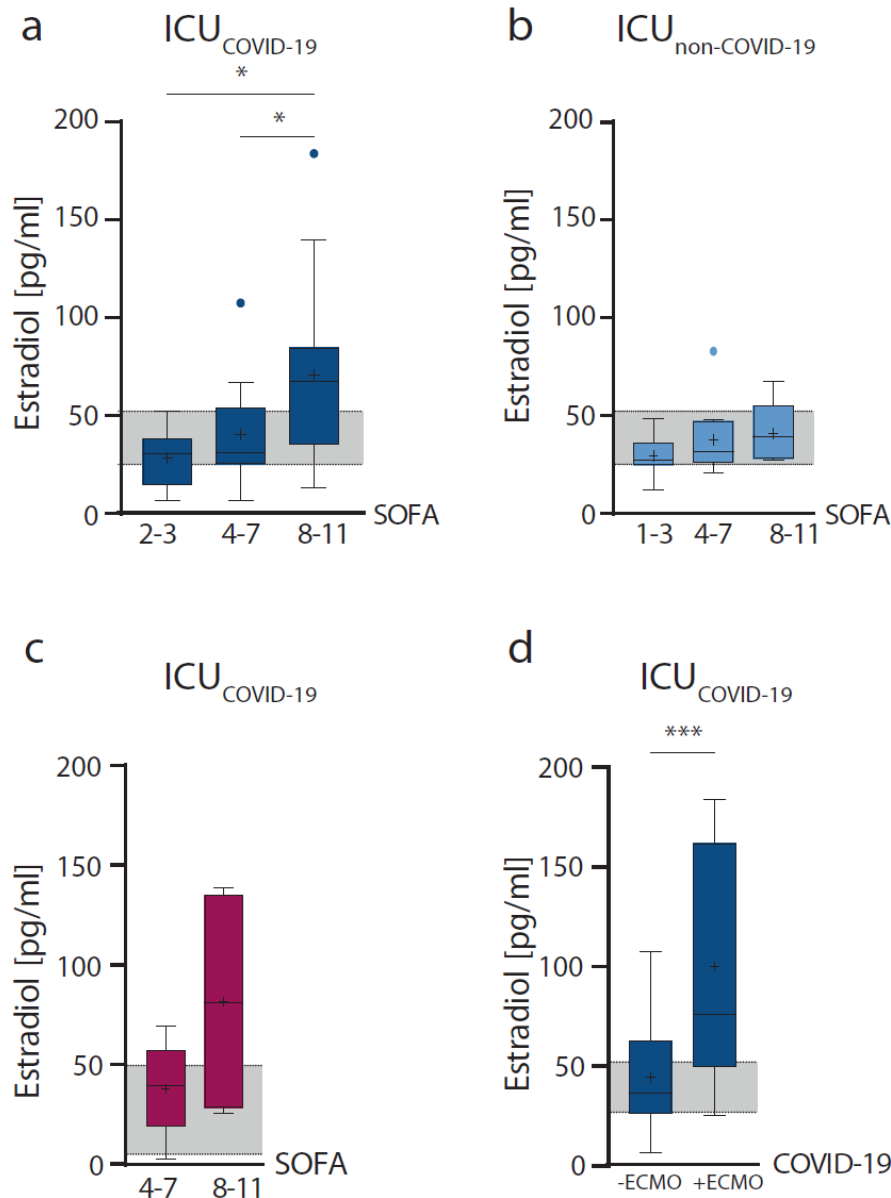


Figure 13: Analyses of sex hormone levels in male and female COVID-19 patients in dependency of disease severity.

Estradiol levels were obtained from critically-ill male (a,b,d) and female (c) COVID-19 or non COVID-19 patients and analyzed in dependency of disease severity. The illness severity was defined by subdividing the patients according to the reported SOFA scores (2-3; 4-7; 8-11) or by COVID-19 patients requiring connection to an ECMO (+ECMO) and patients not being placed on ECMO (-ECMO). Blue graphs represent males (SOFA 2-3, $n=7$; SOFA 4-7, $n=15$; SOFA 8-11, $n=16$; -ECMO, $n=34$; +EMCO, $n=5$) and pink graphs represent females (SOFA 4-7, $n=6$; SOFA 8-11, $n=4$). Percentile boxplots represent 25-75% of values, with the median value indicated by a crossline, and mean values by a plus icon. The laboratory assessed hormone reference ranges are indicated in grey. Statistical significance in males was assessed by non-parametric tests (Kruskal-Wallis test and Dunn's test for multiple comparisons). Statistical significance in females was evaluated by unpaired, two-tailed non-parametric Student's t-test (Mann-Whitney test). Statistical significance was defined as $P < 0.05$ (* $P < 0.05$, *** $P < 0.001$).

Results

All in all, we could observe a strong sex bias in the disease outcome of COVID-19 patients as the mortality in male patients was higher than in female patients. Measuring the sex hormone levels in male COVID-19 patients severe androgen (testosterone and dihydrotestosterone) deficiency and elevated estrogen (estradiol and estrone) levels could be observed, which were not due to primary hypogonadism in the majority of patients. Male COVID-19 patients with a more severe disease course presented higher estradiol and pro-inflammatory cytokine levels. Furthermore, high estradiol levels could be correlated with higher IFN- γ response, which is a hallmark of severe COVID-19 outcome. It is known that immune cells present ER- and AR-receptors on their surface. IFN- γ is suggested to be an activator for the inflammatory macrophage phenotype. We hypothesize that upon COVID-19 infection in males, the sex hormone production is dysregulated. The hereby increase in estradiol levels leads to estrogen primed activated macrophages²²⁵ that produce an enhanced amount of inflammatory cytokines. The excessive inflammation contributes to the activation of endothelial cells (Figure 14).

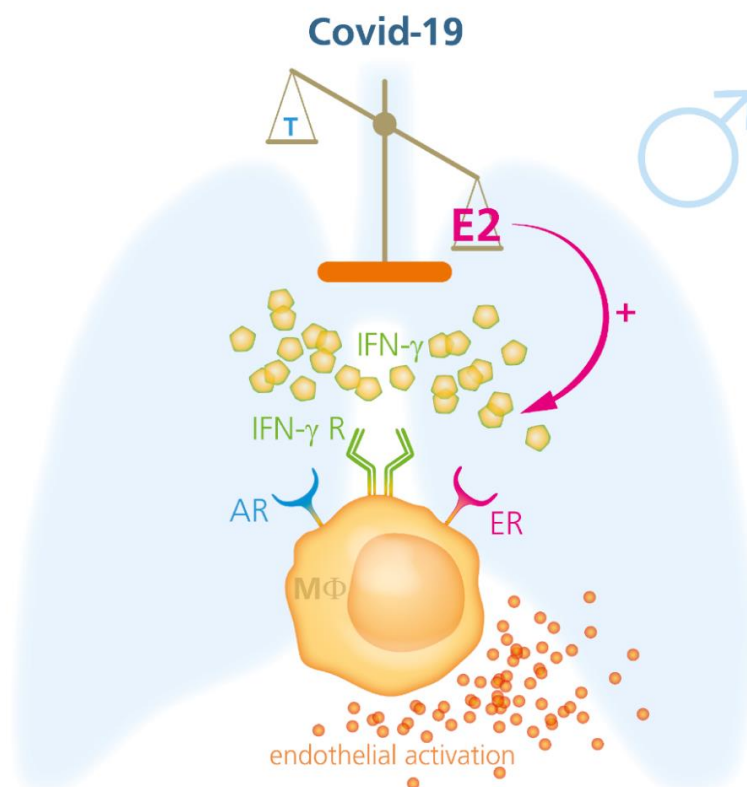


Figure 14: A schematic of the hypothesized model of estradiol activated macrophages in male COVID-19 patients.

5.2 SARS-CoV-2 infection mediates dysregulation of sex hormones in the Syrian golden hamster model

5.2.1 SARS-CoV-2 infection induces weight loss and a systemic infection in Syrian golden hamsters

We wanted to assess whether we could translate our findings in COVID-19 patients into an animal model to further investigate the molecular mechanisms causing the hormonal dysregulation in humans. Therefore, we isolated a SARS-CoV-2 isolate from a PCR-positive male ICU patient and generated a virus stock for our Syrian golden hamster infection model.

Syrian golden hamster have been previously described as a small animal model for SARS-CoV-2 infection^{253,254}. Therefore, we infected 8-10 weeks old male and female golden hamsters with SARS-CoV-2 and monitored the weight loss for 14 days. Both male and female golden hamsters infected with SARS-CoV-2 underwent a significant weight loss peaking at 6 days post infection (d p.i.) compared to PBS and poly(I:C) treated animals (Figure 15a,b). In contrast to our mouse model infected with pH1N1 (Supplemental Figure 4), no lethality in either male or female hamsters was observed. In addition, by calculating the area under the curve there were no differences in weight loss comparing male and female hamster (Figure 15c).

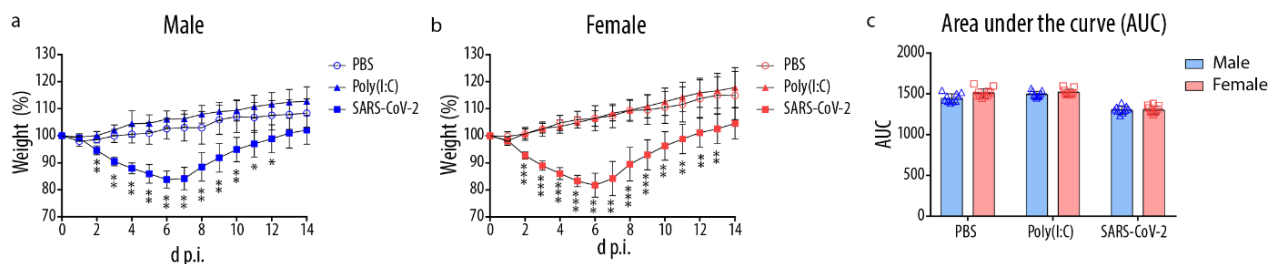


Figure 15: Weight loss of SARS-CoV-2 infected male and female golden hamsters.

Male (a) and female (b) golden hamsters were infected with SARS-CoV-2 (10^5 p.f.u./ml). Weight loss of PBS (n=10), Poly(I:C) (n=9) and SARS-CoV-2- (male, n=9; female, n=10) infected animals was monitored for 14 days and area under the curve (AUC) was calculated. Statistical significance was assessed by Kruskal-Wallis one-way ANOVA. Statistical significance was defined as $P < 0.05$ (* $P < 0.05$, ** $P < 0.01$, *** $P < 0.001$).

Viral replication titers in the lungs and plasma of SARS-CoV-2 infected hamsters were determined (Figure 16a,b) at 3d p.i.. The virus replicated to high titers in the lung and could also be detected in the plasma of four male and three female hamsters implicating a systemic infection. At 6d p.i. virus titers in the lung of male and female hamsters decreased and were

Results

only detectable in 3 male and 2 female hamsters (Supplemental Figure 5). In addition, no virus replication could be detected in the plasma at 6d p.i.. Virus replication did not differ between male and female hamsters in the lungs on day 3 or 6d p.i. or in the plasma on 3d p.i..

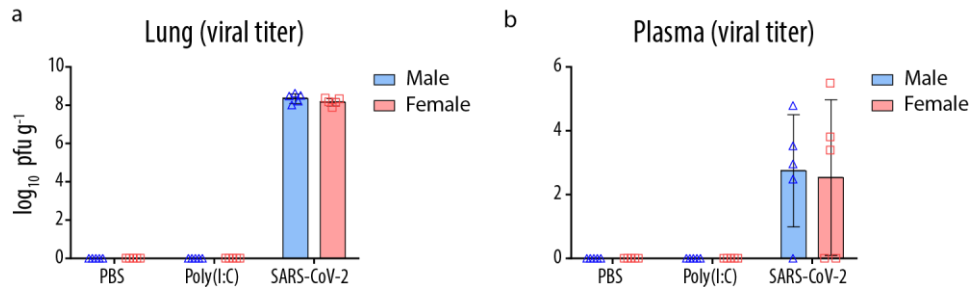


Figure 16: Viral lung and plasma titres of SARS-CoV-2 infected male and female golden hamsters.

Lungs (a) and plasma (b) of SARS-CoV-2 infected male (n=5) and female (n=5) hamsters were harvested at 3d p.i. Viral titers were determined by plaque assay. The individual logarithmic virus titers of each lung and their means are shown.

As we could detect viral replication in the plasma, suggesting a systemic infection at 3d p.i., we also analyzed the reproductive organs (Figure 17). We could observe viral RNA in the testis of infected male hamsters in 3 out of 5 animals and active viral replication in 1 out of 5 infected hamsters. In addition, in infected female hamsters, SARS-CoV-2 RNA could be detected in ovaries of 2 out of 5 animals and in the uterus of 3 out of 5 animals. The virus replicated in the ovaries in 4 out of 5 animals and in the uterus of 2 out of 5 female animals.

Results

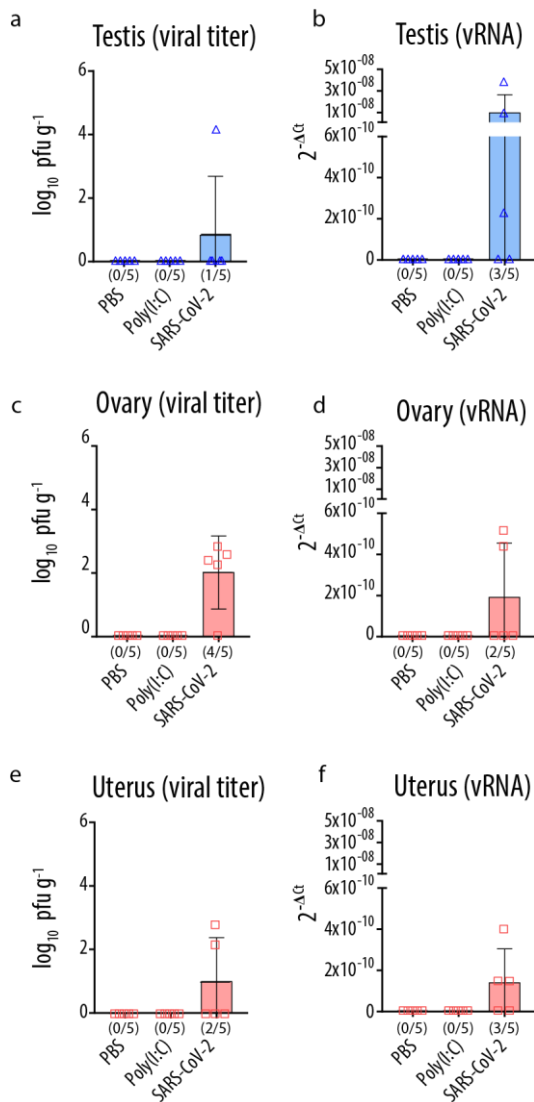


Figure 17: Viral titers and viral RNA levels of SARS-CoV-2 in the reproductive organs of infected male and female golden hamsters.

Testis (a,b), ovaries (c,d) and uterus (e,f) of SARS-CoV-2 infected male (n=5) and female (n=5) hamsters were harvested 3d p.i. Viral titers were determined by plaque assay and viral RNA levels were determined via qPCR. Values are shown as means and error bars were shown as SD.

To sum it up, we could establish an infection model of SARS-CoV-2 in golden hamsters. The virus replicated to high titers in both male and female hamsters causing a systemic infection at 3d p.i.. No differences in weight loss or viral titers of male and female hamsters could be observed.

5.2.2 SARS-CoV-2 infected hamsters present elevated cytokine and chemokine levels

We could observe efficient SARS-CoV-2 replication in the lungs of infected hamsters and wanted to further assess the cytokine and chemokine profiles. Therefore, we analyzed a panel of 13 pro-inflammatory cytokines and chemokines in the lungs of infected hamsters at 1 and 3d p.i.. We could not observe enhanced cytokine or chemokine levels in SARS-CoV-2 infected hamsters 1d p.i. (Supplemental Figure 6). On 3d p.i. several pro-inflammatory cytokines, such as IL-6, IL-1ra, Eotaxin and MIP-1 α were significantly increased in the lungs of male and female infected hamsters compared to hamsters treated with PBS or poly(I:C) (Figure 18a-e). In contrast, VEGF levels were decreased in SARS-CoV-2 infected hamsters compared to uninfected hamsters and IL-10 and IL-12 levels were also decreased in infected female hamsters compared to PBS or poly(I:C) treated female hamsters (Figure 18g-i). Other cytokine and chemokines expression levels, such as IFN- γ , IL-1 β , IL-2, IL-13, MIP-1 β , MCP-1 and TNF- α were not significantly altered in SARS-CoV-2 infected hamsters (Figure 18f,j-o). Interestingly, although IFN- γ levels were not significantly elevated in infected hamsters compared to uninfected hamsters, female infected hamsters presented higher IFN- γ levels compared to infected male hamsters. We also analyzed cytokine and chemokine levels in the plasma 3d p.i. as we could also observe viral replication. However, the majority of proinflammatory cytokine and chemokines were not altered significantly in the plasma of infected male or female hamsters compared to the PBS and poly(I:C) treated hamsters (Supplemental Figure 7).

All in all, SARS-CoV-2 infected hamsters present a similar cytokine profile compared to critically ill COVID-19 patients. Elevated MIP-1 α and MIP-1 β indicate an activation of inflammatory macrophages in the lungs of SARS-CoV-2 infected hamsters.

Results

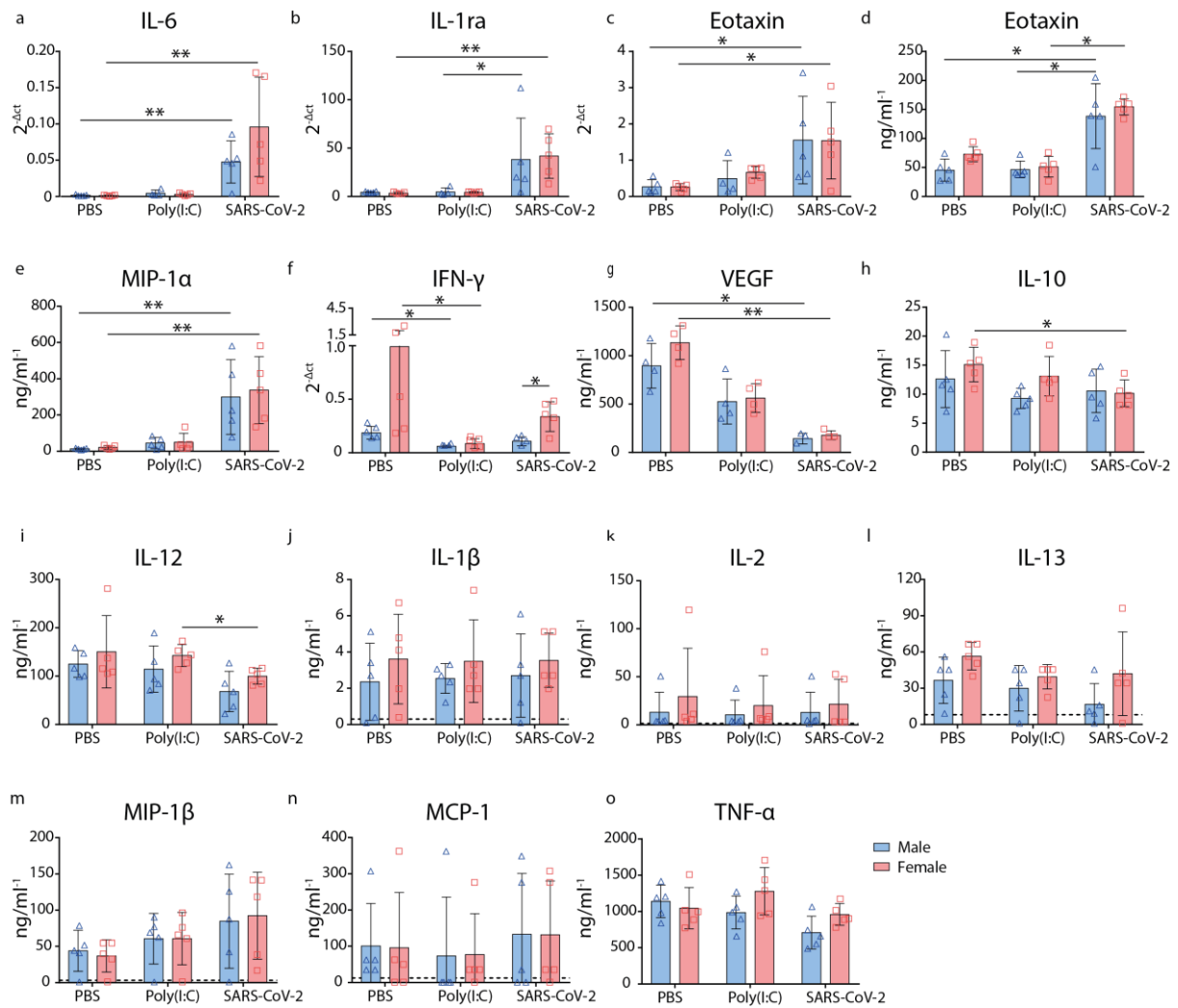


Figure 18: Chemokine and cytokine responses in male and female Syrian golden hamsters infected with SARS-CoV-2.

Shown are cytokine and chemokine levels of male and female golden hamsters infected with SARS-CoV-2. Cytokine and chemokine mRNA levels were analyzed and cytokine and chemokines protein levels were measured in lung homogenates obtained from infected hamsters 3d p.i.. Here: IL-6- (a), IL-1RA- (b), Eotaxin- (c), IFN- γ - (f) mRNA levels and Eotaxin (d), MIP-1 α (e), VEGF (g), IL-10 (h), IL-12 (i), IL-1 β (j), IL-2 (k), IL-13 (l), MIP-1 β (m), MCP-1 (n) and TNF- α (o) protein levels are shown. Statistical significance was evaluated by Kruskal-Wallis one-way ANOVA and by unpaired, two-tailed non-parametric Student's *t*-test. Detection limits are indicated by dotted lines. Statistical significance was defined as $P < 0.05$ (* $P < 0.05$, ** $P < 0.01$). Values are shown as median and interquartile range.

5.2.3 SARS-CoV-2 infection leads to hormone dysregulation in male and female hamsters

Critical ill male COVID-19 patients presented low testosterone levels and male and female patients also had elevated estradiol levels. Next, we wanted to analyze hormone levels in the plasma of SARS-CoV-2 infected hamsters to assess whether the dysregulation in hormone levels is due to the virus infection.

Therefore, we collected plasma on day 1, 3, 6 and 14 post infection and analyzed the plasma hormone levels. Plasma testosterone levels of male infected hamsters were significantly reduced 3d p.i. compared to PBS and poly(I:C) treated male hamsters and recovered completely at 14d p.i. (Figure 19a). Testosterone levels in all female hamsters remained on a low level during the course of infection (Figure 19b). In contrast to the testosterone levels, estradiol levels in male infected hamsters were significantly elevated at 3d p.i. compared to uninfected male hamsters and decreased to comparable levels again on 14d p.i. (Figure 19c). On the other hand, in female infected hamsters estradiol levels were below the estradiol levels of PBS and poly(I:C) treated female hamsters at 3d p.i. (Figure 19d).

Furthermore, cortisol levels were increased in both female and male infected hamsters, most likely due to stress caused by the infection (Figure 19e,f). Interestingly, progesterone levels were also increased in both male and female infected hamsters at 3d p.i. (Figure 19g,h).

To further assess, whether the testosterone deficiency and estradiol increase in infected male hamsters is SARS-CoV-2 specific or is caused by other respiratory viruses, we analyzed testosterone and estradiol levels in mice infected with influenza (2009 pH1N1). Similar to the SARS-CoV-2 infected male hamsters, 2009 pH1N1 infected male mice showed decreased testosterone levels 3d p.i. (Supplemental Figure 1). compared to PBS treated male mice. In contrast, estradiol levels did not change 3d p.i. in pH1N1 infected male mice (Supplemental Figure 8).

Altogether, we could observe a testosterone deficiency and high estradiol levels in SARS-CoV-2 infected male hamsters 3d p.i.. In contrast, female SARS-CoV-2 infected hamsters presented decreased estradiol levels after infection, which could be due to their pre-menopausal state.

Results

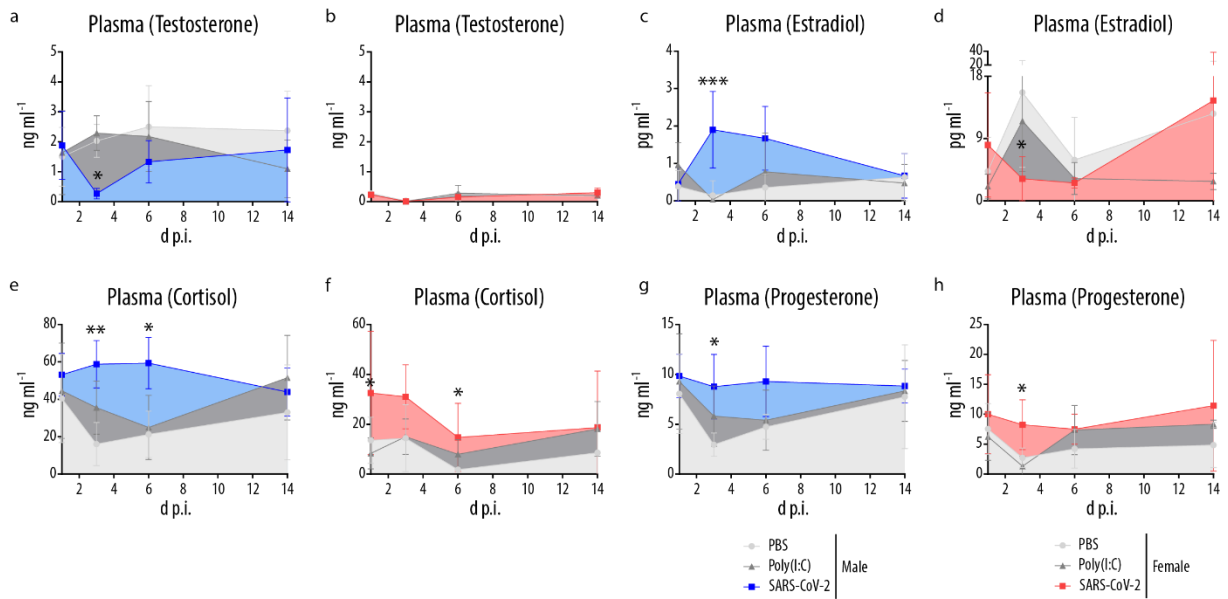


Figure 19: Hormone levels in male and female Syrian golden hamsters infected with SARS-CoV-2.

Shown are hormone levels of male and female golden hamsters infected with SARS-CoV-2. Plasma was obtained from infected hamsters 1, 3, 6 and 14d p.i. and hormone levels were measured. Here testosterone (a,b), estradiol (c,d), cortisol (e,f) and progesterone (g,h) levels are shown. Values are shown as means and error bars are shown as SDs. Statistical significance was evaluated by Kruskal-Wallis one-way ANOVA. Statistical significance was defined as $P < 0.05$ (* $P < 0.05$, *** $P < 0.001$).

5.2.4 SARS-CoV infected hamsters present elevated aromatase mRNA levels in the lungs

Depleted testosterone levels and increased estradiol levels in male hamsters indicate a dysregulation of the testosterone-to-estradiol converting key enzyme of estrogen production aromatase (CYP19A1). The predicted transcription factor binding sites in the promotor regions of the CYP19A1 gene include estrogen, progesterone and testosterone receptor binding sites as well as binding sites for transcription factors that are involved in immunity (Figure 24). The promoters are tissue-selective and regulated by distinct signaling pathways to control aromatase expression.

As we observed enhanced pro-inflammatory cytokine and chemokine levels in the lungs, we measured aromatase CYP19A1 mRNA expression levels on day 1, 3 and 6d p.i. (Figure 20a-c). On day 1p.i. aromatase CYP19A1 levels are comparable between infected hamsters and control groups. In contrast, on day 3p.i. aromatase CYP19A1 mRNA levels are significantly elevated in infected male and female lungs compared to PBS and poly(I:C) treated hamsters. On day 6 p.i. aromatase CYP19A1 levels are elevated by trend in infected male hamsters.

Testosterone is converted to dihydrotestosterone by the enzyme 5- α reductase. 5- α reductase mRNA levels were analyzed in the lungs at 3d p.i. to examine further downstream pathways. However, 5- α reductase expression levels were not altered in infected hamsters compared to control treated hamsters (Figure 20d).

The aromatase is expressed in various tissues. For reproductivity, the expression of the aromatase in the gonads is important. We measured aromatase CYP19A1 mRNA expression levels in testis and ovaries (Figure 20e,f), but could not observe any alteration in expression levels.

Endothelial activation could be observed in COVID-19 patients, which is known to be promoted by inflammatory conditions enhanced by estradiol. At 3 and 6d p.i. endothelial lipase levels were enhanced in infected male hamsters compared to PBS and poly(I:C) control groups (Figure 20g,h) simultaneously to the observed elevated estradiol levels.

The hormonal imbalance in male hamsters could be associated with increased aromatase expression levels in the lungs, which is the main replication site for SARS-CoV-2. Consequently, the pro-inflammatory cytokine and chemokine production is enhanced in the

Results

lungs, which could be further induced by enhanced aromatase expression and production of estradiol.

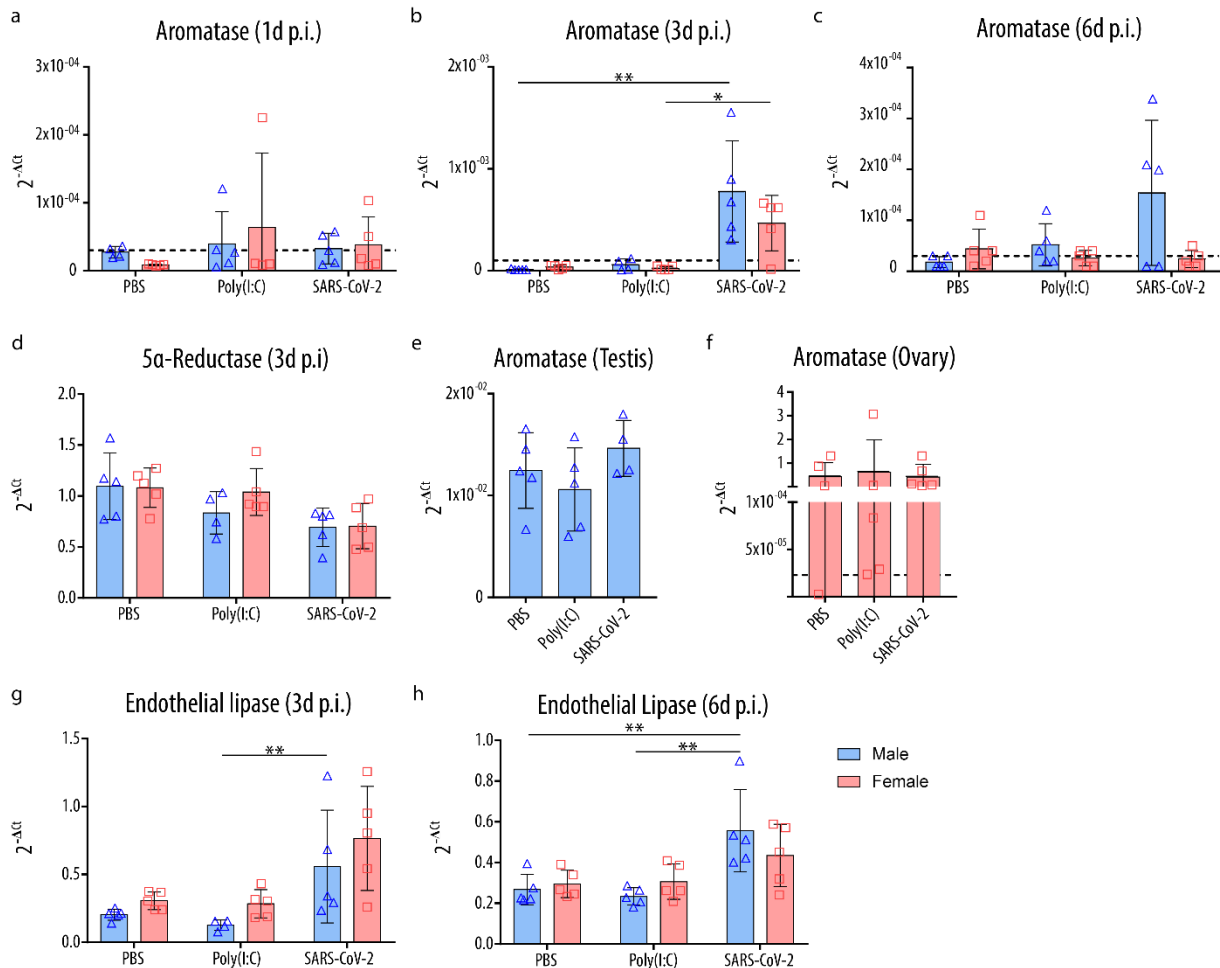


Figure 20: Aromatase expression levels and endothelial activation in male and female Syrian golden hamsters infected with SARS-CoV-2.

Aromatase mRNA expression levels were measured in lung homogenates on 1 (a), 3 (b) and 6 (c) p.i. ($n=5$; Poly(I:C), $n=4$). 5- α reductase mRNA expression levels in the lung were measured on 3 d p.i. (d) ($n=5$; Poly(I:C), $n=4$). Aromatase expression levels in testis (e) and ovaries (f) and endothelial lipase levels were measured on 3d p.i. (g) ($n=5$; male SARS-CoV-2 infected, $n=4$) and on 6d p.i. (h) ($n=5$). Values are shown as means and error bars are shown as SD. Statistical significance was evaluated by Kruskal-Wallis one way ANOVA. Statistical significance was defined as $P < 0.05$ (* $P < 0.05$, ** $P < 0.01$).

5.2.5 SARS-CoV-2 infected male golden hamsters present abundantly high aromatase protein expression levels in perivascular and peribronchiolar infiltrates

As we could observe enhanced aromatase mRNA expression levels in the lungs of infected male hamsters, we wanted to further identify the cell types expressing the aromatase CYP19A1 in the lungs.

Serial lung sections revealed aromatase CYP19A1 expression in endothelial cells, bronchiolar epithelium, the endothelium as well as in the peribronchiolar and perivascular connective tissue in SARS-CoV-2 infected male hamsters as well in the PBS and poly(I:C) treated control groups. In contrast, aromatase CYP19A1 expression in the peribronchiolar epithelium was only present in poly(I:C) and SARS-CoV-2 infected hamsters (Figure 21).

In addition, infiltrations of moderate amounts of macrophages and low amounts of T-lymphocytes could be detected, which was higher in infected hamsters, especially male animal tissue compared to uninfected controls.

All in all, enhanced aromatase CYP19A1 mRNA expression levels in endothelial cells and macrophages of infected hamsters could be confirmed with histological examinations and showed higher amounts in infected male hamsters compared to female hamsters.

Results

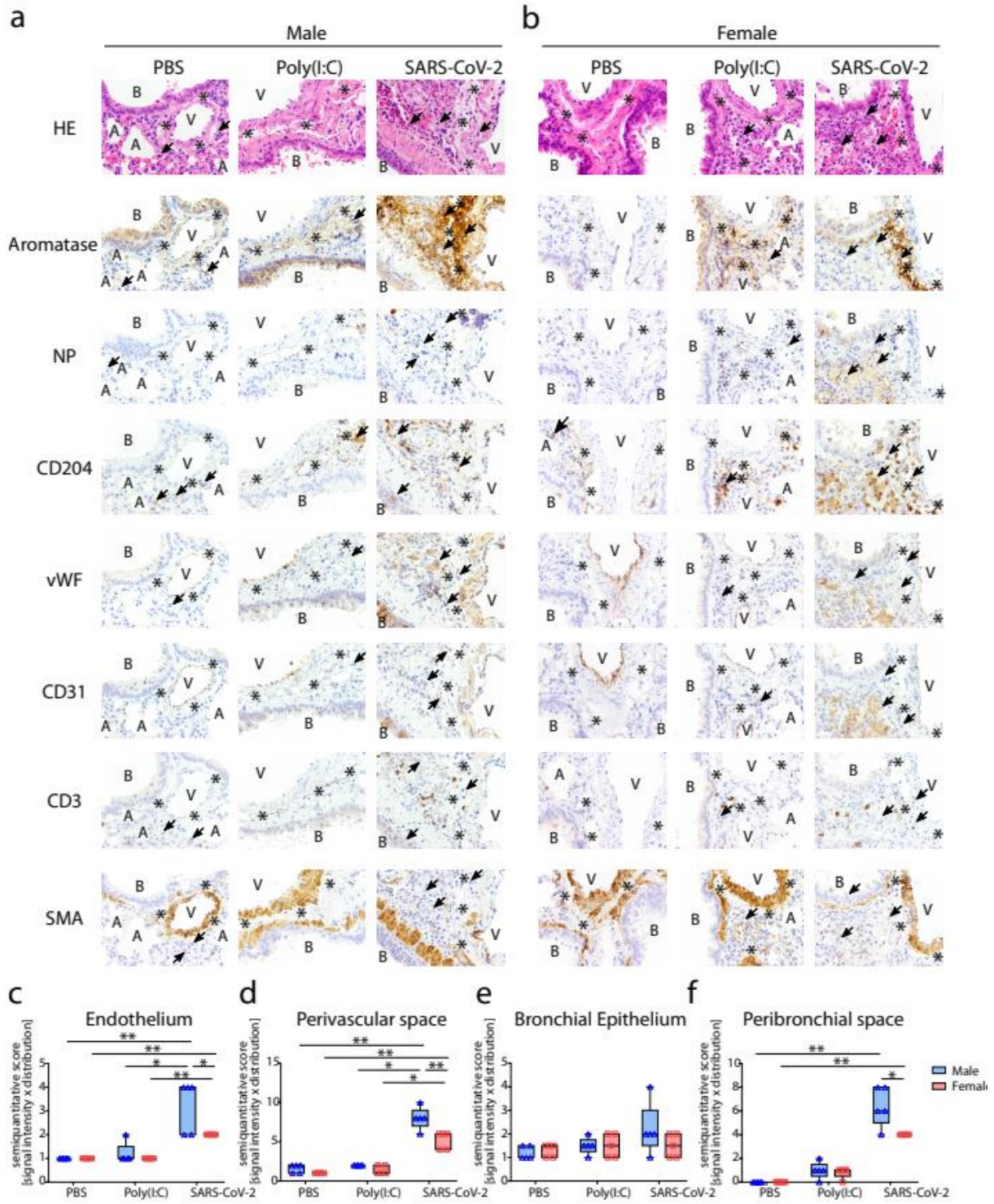


Figure 21: Aromatase expression levels in the lungs of male and female Syrian golden hamsters infected with SARS-CoV-2.

Serial lung sections of male (a) and female (b) hamsters were stained against SARS-CoV-2 NP, macrophages (CD204), endothelial cells (vWF; CD31), T cells (CD3) and smooth muscle (SMA). Representative pictures are shown (c.f). Stars indicate perivascular connective tissue and arrowheads indicate macrophages (bronchus (B), vessel (V), alveola (A)). Aromatase CYP19A1 immunoreactivity was examined and scored semi quantitatively at 3d p.i. ($n=5$) in the endothelium (c), the bronchiolar epithelium (d), the perivascular (e) and peribronchiolar region. Statistical significance was evaluated by Kruskal-Wallis one way ANOVA and Student's t -test. Statistical significance was defined as $P < 0.05$ (* $P < 0.05$, ** $P < 0.01$).

6 Discussion and outlook

6.1 Sex differences in SARS-CoV-2 pathology

Male sex has been identified as risk factor for severe COVID-19 in multiple datasets worldwide with only a few exceptions. While there is no difference in infection rates, male COVID-19 patients are more likely to require intensive care and present higher mortality rates²⁵⁵. The male sex bias could be identified in previous coronavirus outbreaks, such as during the SARS-CoV epidemic²³⁷ and the MERS-CoV outbreak in Saudi Arabia²³⁸.

The male sex bias was confirmed in our human COVID-19 cohort, as the admission to the intensive care unit as well as the mortality was higher in male patients compared to female patients.

In general, differences between male and female COVID-19 disease outcome could be explained by environmental and biological factors. For example, women have a lower prevalence of smoking and cardiovascular diseases, which are risk factors for a worse disease outcome.

To exclude environmental factors, we analysed sex differences in a SARS-CoV-2 golden hamster infection model. We could not observe differences in weight loss in our hamster model between both sexes. In addition, no mortality was observed in SARS-CoV-2 infected hamsters. However, the hamsters were young and without any known comorbidities compared to the COVID-19 patients. The majority of the COVID-19 patients at the intensive care unit represented at least one comorbidity, including obesity and cardiovascular diseases. In addition, studies have shown that the largest sex differences in COVID-19 outcome were found at ages 60-69²⁵⁶. Thus, mortality and sex-specific differences in disease outcome may be expected in hamsters at higher age or with comorbidities infected with SARS-CoV-2.

6.2 The role of testosterone in SARS-CoV-2 infection

It has been demonstrated that male COVID-19 patients are more likely to require intensive care and have higher mortality rates compared to female patients. These observed sex differences may be attributed to sex hormones.

At the beginning of the pandemic it was proposed, that androgens drive the SARS-CoV-2 infection²⁵⁷. Androgen receptor activity is considered to be required for increased transcription of the TMPRSS2 gene, as several androgen receptor elements are located upstream of the transcription start site (Figure 22a)²⁵⁸. Furthermore, there is no other TMPRSS2 gene promotor reported in humans²⁵⁹. TMPRSS2 is important for viral spread and pathogenesis²³, which was thereby hypothesised to be amplified by high testosterone levels and thereby increase the susceptibility to COVID-19 in men. However, studies have shown that there are no differences of TMPRSS2 mRNA expression between men and women²⁶⁰ suggesting, that low levels of testosterone are efficient for TMPRSS2 expression. Interestingly, patients with prostate cancer receiving androgen deprivation therapy had a significantly lower risk of SARS-CoV-2 infection compared to patients, who did not receive androgen deprivation therapy²⁶¹. Nevertheless, it has to be taken into account, that cancer patients have a higher risk of severe COVID-19 outcome.

In addition, androgen receptor and ACE-2 genes are localized on chromosome X (Figure 22b). Inherited genetic polymorphisms, were hypothesized to increase ACE-2 expression, which may enhance male vulnerability towards COVID-19¹³². On the other hand, other studies did not find significant sex differences of ACE-2 expression in human lungs²⁶².

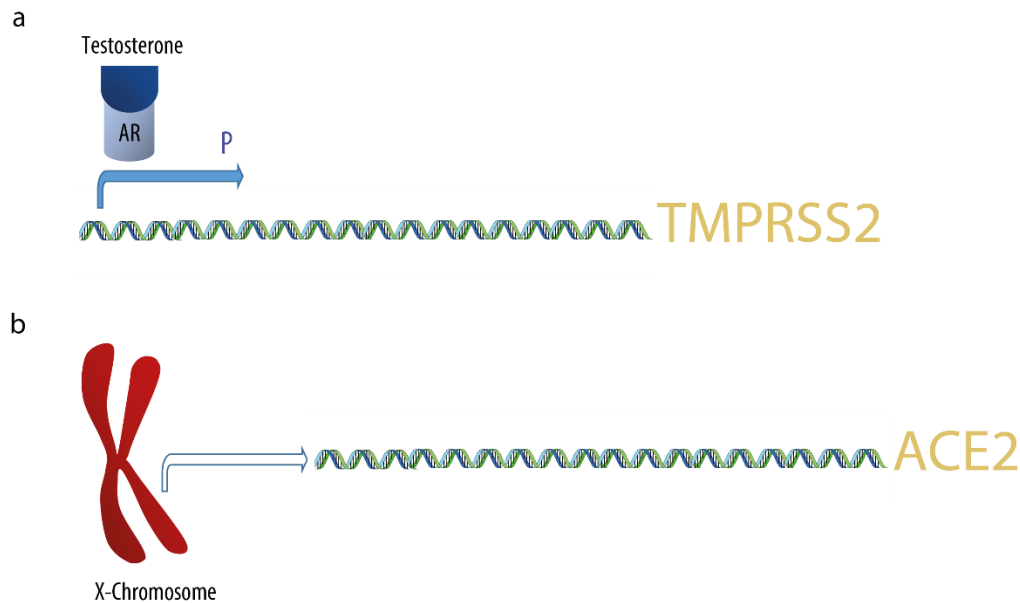


Figure 22: The role of ACE2 and TMPRSS2 in male COVID-19 susceptibility.

Several androgen receptor elements are located upstream of the transcription start site of the TMPRSS2 gene. It is hypothesized that androgen receptor activity is considered to be required for increased transcription of the TMPRSS2 gene (a). The ACE-2 gene, which is important for viral entry is located on the X-chromosome (b). Genetic polymorphisms could contribute to higher ACE-2 expression in men.

Other studies imply that men admitted with COVID-19 have significantly lower testosterone levels than with other acute hospital admissions. Low testosterone levels in male COVID-19 patients could be also detected in male ICU patients in a study from Italy²⁶³ and are hypothesized to have a correlation with increased risk of being admitted to the ICU²⁶⁴. These data combined show the urgency of screening testosterone levels in male patients to identify high risk patients²⁴⁷.

The observed sex differences could be due to differences in immune response, which is known to be influenced by steroid hormones. In our COVID-19 patient cohort the majority of patients presented comorbidities, which are known to have an impact on the hormone levels, for example coronary heart disease, diabetes or obesity.

For coronary heart disease patients, low testosterone levels are a predictor for increased mortality²⁶⁵. Testosterone levels in male COVID-19 patients were significantly lower compared to the coronary heart disease patients, suggesting that low testosterone levels were not due to

their comorbidities but also due to the infection. In addition, we could observe a decrease in testosterone levels in infected hamsters, which is further confirming that low testosterone levels in male COVID-19 patients are a consequence of SARS-CoV-2 infection and are not only a consequence of their comorbidities.

However, we could not observe an association of low testosterone levels with disease severity, likely due to the fact that the majority of patients presented extremely low testosterone levels exacerbating a differential statistical analysis. Including testosterone levels of stationary or mildly infected COVID-19 patients could provide more information on the association of testosterone levels with disease severity. For other infectious diseases, such as HIV²⁶⁶ declining testosterone levels in male patients were previously reported. In addition, in murine infection models, testosterone levels of male mice decreased after influenza²⁶⁷ and tapeworm infections²⁶⁸. Furthermore, we could observe declining testosterone levels in male mice upon 2009 pH1N1 infection.

The low testosterone levels could be explained by virus replication in Leydig cells and impair the testosterone production as we could detect replicating virus in testis of 1 out of 5 SARS-CoV-2 infected hamsters. However, the hamsters without detectable virus levels in the testis also presented low testosterone levels suggesting other pathways being involved.

Testosterone is known to have an anti-inflammatory impact²⁶⁹. The observed low testosterone levels in male COVID-19 patients could contribute to the “cytokine storm” leading to a fatal outcome.

On the other hand, testosterone levels in female COVID-19 patients were not significantly enhanced compared to control groups even though some CHD and COVID-19 patients presented elevated testosterone levels above the reference values. However, it has to be taken into consideration that the female COVID-19 patient cohort is limited. Higher levels of testosterone in postmenopausal women were shown to increase the risk for CHD²⁷⁰ and type 2 diabetes²⁷¹, which could explain the testosterone levels in our CHD patient cohort. Furthermore, obese women tend to develop a condition of functional hyperandrogenism²⁷². Therefore, all comorbidities among the postmenopausal status represented in our female COVID-19 patient cohort could contribute to elevated testosterone levels. Furthermore, SARS-CoV-2 infected young female hamsters did not show elevated testosterone levels.

6.3 The role of estradiol in SARS-CoV-2 infection

In contrast to decreased testosterone levels, we could observe significantly enhanced estrogen levels in male patients as well as in SARS-CoV-2 infected male hamsters. Estradiol is known to promote inflammation^{273,274}. In addition, estradiol was associated with severe disease outcome in male COVID-19 patients and correlated with elevated IFN- γ levels. IFN- γ is known to play an important role in innate and acquired immunity and is produced by mainly by macrophages but also by T-cells, natural killer (NK) cells and dendritic cells^{275,276}. It has been demonstrated that naturally activated macrophages isolated from bronchoalveolar lavage (BAL) produce high levels of IFN- γ ²⁷⁷.

In addition, monocytes and macrophages express all estrogen receptors, ER- α , ER- β and GPER1²⁷⁸. Treatment with estradiol in macrophages in vitro induces increased ER- α expression compared to monocytes that were treated with estradiol²⁷⁹.

There are two types of pulmonary macrophages, alveolar and interstitial macrophages, which are divided into the classical activated pro-inflammatory M1 phenotype, promoted by Th1 cells and the alternatively activated anti-inflammatory M2 phenotype, promoted by Th2 cells. Nahrendorf and Swirski proposed replacing the classical M1/M2 classification by for a network model that accommodates for macrophage function and thereby broaden the macrophage spectrum²⁸⁰. Due to the fact that the studies cited in this thesis referred to the classical nomenclature, M1 and M2 classification will be employed in the following.

The M1 macrophages are responsible for the recruitment of immune cells into the lung²⁸¹ and has been shown to be activated upon infection with influenza, herpes and Zika virus²⁸². Furthermore, upon the cytokine storm in COVID-19 patients, it has been suggested that macrophages contribute to the hyperinflammation state observed in patients with poor prognosis^{283,284}. Estradiol has been shown to promote the M1 macrophage phenotype²⁸⁵. Interestingly, IFN- γ , IL-6 and MIP-1 α levels were elevated in COVID-19 patients. IL-6 and MIP-1 α levels were also elevated in SARS-CoV-2 infected hamsters. IL-6 enhances the polarization of pro-inflammatory macrophages²⁸⁶. In addition, MIP-1 α is secreted by macrophages confirming the macrophage infiltration in COVID-19 patients²⁸⁷. This could be confirmed in our pre-clinical SARS-CoV-2 infected hamster model. Especially high IL-6/IFN- γ ratio was shown to be associated with severe disease in COVID-19 patients²⁸⁸.

On the other hand, in asthmatic patients M2-polarized alveolar macrophages correlate with impaired lung function^{289,290}. The M2 polarization however, is suggested to be regulated in a sex-dependent manner as in female asthmatic patients M2 macrophages are “estrogen-primed” and exhibit an enhanced amount of inflammatory cytokines promoting fibrosis in contrast to male asthmatic patients²²⁵. It is known that the hyper-responsive phenotype can enhance the severity of the tissue injury²⁹¹. In our study, male COVID-19 patients present very high estrogen levels resembling levels in women during their reproductive age, which could contribute to the estrogen-primed M2 macrophage phenotype. This could be confirmed in SARS-CoV-2 infected male hamsters.

Conversely to our results, it is discussed that estradiol might play a protective role in COVID-19 disease²⁹². As females have lower mortality rates than males after SARS-CoV-2 infection, higher estradiol levels were proposed to have a protective effect. In previous studies, female mice that were treated with an ER antagonist or were ovariectomized had a higher mortality rate after infection with SARS-CoV indicating a protective role for ER signalling in female mice²⁴⁶. Conversely, postmenopausal patients have lower levels of estradiol and still present lower mortality rates. Clinical trials are conducted treating COVID-19 patients with estradiol. As of this writing no results are published. However, previous treatments of patients with lung diseases such as cancer, asthma, chronic obstructive pulmonary disease and pulmonary arterial hypertension have not shown any benefits²⁹³. Moreover, estrogen has been implicated as a risk factor for pulmonary arterial hypertension patients and it has been recommended to avoid pregnancy due to extremely high estradiol levels, which could exacerbate lung pathology²⁹⁴.

On the other hand, upon influenza infection, male mice presented low testosterone levels but estradiol levels were not significantly altered, which is in line with previous findings in 2009 pH1N1 and H7N9 infected male patients²⁹⁵. Moreover, administration of estradiol in infected female mice improved the disease outcome²³³. In contrast to COVID-19, the mortality for females in their reproductive age infected with 2009 pH1N1 and H7N9 is higher than for males^{229,296}.

However, enhanced estradiol levels and its effects on the immune system in particularly males requires further research. It could be shown that elevated estradiol levels in critically injured patients regardless of sex are associated with death²⁹⁷.

We hypothesize, that enhanced estradiol levels in male and female patients contribute massive recruitment of macrophages and a cytokine storm as a consequence of excessive secretion of

pro-inflammatory cytokines leading to a severe disease outcome upon SARS-CoV-2 infection (Figure 23).

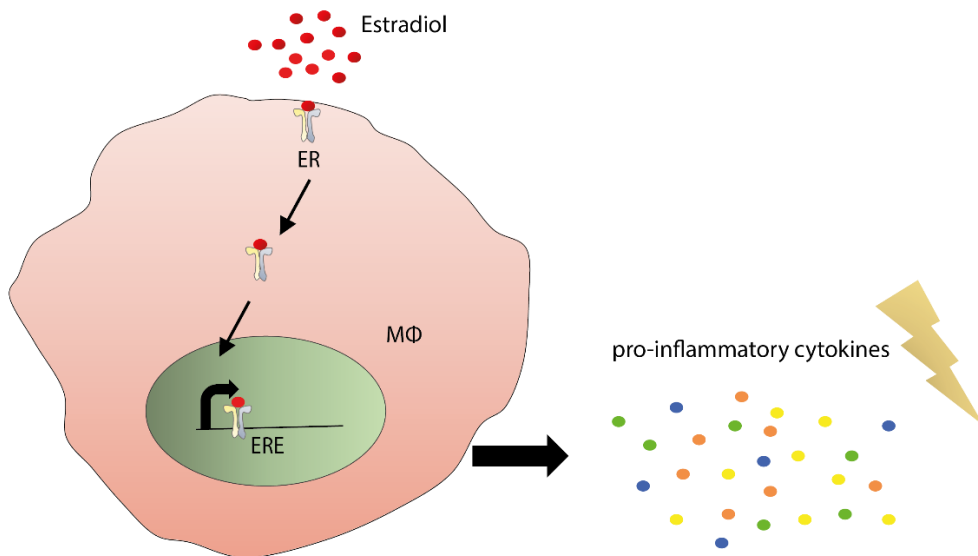


Figure 23: Estradiol promotes macrophage secretion of inflammatory cytokines.

Macrophages express estrogen receptors (ER), which bind to specific DNA sequences called estrogen response elements (ERE) with high affinity and transactivates gene expression in response to estradiol. Elevated estradiol levels in COVID-19 patients may contribute to enhanced secretion of pro-inflammatory cytokines (MIP-1 α , IFN- α , IL-6). Unbound estradiol can diffuse through the cell membrane and bind to estrogen receptors.

6.4 Aromatase CYP19A1 dysregulation upon SARS-CoV-2 infection

Enhanced estradiol levels have been observed in COVID-19 female and male patients. Male patients also presented low testosterone levels at the same time suggesting a dysregulation of the aromatase CYP19A1, which is involved in the metabolism of testosterone to estradiol. In our pre-clinical SARS-CoV-2 hamster infection model, low testosterone levels and elevated estradiol levels could also be observed in infected male hamsters.

The aromatase CYP19A1 is important for regulating the balance of estrogens and androgens²⁹⁸ and is known to be primarily expressed in ovary and testis, but also widely expressed in extraglandular sites, such as brain, lung, placenta, skin fibroblasts and adipose tissue²⁹⁹⁻³⁰¹. In men, extraglandular metabolism of androgens are the major source of estrogen³⁰².

We started measuring CYP19A1 mRNA levels in the male hamster reproductive organs as the primary location for CYP19A1 expression. Analyzing aromatase CYP19A1 mRNA levels in the testis did not reveal significant differences in infected hamsters compared to control groups. The primary replication site for SARS-CoV-2 is the respiratory tract. We could detect high viral titers in the lungs of infected hamsters 3 days post infection. As we could not detect dysregulation of CYP19A1 expression levels at the primary expression site, the testis we further analyzed expression levels in the lungs. Indeed, in the lungs of male hamsters a dysregulation of the aromatase CYP19A1 levels could be confirmed on mRNA level and upon protein level in histological examinations. Therefore, we hypothesize an association of virus replication and dysregulation of the aromatase CYP19A1 in the lung.

CYP19A1 dysregulation is mainly known in breast and endometrial carcinoma patients. Nevertheless, elevated aromatase levels could also be detected in lung cancer patients and lower aromatase levels are a strong predictor of survival³⁰³.

Interestingly, breast cancer studies have shown that the aromatase CYP19A1 is highly expressed in macrophages and autoregulate cytokine production³⁰⁴. The aromatase CYP19A1 gene has several response elements for pro-inflammatory cytokines in the promoter binding sites (Figure 23). Moreover, inflammation in postnatal cerebellum could be correlated with increased aromatase CYP19A1 mRNA expression levels³⁰⁵. Aromatase inhibitors in postmenopausal breast cancer patients have been proven to be effective for adjuvant and neoadjuvant therapy and in the prevention of breast cancer by reducing plasma estradiol levels.

Postmenopausal women belong to the COVID-19 risk groups and were represented in our human COVID-19 cohort with elevated estradiol levels.

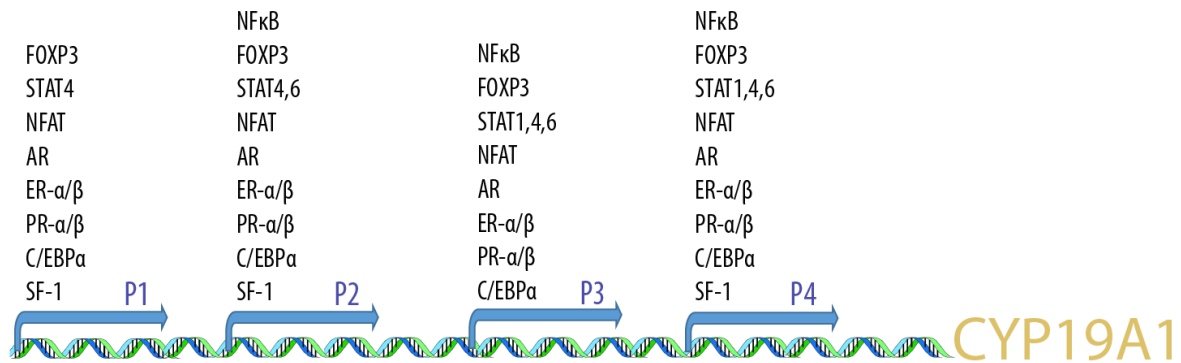


Figure 24: CYP19A1 promotor binding sites.

A schematic model of aromatase gene CYP19A1 promotor binding sites (P1, P2, P3 and P4) for transcription factors.

All in all, our findings suggest that SARS-CoV-2 infection leads to aromatase CYP19A1 dysregulation contributing to elevated plasma estradiol levels, which likely promote inflammation and fibrosis of the lungs. The dysregulation of the aromatase CYP19A1 could be due to the virus induced cytokine and chemokine induction in the lung. The COVID-19 risk groups include patients with underlying diseases with known hormonal imbalances, which could be further enhanced by SARS-CoV-2 infection and thereby promoting a “cytokine storm”. Therefore, screening male and postmenopausal female COVID-19 patients for testosterone and estradiol levels could predict the disease outcome and potential therapies involving aromatase CYP19A1 inhibitors could prevent tissue damage by hyperinflammation.

7 Materials and methods

7.1 Materials

7.1.1 Chemicals

Chemical	Manufacturer
(2-Hydroxypropyl)- β -cyclodextrin	Merck
2-propanol	Sigma-Aldrich/Merck
Acetonitril (99.8%)	Sigma-Aldrich/Merck
Agarose	Serva
Ampicillin sodium-salt	Serva
Avicel	FMC BioPolymer
Bovine serum albumin	Sigma-Aldrich/Merck
Chloroform	Geyer
Crystal violet	Merck
Dimethylsulfoxide (DMSO)	Sigma-Aldrich/Merck
Eosin-Y-solution	Merck
Ethanol	Sigma-Aldrich/Merck
Ethanol (denatured, for disinfection)	Sigma-Aldrich/Merck
Eukitt	Kindler
Formaldehyde solution (37%)	Merck
Glacial acetic acid	Merck
Hematoxylin	Shandon
Hydrochloric acid (HCl) (37%)	Merck
Ottix Plus	DiaPath
Ottix Shaper	DiaPath
Paraffin	DCS
Polyinosinic-polycytidylic acid sodium salt, TLR tested (50 mg)	Sigma-Aldrich/Merck P9582-50MGM
Paraformaldehyde	AppliChem
Potassium chloride (KCl)	Merck
Potassium dihydrogen phosphate	Merck
Pursept-A Xpress, for disinfection	SCHÜLKE & MAYR AG
Sodium chloride (NaCl)	ChemSolute
Testosteron purum (99%)	Sigma-Aldrich/Merck
Triton-X 100	Merck
Tris (hydroxymethyl) amino methane	Merck
TRIzol™	Life Technologies
Tween-20 (pure)	Serva
Virkon S, for disinfection (BSL-3)	MedicAnimal
Xylol	Merck

7.1.2 Buffers and solutions

Buffer / solution	Content/ manufacturer
Avicel solution (2,5%)	2,5% Avicel in ddH ₂ O (autoclaved)
Crystal violet solution	270 ml formaldehyde (37%) 1 g crystal violet in 1 l ddH ₂ O
dNTP mix (10 mM)	Life Technologies
EDTA solution (0.5 M, 100x)	Thermo Scientific
Ethidium bromide solution	Roth
FastDigest Green buffer (10x)	Thermo Scientific
MassRuler DNA ladder mix	Thermo Scientific
MassRuler DNA loading dye	Thermo Scientific
Paraformaldehyde solution (4%)	40g PFA in 1 l PBS, storage at 4°C
Phosphate buffered saline (PBS)	1,37 M NaCl 26,8 mM KCl 51,3 mM Na ₂ HPO ₄ ·2H ₂ O 17,6 mM KH ₂ PO ₄ pH 7.2 – 7.4, autoclaved
Ribolock RNase Inhibitor (40U/μl)	Thermo Scientific
RNase-free H ₂ O	Gibco/ Life Technologies
RNAprotect Tissue Reagent	Qiagen
RNase free DNase Set	Qiagen
TAE buffer (50x)	2 M Tris base 1 M glacial acetic acid 0.05 M EDTA pH 8.0

7.1.3 Kits

Kit	Manufacturer
ADVIA Centaur Testosterone II assays	Siemens Healthcare Diagnostics
Avidin/Biotin Blocking Kit SP2001	Szabo-Scandic
Bio-Plex Pro™ Human Cytokine 27-plex Assay - M500KCAF0Y	Bio-Rad
Bio-Plex Pro™ Mouse Cytokine 7-plex Assay (customized) - L6000004C6 (+Eotaxin, IL-13, MCP-1, MIP-1 α , MIP-1 β , VEGF)	Bio-Rad
Estradiol ELISA (human)	Hölzel Diagnostika
FastStart Essential DNA Green Master	Roche
innuPrep RNA Mini Kit	Analytik Jena
Multiplex mouse immunoassay, custom: (IL-1 β , IL-6, IL-10, IL-17A, TNF α , MCP-1)	Life Technologies
MILLIPLEX MAP Multi-Species Hormone Magnetic Bead Panel - MSHMAG-21K	Merck
QIAamp Viral RNA Mini Kit	Qiagen
RealStar® SARS-CoV-2 RT-PCR Kit RUO	Altona Diagnostics
Superscript™ III Reverse Transcriptase Kit	Invitrogen/Life Technologies

7.1.4 Antibodies

Antibodies	Species/ dilution/ manufacturer
Anti-aromatase antibody (primary)	Rabbit, 1:500 Abcam; ab18995
Anti-influenza NP antibody (primary)	Rabbit, 1:10000 ThermoFisher; PA5-32242
Anti-NP antibody (primary)	Mouse, 1:1000 Abcam; ab43821
Anti-Mouse IgG-HRP	Rabbit, 1:2000 SouthernBiotech; 617005
Anti-SARS-CoV-2 NP (primary)	Mouse, 1:32000 Sino Biological; 40143-MM05
Biotin-SP-AffiniPure F(ab') ₂ Fragment Donkey (secondary)	Rabbit, 1:200 Jackson; 711-066-152

7.1.5 Animals

Species	Sex	Age	Provider
Mouse -C57BL/6	male	6-10 weeks	Charles River
Mouse -C57BL/6	female	6-10 weeks	Charles River
Hamster- RjHan; AURA	male	8-10 weeks	Janvier-Labs
Hamster- RjHan; AURA	female	8-10 weeks	Janvier-Labs

7.1.6 DNA Oligonucleotides

Oligonucleotide ID	Sequence/ manufacturer
murine AR_forward	5'- TGAGTACCGCATGCACAAGT-3'
murine AR_reverse	5'- GCCCATCCACTGGAATAATGC-3'
murine ESR1_forward	5'-AGTGAAGCCTCAATGATGGG-3'
murine ESR2_reverse	5'-GAGCAAGTTAGGAGCAAACAG-3'
hamster Hprt1_forward	5'-TCCCAGCGTCGTGATTAGTG-3'
hamster Hprt1_reverse	5'-GTGATGGCCTCCCATCTCTT-3'
hamster IL-6_forward	5'-TCACCTCTGGTCTTCTGGACT-3'
hamster IL-6_reverse	5'-TCTGGACCCTTTACCTCTTGTT-3'
hamster IL-1 α _forward	5'-ATGGAAATCTGCAGGGGACG-3'
hamster IL-1 α _reverse	5'-TAGCCGGCAATGAGTTGGTT-3'
hamster Eotaxin_forward	5'- AGAGAGCCTGAGACCAACAC-3'
hamster Eotaxin_reverse	5'-AACTGGGATAGAGCCTGGGTG-3'
hamster IFN- γ _forward	5'-ATGGAGGGGACCTCGTCTTT-3'
hamster IFN- γ _reverse	5'-GATGGCCTGGTTGTCCTTCA-3'
hamster CYP19A1_forward	5'-ATGCGGCACATCATGCTGAA-3'
hamster CYP19A1_reverse	5'-TCTTTCAAGTCCTTGGCGGAT-3'
hamster 5- α reductase_forward	5'-ACCCGGGGAAACAGGATACA-3'
hamster 5- α reductase_reverse	5'-GAACAGGGCAAACACTCCAC-3'
hamster EL_forward	5'-GAAACCCAGCGCAAACACTGAC-3'
hamster EL_reverse	5'- TGAGGTCTTCCGTCAAGTGC-3'

7.1.7 Narcotics and supplements

Substance	Manufacturer
Rimadyl® (carprofen)	Zoetis
Isoflurane (100%)	Abbot
Ketamine (100 mg/ml)	WDT
Narcoren	Merial GmbH
Sodium chloride 0.9%	B.Braun Melsungen AG
Xylazine (20 mg/ml)	WDT

7.1.8 Eukaryotic cell lines

Cell lines	Origin/ manufacturer
Mardin-Darby Canine Kidney (MDCK II)	Immortalized canine cell line ATCC (CCL-34)
Vero E6	Immortalized african green monkey cell line ATCC

7.1.9 Media and supplements for eukaryotic cell culture

Medium/ supplement	Content/ manufacturer
Albumin solution from bovine serum, 35% (BSA)	Sigma-Aldrich/Merck
Cryoconservation medium	FBS 10% DMSO
Dulbecco's Modified Eagle's Medium (DMEM)	Sigma-Aldrich/Merck
Dulbecco's Phosphate Buffered Saline (D-PBS)	Sigma-Aldrich/Merck
Fetal bovine serum (FBS) superior	Biochrom GmbH
Infection medium (influenza virus)	MEM 1% L-Glutamine 1% Penicillin & Streptomycin (P/S) 0.2% BSA L-(tosylamido-2-phenyl) ethyl chloromethyl ketone (TPCK)-treated trypsin, 1:1000
Infection medium (corona virus)	DMEM 0.5% L-Glutamine 0.5% P/S 2% FBS
L-Glutamine (200 mM)	Sigma-Aldrich/Merck
Growth medium (MDCK II)	MEM 10% FBS 1% L-Glutamine 1% P/S
Growth medium (VeroE6)	DMEM 10% FBS 1% L-Glutamine 1% P/S
Minimum Essential Medium (MEM)	Sigma-Aldrich/Merck
Modified Eagle Medium 2x (2x MEM) without Phenol Red	Sigma-Aldrich/Merck
Overlay medium for plaque test	1:1 mixture of and 2xMEM (+ 0.4% BSA, 2% L-Glutamine, 2% P/S) 2.5% Avicel in H ₂ O

Medium/ supplement	Content/ manufacturer
Penicillin & Streptomycin	Sigma-Aldrich/Merck
TPCK-treated trypsin	Sigma-Aldrich/Merck
Trypsin-EDTA	Sigma-Aldrich/Merck

7.1.10 Virus strains

Virus strain	Origin
A/Hamburg/NY1580/09 (H1N1)	Sigrid Baumgarte, Institut für Hygiene und Umwelt, Hamburg, Germany ([248])
SARS-CoV-2/Germany/Hamburg/01/2020 ENA study PRJEB41216 and sample ERS5312751	Heinrich-Pette-Institut für experimentelle Virologie, Hamburg, Germany

7.1.11 Consumables

Article	Manufacturer
12-well tissue culture plate	Greiner bio-one Cellstar
24-well tissue culture plate	Falcon / BD Biosciences
6-well tissue culture plate	Falcon / BD Biosciences
96-well tissue culture plate	Sarstedt
ALZet Model 2004 micro-osmotic pump	Charles River
Cannula Microlance™ 3 (25G x 1", 0.5x25 mm)	BD Microlance
Capillaries (EDTA tubes for blood collection)	Kabe Labortechnik GmbH
Cryo vials (1.5 ml)	Sarstedt
Metal beads (Ø 2.0 mm)	RETSCH (#22.455.0010)
Millex-HA Filter, 0.45 µm	Merck
PCR tubes	Sarstedt
Pipette tips, with filter (10, 100, 1000 µl)	Sarstedt
Precision wipe tissue	Kimtech Science
Reaction tubes (1.5 ml, 2.0 ml)	Sarstedt
SafeSeal reaction tubes + screw cap	Sarstedt
S-Monovette® Serum-Gel	Sarstedt
S-Monovette® Lithium-Heparin-Gel	Sarstedt
Syringe TERUMO®, without needle, U-100	TERUMO Cooperation
Insulin (1 ml, 6 % Luer)	
Syringe Omnifix® (3 ml / Luer Lock Solo)	B. Braun Melsungen AG
T25 cell culture flask	Falcon / BD Biosciences
T75 cell culture flask	Sarstedt
Transfer pipettes (5, 10, 25 ml)	Sarstedt

7.1.12 Safety gear

Article	Manufacturer
Duct tape Extra Universal	TESA
Filter/respirator mask, type 9332 FFP3 ventil	3M
Gloves Biogel	3M
Gloves latex	Kimberly-Clark
Gloves purple nitrile	Kimberly-Clark
Lab coat	Leiber
Lab shoes unisex	Suecos
OP mask	Mölnlycke Health Care
OP nurse cap	Mölnlycke Health Care
OP pants (green)	Sattelmacher
Overalls (blue)	ProFit
Safety goggles	UVEX
Shoe covers (blue)	Ansell Health Care
TYVEK® boot covers	DuPont
TYVEK® overalls	DuPont

7.1.13 Laboratory equipment

Article	Manufacturer
ADVIA Centaur XP	Siemens Healthcare Diagnostics
Animal scale	Kern
Biological safety cabinet HeraSafe KS12	Thermo Scientific
Biological safety cabinet HeraSafe KS18	Thermo Scientific
Bio-Plex® 200 Systems	Bio-Rad
Centrifuge Avanti J-E	Beckham Coulter
Centrifuge 5417R	Eppendorf
Centrifuge 5810R	Eppendorf
Centrifuge Varifuge 3.0R	Thermo Scientific
Cryo conservation container Mr. Frosty	Nalgene
Heraeus temperature-controlled CO ₂ incubator B6120	Kendro
Heraeus temperature-controlled CO ₂ incubator BBD 6220	Thermo Scientific
Heraeus temperature-controlled CO ₂ incubator Heracell 150	Thermo Scientific
Isoflurane vaporizer	UNO
LightCycler® 96	Roche
Magnetic stirrer MR3001 (with heating element)	Heidolph
Microliter pipettes Eppendorf Reference (1-10, 10-100, 100-1000 µl)	Eppendorf

Article	Manufacturer
Microplate reader Tecan Safire2	Tecan
Mixer mill MM 400	RETSCH
Multichannel pipettes (8 channel; 5-50 µl; 20-200 µl)	Brand
Paraffin embedding center EG1160	Leica Biosystems
pH calculation device pHenomenal®	VWR
Pipetus	Hirschmann Laborgeräte
Precision scale Extend ED224S	Sartorius
Roche LightCycler® 96	Roche
Shaker MaxQ 6000	Thermo Scientific
Shaker WT 17	Biometra
Shaking waterbathSW22	Julabo
Small centrifuge (1.5 reactions tubes)	Biozym
Small centrifuge (PCR 8-stripes)	Biozym
SpeedVac	Eppendorf
Surgical forceps (for organ harvesting)	F.S.T.
Surgical scissors (for organ harvesting)	F.S.T.
Thermostat Precitherm PFV	Labora Mannheim
Transmitted-light microscope	Zeiss
Vacuum centrifuge	Eppendorf
Vortex-Mixer 7-2020	neoLab

7.1.14 Software

Software	Provider
Adobe Photoshop CS4	Adobe Systems Inc.
Adobe Illustrator CS5.1	Adobe Systems Inc.
Bio-Plex Manager™ software	Bio-Rad
ELISA online analysis tool	https://www.myassays.com/
GraphPad Prism v.8.3.1	GraphPad Software Inc.
LightCycler® 96 software, V 1.1.0.1320	Roche
LinRegPCR	Ruijter et al., 2014
Microsoft Office	Microsoft

7.2 Methods

7.2.1 Ethics statement

Sampling from laboratory-confirmed COVID-19 and non-COVID-19 patients was reviewed and approved by the ethics committee at the Hamburg State Chamber of Physicians (registration no.: WF-053/20 and WF-073/21). The need for an informed consent for healthy blood donors (HC) and patients with coronary heart diseases (CHD) was waived by the ethics committee because data were retrieved retrospectively from electronic health records.

All animal experiments performed in this study were in strict accordance with the guidelines of German animal protection law and all protocols were approved by the German authorities.

7.2.2 Collection of human samples

7.2.2.1 Collection of COVID-19 and non-COVID-19 patient cohort samples

Patient serum and plasma samples, as well as nasopharyngeal swabs were collected from the first 50 laboratory-confirmed COVID-19 patients admitted to the intensive care unit (ICU) at the University Medical Center Hamburg-Eppendorf from March 8th to April 29th, 2020, including 39 male and 11 female patients. Additionally, 42 patients with laboratory-confirmed SARS-CoV-2 PCR, who were admitted to the Department of Intensive Care Medicine at the University Medical Center Hamburg-Eppendorf were recruited as a control group (non-COVID-19 ICU; 27 males, 15 females). Blood samples were collected in either S-Monovette® Serum-Gel or S-Monovette® Lithium-Heparin-Gel tubes on the day of admission and centrifuged for 10 min at 2,500 x g before aliquoting the serum/plasma and storing at -80°C until further analysis.

All demographic and clinical variables were collected retrospectively from the electronic patient data management system (PDMS) (ICM, Dräger, Lübeck, Germany): age, sex, body mass index, comorbidities, Simplified Acute Physiology Score II (SAPS II) on admission, Sequential Organ Failure Assessment Score (SOFA) on admission, and classification of Acute Respiratory Distress Syndrome (ARDS) using the Berlin definition³⁰⁶. Furthermore, antiviral

treatment, supportive and experimental COVID-19 therapies, the need for mechanical ventilation and extracorporeal membrane oxygenation³⁰⁷, as well as the course of the patients were recorded.

7.2.2.2 Collection of coronary heart disease cohort patient samples

Plasma samples from coronary heart disease patients were collected at the University Hospital in Tübingen and sent to the Heinrich Pette Institute on dry ice. The samples were collected in 2020 and patients with laboratory-confirmed COVID-19 were excluded from this study. A total of 24 male patients and 13 female patients over the age of 40 were included in this study.

7.2.2.3 Collection of healthy cohort samples

Plasma samples from healthy donors were collected from the blood donation center of the transfusion medicine at the University Medical Center Hamburg-Eppendorf. The donors blood was collected in blood bags containing anticoagulant citrate. Only donors over the age of 40 were included (30 male donors, 20 female donors). The samples were centrifuged at the collection day for 10 min at 2,500 x g at 4°C and aliquoted for further storage at -80°C.

7.2.3 Animal experiments

All animal experiments were performed in strict accordance with the guidelines of German animal protection law and were approved by the relevant German authority (Behörde für Gesundheit und Verbraucherschutz; protocols N 32/2020 and 01/15). Mice (female and male mice 4-8 weeks old) used in this study were purchased from Envigo and golden hamsters (female and male hamsters 8-10 weeks old) were purchased from Janvier. All animals for infection experiments were housed in individually ventilated cages (IVC). Infections with SARS-CoV-2 were carried out in the biosafety level 3 (BSL-3) facility and infections with 2009 pH1N1 were carried out in the biosafety level 2 (BSL-2) laboratories at the Heinrich Pette Institute following standard operation procedures (SOPs).

7.2.3.1 *In vivo* experiments in mice

7.2.3.1.1 Narcosis of mice

For infection experiments, mice were placed in isoflurane (Forene) narcosis using a vaporizer before injection of an intraperitoneal (i.p.) narcosis composed of 100 mg/kg ketamine and 10 mg/kg xylazine prepared in 0.9% of sterile sodium chloride solution. The narcosis was applied according to the individual animal weight using a 1 ml syringe and a 26G cannula.

Before obtaining blood samples mice were briefly placed in isoflurane narcosis.

7.2.3.1.2 Intranasal infection of mice

Before intranasal infection of the mice with 2009 pH1N1 IAV mice were narcotized and infected with 50 μ l of 2009 pH1N1 (10^4 p.f.u.) or 1x PBS as a control. Therefore, 50 μ l of inoculum were applied carefully onto the nostrils of the mice using a pipette. Afterwards, the breathing rate was observed, and the mice were placed in a recovery position.

7.2.3.1.3 Monitoring of survival and weight loss and euthanization of mice

After infection mice were monitored daily for 14 days after infection. At the human endpoint of 25% weight loss or before organ harvesting, mice had to be euthanized. Therefore, mice were placed in isoflurane narcosis (chapter 7.2.7.1.1) and euthanized by cervical dislocation. After organ harvesting, the mice cadavers were autoclaved, and the organs were either stored at -80°C or in 4% PFA at 4°C until further usage.

7.2.3.1.4 Surgical procedures for testosterone administration

One hour before performing surgical procedures, mice were administered subcutaneously with carprofen (5 mg/kg, Zoetis). The mice were anesthetized with 2.5% isoflurane during the surgery. 6-week-old male mice were assigned to bilaterally gonadectomized or remained intact. On the other hand, 6-week-old female mice were implanted an ALZet Model 2004 micro-osmotic pump subcutaneously releasing either testosterone (5 mg/ml diluted in 45% w/w (2-Hydroxypropyl)- β -cyclodextrin) or a carrier substance as a control. As a postoperative analgetic

the mice were administered subcutaneously with carprofen 24 h after surgery. Two weeks after the surgeries the mice were infected with 10^4 p.f.u. 2009 pH1N1.

7.2.3.1.5 Harvesting of blood and organs

Organs were harvested 1 and 3 days post infection. Under isoflurane narcosis, blood was collected retrobulbary in EDTA tubes and mice were euthanized by cervical dislocation. For the collection of EDTA-plasma the whole blood tubes were centrifuged for 10 min at 2500 x g. The plasma was aliquoted and stored at -80°C . The remaining blood pellet was diluted in TRIzol and further used for RNA isolation of PBMCs (chapter 7.2.3.1). The lung was removed and divided into tubes pre-filled with metal beads for homogenization or filled with 4% PFA for histological examination (chapter 7.2.6).

The weight of lung tissue in the tubes for homogenization was recorded and the tissue was directly homogenized in 1 ml 1x PBS. The lung tissue was homogenized using a RETSCH homogenizer (20 Hz, 4°C , 10 min), following a centrifugation step for 10 min at 6000 x g. The supernatant was aliquoted and stored at -80°C until further analysis.

7.2.3.2 *In vivo* experiments in golden hamsters

7.2.3.2.1 Narcosis of golden hamsters

For SARS-CoV-2 infection experiments, hamsters were injected an intraperitoneal (i.p.) narcosis with 150 mg/kg ketamine and 10 mg/kg xylazine prepared in 0.9% of sterile sodium chloride solution. The narcosis was applied according to the individual animal weight using a 1 ml syringe and a 26G cannula.

7.2.3.2.2 Intranasal infection of hamster

Before intranasal infection the hamsters were narcotized and infected with 80 μl of SARS-CoV-2 (10^5 p.f.u.) or 1x PBS and 1 mg/kg poly(I:C) as a control. Therefore, 80 μl of inoculum were applied carefully onto the nostrils of the hamsters using a pipette. Afterwards, the breathing rate was observed, and the hamsters were placed in a recovery position.

7.2.3.2.3 Monitoring of survival and weight loss and euthanization of hamsters

Hamsters were monitored for weight loss and signs of disease for 14 days post infection. Subsequently, hamsters were euthanized for organ explants or when reaching the human endpoint of losing 25% of their body weight. Therefore, hamsters were euthanized by intraperitoneal injection of an overdosis of pentobarbital. After organ harvesting, the hamster cadavers were autoclaved, and the organs were either stored at -80°C or at 4°C until further usage.

7.2.3.2.4 Harvesting of blood and organs

Hamster organs were harvested 1, 3 and 6 days post infection. After euthanizing the animals blood was collected by cardiac puncture in EDTA tubes. For the collection of EDTA-plasma the whole blood tubes were centrifuged for 10 min at 2500 x g. The plasma was aliquoted and stored at -80°C. Lungs and gonads were separated into tubes filled with metal tubes, RNAprotect Tissue Reagent (QIAGEN)-filled tubes for RNA isolation and tubes filled with 10% neutral-buffered formalin for histopathological examination.

The weight of lungs and gonads was recorded, and the tissue was homogenized in PBS using a RETSCH homogenizer (20 Hz, 4°C, 10 min) following a centrifugation step for 10 min at 6,000 x g. The supernatant was aliquoted and stored at -80°C.

7.2.4 Cell culture techniques

7.2.4.1 Cultivation of eukaryotic cells

Eukaryotic cell lines were cultivated in a temperature-controlled incubator at 37°C, 5% CO₂ and 95% relative humidity (rH). MDCK II cells were cultivated in Minimal Essential Medium (MEM), supplemented with 10% FBS, 1% L-Glu and 1% P/S. VeroE6 cells were maintained in Dulbecco's Modified Eagles Medium (DMEM), supplemented with 10% FBS, 1% L-Glu and 1% P/S. All cell lines were regularly tested for *Mycoplasma sp* (chapter 7.2.2.3).

7.2.4.2 Freezing and thawing of eukaryotic cells

For long-term storage eukaryotic cell lines were stored in liquid nitrogen. The cells of a confluent flask were trypsinized and pelleted at 1000 x g for 5 min at room temperature for cryoconservation. The pelleted cells were resuspended in cryoconservation medium (FBS + 10% DMSO) and aliquoted into cryo vials, which were stored in cryoconservation containers “Mr. Frosty” at -80°C for at least 24 hours before transferring into liquid nitrogen.

For re-cultivating frozen cells, the cryo vials were thawed at 37°C in a water bath. To remove residual DMSO the cells were washed with growth medium and centrifuged at 300 x g for 8 min before resuspension in growth medium. The cells were then seeded into T25 cell culture flasks at 37°C, 5% CO₂ and 96% rH.

7.2.4.3 Mycoplasma sp PCR

All eukaryotic cell lines in this study were regularly tested negative for *Mycoplasma sp* contamination using the Venor®GeM Classic Mycoplasma PCR Detection Kit (Minerva Biolabs GmbH) according to manufacturer’s instructions.

7.2.5 Nucleic acid techniques

7.2.5.1 Isolation of total RNA from murine PBMCs

Total RNA was isolated from murine PBMCs following a guanidiniumthiocyanate-phenol-chloroform extraction protocol. After extraction of plasma (chapter 7.2.7.1.5), the samples were lysed by diluting the cell pellet 1:1 in Trizol reagent (total volume 500 µl) and stored at -80°C until further preparation. To extract the RNA, the samples were thawed, 100 µl of chloroform were added and the samples were incubated for 3 min at room temperature. Following a centrifugation step at 12,000 x g for 15 min at 4°C, the aqueous phase was separated and mixed with 500 µl isopropanol. After incubation for 10 min at room temperature the samples were centrifuged at 12,000 x g for 10 min at 4°C. The RNA pellet fraction was then washed with 500 µl 75% ethanol and centrifuged at 12,000 x g for 5 min at 4°C. After discarding the supernatant, the pellet was dried in a heat block at 37°C for 30 min and reconstituted in 40 µl RNase-free ddH₂O. Ribolock RNA inhibitor (0.75 µl / 30 µl of eluted RNA) was added and the RNA concentration was measured on NanoDrop1000 before storing the RNAs at -80°C until subsequent analysis.

7.2.5.2 Isolation of total RNA from hamster tissues

Total RNA was isolated from RNeasy Protect[®] fixated hamster tissues (lung, testis, ovaries, uterus). The tissue was separated into sterile 2 ml SafeSeal reaction tubes containing 4-6 metal beads (\varnothing 2 mm). 900 μ l lysis buffer RL were added to about 50 mg of tissue and the samples were homogenized for 6 min at 30 Hz in a Mixer mill MM 400. To prevent clogged columns hamster testis tissue samples were additionally treated with 450 μ l of Trizol reagent following centrifugation at 12000 x g for 15 min at 4°C. The upper, aqueous phase was then transferred to spin-filter D. The following RNA extraction was performed using the innuPrep RNA Mini Kit (Analytik Jena) according to manufacturer's instructions ("protocol 1: RNA extraction from tissue samples") with minor modifications. After a HS buffer washing step a DNase I treatment (RNase-Free DNase Set; Qiagen) was performed to digest genomic DNA. Therefore, 10 μ l DNase I were diluted in RDD buffer and applied to the columns. After incubation for 15 min at room temperature, the columns were washed with 500 μ l HS buffer. Isolated RNA was eluted with 30 μ l RNase-free ddH₂O and the RNA concentration was measured on NanoDrop1000 before storing the RNAs at -80°C until subsequent analyses.

7.2.5.3 Isolation of viral RNA from patient and hamster samples

For detection of SARS-CoV-2 RNA in patient (nasal/tracheal swabs, plasma/serum, urine) and hamster samples (lung, plasma, testis, uterus, ovaries), viral RNA was isolated using the QIAamp Viral RNA Mini Kit according to the manufacturer's instructions. 10 μ l of the sample were diluted in 130 μ l PBS and 560 μ l AVL buffer containing carrier RNA was added. RNA was eluted with 30 μ l RNase-free ddH₂O. Ribolock[™] RNA inhibitor (0.75 μ l / 30 μ l of eluted RNA) was added and subsequently used for analyses.

7.2.5.4 Reverse transcription PCR (RT-PCR)

In this study, a reverse transcription reaction was carried out to generate complementary DNA (cDNA) based on RNA templates using a random nonamer primer mix for synthesizing a pool of cDNAs from all RNAs present in the samples (chapters 7.2.3.1 and 7.2.3.2). The reaction set up is displayed in table 4.

Table 4: Setup of cDNA synthesis using a random nonamer (p9) primer mix.

Component	Volume
RNase free ddH ₂ O	8.5 µl
Primer (p(dN) ₉) [50 µM]	2.0 µl
dNTP mix [10 mM]	1.0 µl
Template RNA [0.5 - 1.5 µg]	1.5 µl
Total	13 µl
<hr/>	
<i>PCR cycling</i>	65°C 5 min
<hr/>	
First strand Buffer (5x)	4.0 µl
DTT, 0.1 mM	1.0 µl
Ribolock RNase Inhibitor (40 U/µl)	1.0 µl
Superscript III RT (200 U/µl)	1.0 µl
Total	20 µl
<hr/>	
	25°C, 5 min
<i>PCR cycling</i>	50°C, 60 min
	70°C, 15 min
<hr/>	

7.2.5.5 Real-time reverse transcription PCR (RT-PCR)

Quantitative real-time reverse transcription PCR (qRT-PCR)

To determine expression levels of receptor levels in murine peripheral blood mononuclear cells (PBMCs) (AR, ESR1) as well as pro-inflammatory genes and enzymes in hamster tissue, qRT-PCR was performed. The qRT-PCR reactions were set up in LightCycler® 480 Multiwell Plate 96 Reaction Plates (Roche) and were conducted on a LightCycler® 96 Real-Time PCR System (Roche). The reaction set up is described in table 5. For the analysis, Ct values of each samples were normalized to Ct values of the reference gene of the respective sample and the average of the Δ Ct value was determined. The relative $2^{-\Delta$ Ct expression values were calculated and presented.

Table 5: Setup of qRT-PCR reaction.

Component	Volume	
ddH ₂ O	7.4 µl	
Primer forward [20 µM]	0.3 µl	
Primer reverse [20 µM]	0.3 µl	
Fast Start Essential Green Master (2x)	10 µl	
cDNA template	2.0 µl	
Total	20 µl	
	95°C, 5 min	45 cycles
	95°C, 15 sec	
PCR cycling	60°C 10 sec	
	72°C 20 sec	
	95°C, 15 sec	
	67°C, 15 sec	

7.2.5.6 Qualitative real-time reverse transcription PCR

For qualitative detection of SARS-CoV-2 specific RNA in patient and hamster samples the RealStar® SARS-CoV-2 RT-PCR Kit RUO (Altona Diagnostics) was used following the manufacturer's instructions. For the reactions 10 µl of isolated viral RNA (chapter 7.2.3.3) were used.

7.2.6 Protein biochemical methods

7.2.6.1 Cytokine/chemokine and hormone quantification by Multiplex-Immunoassay

To determine differences in cytokine and hormone expression during influenza virus or SARS-CoV-2 infection pro-inflammatory cytokine/chemokine and hormone levels were determined by Multiplex-Immunoassay. The luminex technology is based on diverse secretory proteins coupled to magnetic beads and allowing the simultaneous detection of a large number of cytokines and chemokines, as well as hormones in tissue samples and plasma.

For cytokine and chemokine measurements custom-made Bio-Plex Pro™ Human or Mouse Cytokine multiplex (Bio-Rad) according to the manufacturer's instructions in a Bio-Plex 200 System with high-throughput fluidics (HTF; Bio-Rad) were used.

Materials and methods

In this study, a panel of 27 cytokines and chemokines (Eotaxin, FGF, G-CSF, IFN- γ , IP-10, IL-2, IL-4, IL-5, IL-6, IL-7, IL-8, IL-9, IL-10, IL-12, IL-13, IL-15, IL-17, IL-1 β , IL-1RA, MCP-1, PDGF-BB, RANTES, TNF- α , VEGF) were measured in the serum/plasma of COVID-19 patients. A panel of 13 cytokines and chemokines (Eotaxin, CCL3, CCL4, IFN- γ , IL-2, IL-6, IL-10, IL-12, IL-13, IL-1 β , MCP-1, TNF- α and VEGF) were measured in homogenized lungs and plasma of golden hamsters. In addition, a panel of 6 cytokines and chemokines (MCP-1, IL-1 β , IL-6, IL-10, IL17A and TNF- α) were analysed in homogenized lungs of 2009 pH1N1 infected mice.

For the detection of hormones in plasma of coronary heart disease patients and hamster samples including plasma, homogenized testis or ovaries a custom-made MILLIPLEX MAP Multi-Species Hormone Magnetic Bead Panel (Merck), analysing testosterone, cortisol and progesterone according to the manufacturer's instructions in a Bio-Plex 200 System with high-throughput fluidics (HTF; Bio-Rad) was used. Therefore, 150 μ l of the samples were mixed with 225 μ l acetonitrile. After incubation for 10 min at room temperature, the samples were mixed again and centrifuged at 17000 x g for 5 min at room temperature. The supernatant samples were dried in a SpeedVac at highest vacuum setting for 2 hours and reconstituted in 120 μ l assay buffer.

7.2.6.2 Hormone quantification by external institutes/companies

Hormone levels in plasma samples of COVID-19 patients and plasma of the healthy cohort were measured by an external laboratory accredited for measurements of human samples (Labor Lademannbogen, Hamburg, Germany). Cortisol, TSH, T3, T4, LH, FSH, TT, E2 and SHBG were measured by ECLIA. Estrone levels were analysed by RIA. Free Testosterone was analysed by ELISA and DHY-TT was measured by LC-MS/MS. All measurements were performed according to standardized clinical protocols.

Testosterone in plasma of mice infected with 2009 pH1N1 were determined by a chemiluminescence immunoassay (ADVIA Centaur Testosterone II assays; Siemens Healthcare Diagnostics) and the measurements were performed with the ADVIA Centaur XP (Siemens Healthcare Diagnostics) at the Institute for Clinical Chemistry and Laboratory Medicine, University Medical Center Hamburg-Eppendorf.

7.2.6.3 Enzyme-linked immunosorbent assay (ELISA)

To quantify protein levels a sandwich ELISA measures an antigen, which is bound to a specific primary antibody (capture antibody). The primary antibody can be detected by secondary enzyme-linked antibody (detection antibody). In this study, commercially available ELISA kits were used to quantify serum/plasma levels of

- a) E2 (CHD patient cohort, hamster samples); Hölzel Diagnostika
- b) EL (hamster samples); IBL international
- c) Adiponectin (hamster samples); Sigma-Aldrich/Merck

The ELISAs were performed according to the manufacturer's protocols. For quantification the purified antigen was applied to the microtiter plates in a serial dilution. The adsorption was measured in a multimode microplate reader (Tecan) at the respective wavelength. Magellan 7.1 Software and MyAssays: assay data analysis software were used for analysis.

7.2.7 Virological techniques

7.2.7.1 Isolation of SARS-CoV-2

The SARS-CoV-2 strain (SARS-CoV-2/Germany/Hamburg/01/2020) used in this study was isolated from a sample of a confirmed male intensive care patient with COVID-19 in Hamburg. Therefore, 250 µl of a nasopharyngeal swab were centrifuged for 5 min at 5000 x g at 4°C. The supernatant (200 µl) was diluted in 200 µl of inoculation medium (DMEM + 1% penicillin-streptomycin, 1% L-glutamine and 1 µg/ml TPCK-treated trypsin). VeroE6 cells seeded in a 24 well plate were inoculated with the diluted supernatant at 37°C in a CO₂ incubator. After 1 hour of incubation the supernatant was removed and the cells were washed two times with 1x PBS before replacing the medium with 1 ml of infection medium (DMEM + 2% FBS, + 0.5% penicillin-streptomycin and 0.5% L-glutamine). The cells were incubated for 72 h at 37°C in a CO₂ incubator before transferring the supernatant into 1.5 ml tubes. After centrifugation of the supernatant for 5 min at 5000 x g at 4°C, 10 µl of the supernatants were transferred on VeroE6 cells in 3x T-25 cell culture flasks. 72 h after incubation at 37°C in a CO₂ incubator the supernatants of the three T-25 cell culture flasks were united and the virus was harvested (chapter 7.2.5.3).

7.2.7.2 Propagation of SARS-CoV-2 on VeroE6 cells

The SARS-CoV-2 stock (SARS-CoV-2/Germany/Hamburg/01/2020) was isolated in this study and propagated on VeroE6 cells. Briefly, VeroE6 cells were grown in T-25 cell culture flasks to 90% confluence. The growth medium (DMEM + 10% FBS, + 1% penicillin-streptomycin and 1% L-glutamine) was replaced by 5 ml infection medium (DMEM + 2% FBS, + 0.5% penicillin-streptomycin and 0.5% L-glutamine) and inoculated with 10 µl of virus stock. The cells were incubated at 37°C in a CO₂ incubator. After 72 hours the supernatants of three inoculated T-25 flasks were united and centrifuged for 10 min at 1000 x g at 4°C. To remove remaining cell debris the supernatant was additionally filtered through a 0,45 µm syringe filter and aliquoted in cryo vials (100 µl). All virus stocks were stored at -80°C and the plaque forming units were determined by plaque assay on VeroE6 cells after one freeze-thaw cycle (chapter 7.2.5.4).

7.2.7.3 Propagation of influenza A viruses on MDCK II cells

The 2009 pH1N1 stock (A/Hamburg/NY1580/2009) used in this study already existed and was propagated on MDCK II cells.

The method for propagation of influenza A virus on eukaryotic cells was performed according to a modified protocol following Gaush *et al.*³⁰⁸. MDCK II cells were grown in T-75 cell culture flasks until they were 90% confluent. The cells were washed 2x with 1x PBS and inoculated with 5 ml infection medium (MEM +0.2% BSA, 1% penicillin-streptomycin and 1% L-glutamine) containing 5 µl of virus for 30 min at 37°C in a CO₂ incubator. The flasks were moved every 10 min to ensure an optimal distribution of virus on the cells. After 30 min the inoculum was removed and replaced with infection medium (MEM +0.2% BSA, 1% penicillin-streptomycin, 1% L-glutamine and 1 µg/ml TPCK-treated trypsin).

The virus was harvested after observing a cytopathic effect of about 80%. The medium containing the virus particles was centrifuged for 5 min at 1000 x g at 4°C and filtered through a 0,45 µm syringe filter to remove remaining cell debris. For storage, the virus was aliquoted in cryo vials (100 µl) and the plaque forming units were determined by plaque assay on MDCK II cells (chapter 7.2.5.4) after one freeze-thaw cycle. All virus stocks were stored at -80°C until further usage.

7.2.7.4 Determination of virus titers by plaque assay

To determine viral titers in virus stocks and organ homogenates a plaque assay using a semi-viscose overlay medium was performed according to a modified protocol following Matrosovich *et al.*³⁰⁹. In this study viral lung titers of 2009 pH1N1 infected mice, SARS-CoV-2 virus stock titers as well as lung, testis, ovaries, uterus, fat and mesenchymal fat virus titers of infected golden hamsters were analysed via plaque assay.

For 2009 pH1N1 a plaque assay on MDCK II cells is commonly used, whereas for SARS-CoV-2 a plaque assay on VeroE6 cells was performed.

The cells were seeded in 6 well plates for virus stock titers and organ titers of infected animals. The samples were diluted in PBS in a 10- fold dilution series. After washing the cells with PBS, they were inoculated with 333 μ l of the virus dilutions and incubated at 37°C in a CO₂ incubator for 30 min. To prevent drying out of the cells, the plates were moved every 10 min. After the incubation time 3 ml of Avicel-Overlay-Medium with 1 μ g/ml TPCK-treated trypsin were added to every well. The cells were incubated for 72 h at 37°C in a CO₂ incubator. The overlay medium was removed and after washing the cells with PBS 1 ml of 4% PFA were added for at least 30 min at 4°C.

2009 pH1N1 viral titers were determined by IAV nucleoprotein-specific antibody staining. After washing the cells with PBS they were incubated for 30 min with 0.3% Triton-X for permeabilisation. The cells were then incubated with 500 μ l of the primary anti-IAV NP antibody (Abcam) for 1 h at room temperature. Following three washing steps with PBS (+0.05% Tween) the cells were incubated with 500 μ l of secondary HRP-coupled anti-mouse antibody (SouthernBiotech). In this study, the antibodies were diluted 1:1000 in Superblock buffer. For the detection the HRP substrate containing True-Blue dye was applied to the cell layer after two washing steps.

SARS-CoV-2 viral titers could be detected by counterstaining with crystal violet due to formation of large, visible plaques in the cell layer.

Viral titers were determined in plaque forming units per milliliter (p.f.u./ml) by counting the plaques per well.

7.2.8 Histological techniques

To analyse the impact of an IAV or SARS-CoV-2 infection on organs of infected animals, histological crosssections were prepared. The crosssections were stained by hematoxylin-eosin (HE) and an immunohistochemical staining (ICH-P). The stained crosssections were imaged

using *Nikon Eclipse 80i upright* light microscope coupled with *Color Camera Nikon DS-Ri2*. Images were captured at 10x magnification and three independent fields were taken from each slide. The images were edited with Adobe® Photoshop® CS6 (64 bit).

7.2.8.1 Preparation of murine and hamster organ tissues for histology

The histological samples were fixated in 4% PFA for 1-2 weeks or 10% neutral-buffered formalin for 24 h. To extract the PFA afterwards, samples were stored in 1x PBS before paraffin embedding of the organ samples. The following steps were performed, and paraffin treatment was carried out in the tissue infiltration system ASP300 (Leica Biosystems)

- 70% EtOH, 1 h at RT
- 80% EtOH, 1 h at RT
- 90% EtOH, 1 h at RT
- 95% EtOH, 1 h at RT
- 100% EtOH, 2,5 h at RT
- Xylol I, 1 h at RT
- Xylol II, 1 h at RT
- Paraffin type 3, 1 h at 58°C

The paraffin wax blocks with the embedded tissues were stored in the dark at RT until further usage. To prepare the 4 µm microtome sections the samples were cooled down to -12°C. After sectioning the microtome slides, they were transferred into a water bath at 42°C and dried on an object slide at 37°C overnight.

7.2.8.2 Deparaffining and rehydration of FFPE- tissue sections

The tissue section on object slides (FFPE- formalin-fixed paraffin-embedded tissue sections) can be stored at RT until further usage. Before histochemical or immunohistochemical stainings the tissue sections were deparaffined and rehydrated using Xylol and decreasing ethanol concentrations according to the following steps:

- Incubation of FFPE slides at 56°C for 25 min

Materials and methods

- Xylol I, 5 min at RT
- Xylol II, 5 min at RT
- 100% EtOH I, 5 min
- 100% EtOH II, 5 min (10x)
- 95% EtOH, 5 min (10x)
- 90% EtOH, 5 min (10x)
- 80% EtOH, 5 min (10x)
- 70% EtOH, 5 min (10x)
- 50% EtOH, 5 min (10x)
- ddH₂O, 2 min

7.2.8.3 Hematoxylin and eosin (H&E)- staining of murine and hamster organ tissue

To differentiate between nuclear and cytoplasmic parts of the cells the tissue sections were stained with hematoxylin and eosin. Hematoxylin is staining acidic and basophilic compartments of the cell, as nucleus and rough endoplasmic reticulum, blue to violet. Eosin, on the other hand, is staining alkaline cell compartments, such as the cytoplasm, mitochondria and smooth endoplasmic reticulum, pink. The H&E-staining was performed on deparaffined FFPE- tissue sections:

- ddH₂O, 2 min
- hematoxylin, 4 min
- running tap water, 10 sec
- EtOH-HCl solution (97% EtOH; 3% HCl), 10 sec
- running tap water, 5 min
- eosin, 25 sec

After H&E-staining, the samples were dehydrated with EtOH and Xylol:

- Ottix Shaper I, (10x dipping)
- Ottix Shaper II, (10x dipping)
- Ottix Shaper III, (10x dipping)

Materials and methods

- Ottix Shaper IV, 5 min
- Ottix Plus I, (10x dipping)
- Ottix Plus II, (10x dipping)
- Ottix Plus III, (10x dipping)
- Ottix Plus IV, (10x dipping)
- Xylol, (10x dipping)
- Xylol, 10 min

Afterwards the tissue sections were mounted with Eukitt and stored at RT in the dark until imaging.

7.2.8.4 Immunohistochemical staining (ICH-P)

To evaluate virus tropism and detect virus-infected cells, the FFPE tissue sections were stained using an immunohistochemical procedure. Therefore deparaffined and dehydrated tissue sections (chapter 7.2.6.2) were used. The procedure is described in the following:

- Microwave (850 W, 16 min)
- Microwave (450 W, 5 min) *Citrat Plus Buffer*
- Cooling down, 20 min
- Washing step with 1x PBS (5 min)

The endogenously expressed peroxidase, which can lead to high background staining as the detection is based on an HRP-coupled secondary antibody, had to be blocked. Therefore, the tissue sections were treated with methanol with 3% H₂O₂ for 5 min at RT. After a washing step with 1x PBS for 5 min avidin binding sites as well as endogenous biotin were blocked using an avidin/biotin blocking kit (Szabo-Scandic) for 15 min at RT. In the following, the sections were washed three times with 1x PBS for 5 min and incubated with the primary antibody for 75 min (rabbit, Anti-NP, Thermo Fischer, PA5-32242) diluted 1:2,000 in 1x PBS at RT. After incubation with secondary antibody diluted 1:200 in 1x PBS with 2% donkey serum (anti-rabbit, Jackson ImmunoResearch, 711-066-152) the samples were incubated for 15 min with the ZytoChemPkus (HRP) Broad Spectrum (DAB) Kit to ensure binding of the streptavidin-HRP-conjugate on the biotinylated secondary antibody. The sections were then washed three

times with 1x PBS for 5 min. To exclude unspecific binding of the secondary antibody the sections were incubated with 10% donkey serum for 30 min at RT. The immunohistochemical staining of the viral antigen resulted by addition of the HRP- substrate; 3,3'-diaminobenzidin (DAB). The reaction was stopped after about 5 min with ddH₂O. To improve the analysis with the light microscopy a H&E counterstaining (chapter 7.2.6.3) was performed. The slides were mounted with Eukitt and stored in the dark at RT.

7.2.9 Statistical evaluations

Statistical evaluation for quantitative data was performed with two-way-ANOVA including the cohort and sex as independent variable as well as its interaction. For non-normal data unpaired Mann-Whitney or Kruskal-Wallis test ignoring any multiple comparisons were used. Statistical significance was defined as $P < 0.05$ (* $P < 0.05$, ** $P < 0.01$ and *** $P < 0.001$). All statistical evaluations mentioned above were performed with SAS®, version 9.4 TS level 1M5 (SAS Institute Inc., Cary, NC, United States). Graphical representation of the data was performed via GraphPad Prism 8 v. 8.4.2 (GraphPad Software, Inc.).

All data regarding the animal models were analysed with the Prism software (GraphPad, 8.4.3) using Kruskal-Wallis one-way analysis of variance (ANOVA) followed by Dunn's multiple comparisons test or unpaired two-tailed Student's *t*-test as indicated in the respective legends. Statistical significance was defined as $p < 0.05$ (* $p < 0.05$, ** $p < 0.01$, *** $p < 0.001$).

Detection of outliers were performed using Grubbs' test in GraphPad QuickCalcs Outlier Calculator.

Additionally, all ELISA data were evaluated using the "Four Parameter Logistic Curve" online data analysis tool, MyAssays Ltd., 25th October 2012, <http://www.myassays.com/four-parameter-logistic-curve.assay>.

7.2.10.4 Immunohistology and histopathology

Histological preparations and staining of murine tissue were performed by Gundula Pilnitz-Stolze. This includes treatment of formalin fixed samples, preparation of slides, staining and fixation.

Contact: Gundula Pilnitz-Stolze Heinrich Pette Institute

Heinrich-Pette-Institute- Leibniz Institute for Experimental Virology, Core facility: Imaging

Histological preparations and staining of hamster tissue were performed by Kathrin Becker and Georg Beythien. This includes treatment of formalin fixed samples, preparation of slides, staining and fixation.

Contact: Dr. Kathrin Becker, Georg Beythien

University of Veterinary Medicine, Hannover, Institute for Pathology

7.2.10.5 Statistical evaluation of COVID-19 patient cohort data analyzes

The statistical analyzes of all data referring to the COVID-19 patient cohort were evaluated by Prof. Dr. Lothar Kreienbrock and Bettina Schneider.

Contact: Prof. Dr. Lothar Kreienbrock, Bettina Schneider

University of Veterinary Medicine, Hannover, Institute for Biometrics, Epidemiology and Information processing

8 Literature

1. Johns Hopkins Coronavirus Resource Center. COVID-19 Map - Johns Hopkins Coronavirus Resource Center. *Johns Hopkins Coronavirus Resource Center* (2020).
2. Carstens, E. B. Ratification vote on taxonomic proposals to the International Committee on Taxonomy of Viruses (2009). *Arch. Virol.* (2010) doi:10.1007/s00705-009-0547-x.
3. Mihindukulasuriya, K. A., Wu, G., St. Leger, J., Nordhausen, R. W. & Wang, D. Identification of a Novel Coronavirus from a Beluga Whale by Using a Panviral Microarray. *J. Virol.* (2008) doi:10.1128/jvi.02722-07.
4. Woo, P. C. Y. *et al.* Comparative Analysis of Complete Genome Sequences of Three Avian Coronaviruses Reveals a Novel Group 3c Coronavirus. *J. Virol.* (2009) doi:10.1128/jvi.01977-08.
5. McIntosh, K. Coronaviruses: A Comparative Review. in *Current Topics in Microbiology and Immunology / Ergebnisse der Mikrobiologie und Immunitätsforschung* (1974). doi:10.1007/978-3-642-65775-7_3.
6. Artika, I. M., Dewantari, A. K. & Wiyatno, A. Molecular biology of coronaviruses: current knowledge. *Heliyon* (2020) doi:10.1016/j.heliyon.2020.e04743.
7. Beniac, D. R., Andonov, A., Grudeski, E. & Booth, T. F. Architecture of the SARS coronavirus prefusion spike. *Nat. Struct. Mol. Biol.* (2006) doi:10.1038/nsmb1123.
8. Walls, A. C. *et al.* Cryo-electron microscopy structure of a coronavirus spike glycoprotein trimer. *Nature* (2016) doi:10.1038/nature16988.
9. Bosch, B. J. & Rottier, P. J. M. Nidovirus Entry into Cells. in *Nidoviruses* (2014). doi:10.1128/9781555815790.ch11.
10. Weiss, S. R. & Navas-Martin, S. Coronavirus Pathogenesis and the Emerging Pathogen Severe Acute Respiratory Syndrome Coronavirus. *Microbiol. Mol. Biol. Rev.* (2005) doi:10.1128/mnbr.69.4.635-664.2005.
11. Du, L. *et al.* The spike protein of SARS-CoV - A target for vaccine and therapeutic development. *Nature Reviews Microbiology* (2009) doi:10.1038/nrmicro2090.
12. Cavanagh, D. Coronaviridae: a review of coronaviruses and toroviruses. in *Coronaviruses with Special Emphasis on First Insights Concerning SARS* (2005). doi:10.1007/3-7643-7339-3_1.
13. Sturman, L. S., Holmes, K. V & Behnke, J. Isolation of coronavirus envelope glycoproteins and interaction with the viral nucleocapsid. *J. Virol.* (1980) doi:10.1128/jvi.33.1.449-462.1980.
14. Armstrong, J., Niemann, H., Smeeckens, S., Rottier, P. & Warren, G. Sequence and topology of a model intracellular membrane protein, E1 glycoprotein, from a coronavirus. *Nature* (1984) doi:10.1038/308751a0.
15. Neuman, B. W. *et al.* A structural analysis of M protein in coronavirus assembly and morphology. *J. Struct. Biol.* (2011) doi:10.1016/j.jsb.2010.11.021.
16. Godet, M., L'Haridon, R., Vautherot, J. F. & Laude, H. TGEV corona virus ORF4

- encodes a membrane protein that is incorporated into virions. *Virology* (1992) doi:10.1016/0042-6822(92)90521-P.
17. Hogue, B. G. & Machamer, C. E. Coronavirus Structural Proteins and Virus Assembly. in *Nidoviruses* (2014). doi:10.1128/9781555815790.ch12.
 18. Chang, C. K. *et al.* Modular organization of SARS coronavirus nucleocapsid protein. *J. Biomed. Sci.* (2006) doi:10.1007/s11373-005-9035-9.
 19. Hurst, K. R., Koetzner, C. A. & Masters, P. S. Identification of In Vivo-Interacting Domains of the Murine Coronavirus Nucleocapsid Protein. *J. Virol.* (2009) doi:10.1128/jvi.00440-09.
 20. Cornelissen, L. A. *et al.* Hemagglutinin-esterase, a novel structural protein of torovirus. *J. Virol.* (1997) doi:10.1128/jvi.71.7.5277-5286.1997.
 21. Zhand, S. *et al.* Covid-19: The immune responses and clinical therapy candidates. *Int. J. Mol. Sci.* (2020) doi:10.3390/ijms21155559.
 22. Letko, M., Marzi, A. & Munster, V. Functional assessment of cell entry and receptor usage for SARS-CoV-2 and other lineage B betacoronaviruses. *Nat. Microbiol.* (2020) doi:10.1038/s41564-020-0688-y.
 23. Hoffmann, M. *et al.* SARS-CoV-2 Cell Entry Depends on ACE2 and TMPRSS2 and Is Blocked by a Clinically Proven Protease Inhibitor. *Cell* (2020) doi:10.1016/j.cell.2020.02.052.
 24. Walls, A. C. *et al.* Structure, Function, and Antigenicity of the SARS-CoV-2 Spike Glycoprotein. *Cell* (2020) doi:10.1016/j.cell.2020.02.058.
 25. Zhou, P. *et al.* A pneumonia outbreak associated with a new coronavirus of probable bat origin. *Nature* (2020) doi:10.1038/s41586-020-2012-7.
 26. Cantuti-Castelvetri, L. *et al.* Neuropilin-1 facilitates SARS-CoV-2 cell entry and infectivity. *Science* (80-.). (2020) doi:10.1126/science.abd2985.
 27. Daly, J. L. *et al.* Neuropilin-1 is a host factor for SARS-CoV-2 infection. *Science* (80-.). (2020) doi:10.1126/science.abd3072.
 28. Tortorici, M. A. & Veerler, D. Structural insights into coronavirus entry. in *Advances in Virus Research* (2019). doi:10.1016/bs.aivir.2019.08.002.
 29. Li, F. Structure, Function, and Evolution of Coronavirus Spike Proteins. *Annual Review of Virology* (2016) doi:10.1146/annurev-virology-110615-042301.
 30. Shang, J. *et al.* Cell entry mechanisms of SARS-CoV-2. *Proc. Natl. Acad. Sci. U. S. A.* (2020) doi:10.1073/pnas.2003138117.
 31. Gierer, S. *et al.* The Spike Protein of the Emerging Betacoronavirus EMC Uses a Novel Coronavirus Receptor for Entry, Can Be Activated by TMPRSS2, and Is Targeted by Neutralizing Antibodies. *J. Virol.* (2013) doi:10.1128/jvi.00128-13.
 32. Matsuyama, S. *et al.* Efficient Activation of the Severe Acute Respiratory Syndrome Coronavirus Spike Protein by the Transmembrane Protease TMPRSS2. *J. Virol.* (2010) doi:10.1128/jvi.01542-10.
 33. Perlman, S. & Netland, J. Coronaviruses post-SARS: Update on replication and pathogenesis. *Nature Reviews Microbiology* (2009) doi:10.1038/nrmicro2147.

Literature

34. Finkel, Y. *et al.* The coding capacity of SARS-CoV-2. *Nature* (2020) doi:10.1038/s41586-020-2739-1.
35. Snijder, E. J., Decroly, E. & Ziebuhr, J. The Nonstructural Proteins Directing Coronavirus RNA Synthesis and Processing. in *Advances in Virus Research* (2016). doi:10.1016/bs.aivir.2016.08.008.
36. Eckerle, L. D., Lu, X., Sperry, S. M., Choi, L. & Denison, M. R. High Fidelity of Murine Hepatitis Virus Replication Is Decreased in nsp14 Exoribonuclease Mutants. *J. Virol.* (2007) doi:10.1128/jvi.01296-07.
37. Zumla, A., Hui, D. S. & Perlman, S. Middle East respiratory syndrome. *The Lancet* (2015) doi:10.1016/S0140-6736(15)60454-8.
38. Sola, I., Almazán, F., Zúñiga, S. & Enjuanes, L. Continuous and Discontinuous RNA Synthesis in Coronaviruses. *Annual Review of Virology* (2015) doi:10.1146/annurev-virology-100114-055218.
39. de Haan, C. A. M. & Rottier, P. J. M. Molecular Interactions in the Assembly of Coronaviruses. *Advances in Virus Research* (2005) doi:10.1016/S0065-3527(05)64006-7.
40. Stertz, S. *et al.* The intracellular sites of early replication and budding of SARS-coronavirus. *Virology* (2007) doi:10.1016/j.virol.2006.11.027.
41. Ghosh, S. *et al.* β -Coronaviruses Use Lysosomal Organelles for Cellular Egress. *SSRN Electron. J.* (2020) doi:10.1101/2020.07.25.192310.
42. V'kovski, P., Kratzel, A., Steiner, S., Stalder, H. & Thiel, V. Coronavirus biology and replication: implications for SARS-CoV-2. *Nature Reviews Microbiology* (2020) doi:10.1038/s41579-020-00468-6.
43. Vijaykrishna, D. *et al.* Evolutionary Insights into the Ecology of Coronaviruses. *J. Virol.* (2007) doi:10.1128/jvi.02605-06.
44. Duffy, S., Shackelton, L. A. & Holmes, E. C. Rates of evolutionary change in viruses: Patterns and determinants. *Nature Reviews Genetics* (2008) doi:10.1038/nrg2323.
45. Li, W. *et al.* Bats are natural reservoirs of SARS-like coronaviruses. *Science* (80-.). (2005) doi:10.1126/science.1118391.
46. Wang, W. *et al.* Discovery, diversity and evolution of novel coronaviruses sampled from rodents in China. *Virology* (2015) doi:10.1016/j.virol.2014.10.017.
47. Woo, P. C. Y., Lau, S. K. P., Huang, Y. & Yuen, K. Y. Coronavirus diversity, phylogeny and interspecies jumping. *Experimental Biology and Medicine* (2009) doi:10.3181/0903-MR-94.
48. Forni, D., Cagliani, R., Clerici, M. & Sironi, M. Molecular Evolution of Human Coronavirus Genomes. *Trends in Microbiology* (2017) doi:10.1016/j.tim.2016.09.001.
49. Tao, Y. *et al.* Surveillance of Bat Coronaviruses in Kenya Identifies Relatives of Human Coronaviruses NL63 and 229E and Their Recombination History. *J. Virol.* (2017) doi:10.1128/jvi.01953-16.
50. Cui, J., Li, F. & Shi, Z. L. Origin and evolution of pathogenic coronaviruses. *Nature Reviews Microbiology* (2019) doi:10.1038/s41579-018-0118-9.

Literature

51. Lau, S. K. P. *et al.* Severe acute respiratory syndrome coronavirus-like virus in Chinese horseshoe bats. *Proc. Natl. Acad. Sci. U. S. A.* (2005) doi:10.1073/pnas.0506735102.
52. Ge, X. Y. *et al.* Isolation and characterization of a bat SARS-like coronavirus that uses the ACE2 receptor. *Nature* (2013) doi:10.1038/nature12711.
53. Hu, B. *et al.* Discovery of a rich gene pool of bat SARS-related coronaviruses provides new insights into the origin of SARS coronavirus. *PLoS Pathog.* (2017) doi:10.1371/journal.ppat.1006698.
54. Zhou, H. *et al.* A Novel Bat Coronavirus Closely Related to SARS-CoV-2 Contains Natural Insertions at the S1/S2 Cleavage Site of the Spike Protein. *Curr. Biol.* (2020) doi:10.1016/j.cub.2020.05.023.
55. Xiao, K. *et al.* Isolation of SARS-CoV-2-related coronavirus from Malayan pangolins. *Nature* (2020) doi:10.1038/s41586-020-2313-x.
56. Liu, P. *et al.* Are pangolins the intermediate host of the 2019 novel coronavirus (SARS-CoV-2)? *PLoS Pathogens* (2020) doi:10.1371/journal.ppat.1008421.
57. Drexler, J. F., Corman, V. M. & Drosten, C. Ecology, evolution and classification of bat coronaviruses in the aftermath of SARS. *Antiviral Research* (2014) doi:10.1016/j.antiviral.2013.10.013.
58. Anthony, S. J. *et al.* Global patterns in coronavirus diversity. *Virus Evol.* (2017) doi:10.1093/ve/vex012.
59. Wong, A. C. P., Li, X., Lau, S. K. P. & Woo, P. C. Y. Global epidemiology of bat coronaviruses. *Viruses* (2019) doi:10.3390/v11020174.
60. Smith, A. T. & Xie, Y. *Mammals of China. Mammals of China* (2013). doi:10.1093/jmammal/gyu023.
61. Olival, K. J. *et al.* Host and viral traits predict zoonotic spillover from mammals. *Nature* (2017) doi:10.1038/nature22975.
62. Zhang, G. *et al.* Comparative analysis of bat genomes provides insight into the evolution of flight and immunity. *Science* (80-.). (2013) doi:10.1126/science.1230835.
63. Peck, K. M., Burch, C. L., Heise, M. T. & Baric, R. S. Coronavirus Host Range Expansion and Middle East Respiratory Syndrome Coronavirus Emergence: Biochemical Mechanisms and Evolutionary Perspectives. *Annual Review of Virology* (2015) doi:10.1146/annurev-virology-100114-055029.
64. Andersen, K. G., Rambaut, A., Lipkin, W. I., Holmes, E. C. & Garry, R. F. The proximal origin of SARS-CoV-2. *Nature Medicine* (2020) doi:10.1038/s41591-020-0820-9.
65. Coutard, B. *et al.* The spike glycoprotein of the new coronavirus 2019-nCoV contains a furin-like cleavage site absent in CoV of the same clade. *Antiviral Res.* (2020) doi:10.1016/j.antiviral.2020.104742.
66. Wrobel, A. G. *et al.* SARS-CoV-2 and bat RaTG13 spike glycoprotein structures inform on virus evolution and furin-cleavage effects. *Nat. Struct. Mol. Biol.* (2020) doi:10.1038/s41594-020-0468-7.
67. Corman, V. M., Muth, D., Niemeyer, D. & Drosten, C. Hosts and Sources of Endemic Human Coronaviruses. in *Advances in Virus Research* (2018).

- doi:10.1016/bs.aivir.2018.01.001.
68. Killerby, M. E. *et al.* Human coronavirus circulation in the United States 2014–2017. *J. Clin. Virol.* (2018) doi:10.1016/j.jcv.2018.01.019.
 69. Varghese, L. *et al.* Epidemiology and clinical features of human coronaviruses in the pediatric population. *J. Pediatric Infect. Dis. Soc.* (2018) doi:10.1093/jpids/pix027.
 70. Gorse, G. J., O’Connor, T. Z., Hall, S. L., Vitale, J. N. & Nichol, K. L. Human coronavirus and acute respiratory illness in older adults with chronic obstructive pulmonary disease. *J. Infect. Dis.* (2009) doi:10.1086/597122.
 71. Walsh, E. E., Shin, J. H. & Falsey, A. R. Clinical impact of human coronaviruses 229E and OC43 infection in diverse adult populations. *J. Infect. Dis.* (2013) doi:10.1093/infdis/jit393.
 72. Pyrc, K., Berkhout, B. & van der Hoek, L. The Novel Human Coronaviruses NL63 and HKU1. *J. Virol.* (2007) doi:10.1128/jvi.01466-06.
 73. Abdul-Rasool, S. & Fielding, B. C. Understanding Human Coronavirus HCoV-NL63. *Open Virol. J.* (2010).
 74. Kaye, H. S. & Dowdle, W. R. Seroepidemiologic survey of coronavirus (strain 229e) infections in a population of children. *Am. J. Epidemiol.* (1975) doi:10.1093/oxfordjournals.aje.a112091.
 75. Isaacs, D., Flowers, D., Clarke, J. R., Valman, H. B. & MacNaughton, M. R. Epidemiology of coronavirus respiratory infections. *Arch. Dis. Child.* (1983) doi:10.1136/adc.58.7.500.
 76. Zhong, N. S. *et al.* Epidemiology and cause of severe acute respiratory syndrome (SARS) in Guangdong, People’s Republic of China, in February, 2003. *Lancet* (2003) doi:10.1016/S0140-6736(03)14630-2.
 77. Centers for Disease, C. & Prevention. Update: Outbreak of severe acute respiratory syndrome--worldwide, 2003.[Erratum appears in MMWR Morb Mortal Wkly Rep. 2003 Apr 4;52(13):284]. *MMWR - Morb. Mortal. Wkly. Rep.* (2003).
 78. Peiris, J. S. M. *et al.* Coronavirus as a possible cause of severe acute respiratory syndrome. *Lancet* (2003) doi:10.1016/S0140-6736(03)13077-2.
 79. Poutanen, S. M. *et al.* Identification of Severe Acute Respiratory Syndrome in Canada. *N. Engl. J. Med.* (2003) doi:10.1056/nejmoa030634.
 80. Ksiazek, T. G. *et al.* A Novel Coronavirus Associated with Severe Acute Respiratory Syndrome. *N. Engl. J. Med.* (2003) doi:10.1056/nejmoa030781.
 81. Drosten, C. *et al.* Identification of a Novel Coronavirus in Patients with Severe Acute Respiratory Syndrome. *N. Engl. J. Med.* (2003) doi:10.1056/nejmoa030747.
 82. Guan, Y. *et al.* Isolation and characterization of viruses related to the SARS coronavirus from animals in Southern China. *Science* (80-.). (2003) doi:10.1126/science.1087139.
 83. Leung, D. T. M. *et al.* Extremely Low Exposure of a Community to Severe Acute Respiratory Syndrome Coronavirus: False Seropositivity due to Use of Bacterially Derived Antigens. *J. Virol.* (2006) doi:10.1128/jvi.00649-06.

84. Chan, K. H. *et al.* Detection of SARS Coronavirus in Patients with Suspected SARS. *Emerg. Infect. Dis.* (2004) doi:10.3201/eid1002.030610.
85. Seto, W. H. *et al.* Effectiveness of precautions against droplets and contact in prevention of nosocomial transmission of severe acute respiratory syndrome (SARS). *Lancet* (2003) doi:10.1016/S0140-6736(03)13168-6.
86. Lee, N. *et al.* A Major Outbreak of Severe Acute Respiratory Syndrome in Hong Kong. *N. Engl. J. Med.* (2003) doi:10.1056/nejmoa030685.
87. Christian, M. D. *et al.* Possible SARS Coronavirus Transmission during Cardiopulmonary Resuscitation. *Emerg. Infect. Dis.* (2004) doi:10.3201/eid1002.030700.
88. Varia, M. *et al.* Investigation of a nosocomial outbreak of severe acute respiratory syndrome (SARS) in Toronto, Canada. *CMAJ* (2003).
89. Hung, I. F. N. *et al.* Viral loads in clinical specimens and SARS manifestations. *Emerg. Infect. Dis.* (2004) doi:10.3201/eid1009.040058.
90. Peiris, J. S. M. *et al.* Clinical progression and viral load in a community outbreak of coronavirus-associated SARS pneumonia: A prospective study. *Lancet* (2003) doi:10.1016/S0140-6736(03)13412-5.
91. Liang, G. *et al.* Laboratory diagnosis of four recent sporadic cases of community-acquired SARS, Guangdong Province, China. *Emerg. Infect. Dis.* (2004) doi:10.3201/eid1010.040445.
92. Lim, P. L. *et al.* Laboratory-Acquired Severe Acute Respiratory Syndrome. *N. Engl. J. Med.* (2004) doi:10.1056/nejmoa032565.
93. Zaki, A. M., van Boheemen, S., Bestebroer, T. M., Osterhaus, A. D. M. E. & Fouchier, R. A. M. Isolation of a Novel Coronavirus from a Man with Pneumonia in Saudi Arabia. *N. Engl. J. Med.* (2012) doi:10.1056/nejmoa1211721.
94. de Groot, R. J. *et al.* Middle East Respiratory Syndrome Coronavirus (MERS-CoV): Announcement of the Coronavirus Study Group. *J. Virol.* (2013) doi:10.1128/jvi.01244-13.
95. Bermingham, A. *et al.* Severe respiratory illness caused by a novel coronavirus, in a patient transferred to the United Kingdom from the Middle East, September 2012. *Eurosurveillance* (2012) doi:10.2807/ese.17.40.20290-en.
96. Lee, J. Y. *et al.* The clinical and virological features of the first imported case causing MERS-CoV outbreak in South Korea, 2015. *BMC Infect. Dis.* (2017) doi:10.1186/s12879-017-2576-5.
97. Hsieh, Y. H. 2015 Middle East Respiratory Syndrome Coronavirus (MERS-CoV) nosocomial outbreak in South Korea: Insights from modeling. *PeerJ* (2015) doi:10.7717/peerj.1505.
98. Cowling, B. J. *et al.* Preliminary epidemiological assessment of MERS-CoV outbreak in South Korea, may to june 2015. *Eurosurveillance* (2015) doi:10.2807/1560-7917.ES2015.20.25.21163.
99. Ki, M. 2015 MERS outbreak in Korea: hospital-to-hospital transmission. *Epidemiol. Health* (2015) doi:10.4178/epih/e2015033.

100. Alagaili, A. N. *et al.* Middle east respiratory syndrome coronavirus infection in dromedary camels in Saudi Arabia. *MBio* (2014) doi:10.1128/mBio.00884-14.
101. Chan, R. W. Y. *et al.* Tropism and replication of Middle East respiratory syndrome coronavirus from dromedary camels in the human respiratory tract: An in-vitro and ex-vivo study. *Lancet Respir. Med.* (2014) doi:10.1016/S2213-2600(14)70158-4.
102. Yusof, M. F. *et al.* Prevalence of Middle East respiratory syndrome coronavirus (MERS-CoV) in dromedary camels in Abu Dhabi Emirate, United Arab Emirates. *Virus Genes* (2015) doi:10.1007/s11262-015-1174-0.
103. Müller, M. A. *et al.* Mers coronavirus neutralizing antibodies in camels, eastern Africa, 1983–1997. *Emerg. Infect. Dis.* (2014) doi:10.3201/eid2012.141026.
104. Corman, V. M. *et al.* Rooting the Phylogenetic Tree of Middle East Respiratory Syndrome Coronavirus by Characterization of a Conspecific Virus from an African Bat. *J. Virol.* (2014) doi:10.1128/jvi.01498-14.
105. Conzade, R. *et al.* Reported direct and indirect contact with dromedary camels among laboratory-confirmed MERS-CoV cases. *Viruses* (2018) doi:10.3390/v10080425.
106. Assiri, A. *et al.* Multifacility outbreak of middle east respiratory syndrome in Taif, Saudi Arabia. *Emerg. Infect. Dis.* (2016) doi:10.3201/eid2201.151370.
107. Assiri, A. *et al.* Hospital Outbreak of Middle East Respiratory Syndrome Coronavirus. *N. Engl. J. Med.* (2013) doi:10.1056/nejmoa1306742.
108. Balkhy, H. H. *et al.* Description of a hospital outbreak of middle east respiratory syndrome in a large tertiary care hospital in Saudi Arabia. *Infect. Control Hosp. Epidemiol.* (2016) doi:10.1017/ice.2016.132.
109. Oboho, I. K. *et al.* 2014 MERS-CoV Outbreak in Jeddah — A Link to Health Care Facilities. *N. Engl. J. Med.* (2015) doi:10.1056/nejmoa1408636.
110. Drosten, C. *et al.* Transmission of MERS-Coronavirus in Household Contacts. *N. Engl. J. Med.* (2014) doi:10.1056/nejmoa1405858.
111. Memish, Z. A., Zumla, A. I., Al-Hakeem, R. F., Al-Rabeeh, A. A. & Stephens, G. M. Family Cluster of Middle East Respiratory Syndrome Coronavirus Infections. *N. Engl. J. Med.* (2013) doi:10.1056/nejmoa1303729.
112. Omrani, A. S., Al-Tawfiq, J. A. & Memish, Z. A. Middle east respiratory syndrome coronavirus (Mers-coV): Animal to human interaction. *Pathogens and Global Health* (2015) doi:10.1080/20477724.2015.1122852.
113. Azhar, E. I. *et al.* Detection of the middle east respiratory syndrome coronavirus genome in an air sample originating from a camel barn owned by an infected patient. *MBio* (2014) doi:10.1128/mBio.01450-14.
114. Alraddadi, B. M. *et al.* Risk factors for primary middle east respiratory syndrome coronavirus illness in humans, Saudi Arabia, 2014. *Emerg. Infect. Dis.* (2016) doi:10.3201/eid2201.151340.
115. mers-cases-2019e2d47241b73348d5aaf74068c74fddb9. (2019).
116. WHO. *Novel Coronavirus (2019-nCoV). Situation Report-1* (2020).
117. Lu, H., Stratton, C. W. & Tang, Y. W. Outbreak of pneumonia of unknown etiology in

- Wuhan, China: The mystery and the miracle. *Journal of Medical Virology* (2020) doi:10.1002/jmv.25678.
118. Huang, C. *et al.* Clinical features of patients infected with 2019 novel coronavirus in Wuhan, China. *Lancet* (2020) doi:10.1016/S0140-6736(20)30183-5.
 119. WHO. *World Health Organization. Pneumonia of unknown cause – China. Disease outbreak news: 5 January 2020* (2020).
 120. Chan, J. F. W. *et al.* A familial cluster of pneumonia associated with the 2019 novel coronavirus indicating person-to-person transmission: a study of a family cluster. *Lancet* (2020) doi:10.1016/S0140-6736(20)30154-9.
 121. Gralinski, L. E. & Menachery, V. D. Return of the coronavirus: 2019-nCoV. *Viruses* (2020) doi:10.3390/v12020135.
 122. Zhu, N. *et al.* A Novel Coronavirus from Patients with Pneumonia in China, 2019. *N. Engl. J. Med.* (2020) doi:10.1056/nejmoa2001017.
 123. Deng, S.-Q. & Peng, H.-J. Characteristics of and Public Health Responses to the Coronavirus Disease 2019 Outbreak in China. *J. Clin. Med.* (2020) doi:10.3390/jcm9020575.
 124. Wang, R., Zhang, X., Irwin, D. M. & Shen, Y. Emergence of SARS-like coronavirus poses new challenge in China. *Journal of Infection* (2020) doi:10.1016/j.jinf.2020.01.017.
 125. Eurosurveillance Editorial Team. Note from the editors: World Health Organization declares novel coronavirus (2019-nCoV) sixth public health emergency of international concern. *Euro Surveill.* (2020) doi:10.2807/1560-7917.ES.2020.25.5.200131e.
 126. Fisher, D. & Heymann, D. Q&A: The novel coronavirus outbreak causing COVID-19. *BMC Medicine* (2020) doi:10.1186/s12916-020-01533-w.
 127. Lai, C. C., Shih, T. P., Ko, W. C., Tang, H. J. & Hsueh, P. R. Severe acute respiratory syndrome coronavirus 2 (SARS-CoV-2) and coronavirus disease-2019 (COVID-19): The epidemic and the challenges. *International Journal of Antimicrobial Agents* (2020) doi:10.1016/j.ijantimicag.2020.105924.
 128. World Health Organization. Situation Report-51 SITUATION IN NUMBERS total and new cases in last 24 hours. *Coronavirus Dis. 2019* (2020).
 129. Wang, D. *et al.* Clinical Characteristics of 138 Hospitalized Patients with 2019 Novel Coronavirus-Infected Pneumonia in Wuhan, China. *JAMA - J. Am. Med. Assoc.* (2020) doi:10.1001/jama.2020.1585.
 130. Zhang, J. jin *et al.* Clinical characteristics of 140 patients infected with SARS-CoV-2 in Wuhan, China. *Allergy Eur. J. Allergy Clin. Immunol.* (2020) doi:10.1111/all.14238.
 131. Cao, M. *et al.* Clinical Features of Patients Infected with the 2019 Novel Coronavirus (COVID-19) in Shanghai, China. *medRxiv Prepr. Serv. Heal. Sci.* (2020) doi:10.1101/2020.03.04.20030395.
 132. Jin, J. M. *et al.* Gender Differences in Patients With COVID-19: Focus on Severity and Mortality. *Front. Public Heal.* (2020) doi:10.3389/fpubh.2020.00152.
 133. Rubin, S. J. S., Falkson, S. R., Degner, N. R. & Blish, C. Clinical characteristics associated with COVID-19 severity in California. *J. Clin. Transl. Sci.* (2020)

- doi:10.1017/cts.2020.40.
134. Petrilli, C. M. *et al.* Factors associated with hospital admission and critical illness among 5279 people with coronavirus disease 2019 in New York City: Prospective cohort study. *BMJ* (2020) doi:10.1136/bmj.m1966.
 135. Hu, L. *et al.* Risk Factors Associated With Clinical Outcomes in 323 Coronavirus Disease 2019 (COVID-19) Hospitalized Patients in Wuhan, China. *Clin. Infect. Dis.* (2020) doi:10.1093/cid/ciaa539.
 136. Qu, R. *et al.* Platelet-to-lymphocyte ratio is associated with prognosis in patients with coronavirus disease-19. *J. Med. Virol.* (2020) doi:10.1002/jmv.25767.
 137. Guo, W. *et al.* Diabetes is a risk factor for the progression and prognosis of COVID-19. *Diabetes. Metab. Res. Rev.* (2020) doi:10.1002/dmrr.3319.
 138. Ding, T. *et al.* Potential Influence of Menstrual Status and Sex Hormones on female SARS-CoV-2 Infection: A Cross-sectional Study from Multicentre in Wuhan, China. *Clin. Infect. Dis.* (2020) doi:10.1093/cid/ciaa1022.
 139. Johns Hopkins. Coronavirus Resource Center. *Johns Hopkins Coronavirus Resource Center* (2021).
 140. European Center for Disease Prevention and Control. Outbreak of novel coronavirus disease 2019 (COVID-19): increased transmission globally – fifth update. *Rapid Risk Assess.* (2020).
 141. Hu, B., Guo, H., Zhou, P. & Shi, Z. L. Characteristics of SARS-CoV-2 and COVID-19. *Nature Reviews Microbiology* (2020) doi:10.1038/s41579-020-00459-7.
 142. Medicine, L. S. of H. and T. COVID-19 Vaccine Tracker. *COVID-19 Vaccine Tracker* (2021).
 143. Zumla, A., Chan, J. F. W., Azhar, E. I., Hui, D. S. C. & Yuen, K. Y. Coronaviruses—drug discovery and therapeutic options. *Nature Reviews Drug Discovery* (2016) doi:10.1038/nrd.2015.37.
 144. Chan, J. F. W. *et al.* Middle East Respiratory syndrome coronavirus: Another zoonotic betacoronavirus causing SARS-like disease. *Clin. Microbiol. Rev.* (2015) doi:10.1128/CMR.00102-14.
 145. Smith, T. R. F. *et al.* Immunogenicity of a DNA vaccine candidate for COVID-19. *Nat. Commun.* (2020) doi:10.1038/s41467-020-16505-0.
 146. Zhu, F. C. *et al.* Safety, tolerability, and immunogenicity of a recombinant adenovirus type-5 vectored COVID-19 vaccine: a dose-escalation, open-label, non-randomised, first-in-human trial. *Lancet* (2020) doi:10.1016/S0140-6736(20)31208-3.
 147. Gao, Q. *et al.* Development of an inactivated vaccine candidate for SARS-CoV-2. *Science* (80-.). (2020) doi:10.1126/science.abc1932.
 148. Krammer, F. SARS-CoV-2 vaccines in development. *Nature* (2020) doi:10.1038/s41586-020-2798-3.
 149. Lian, N. *et al.* Umifenovir treatment is not associated with improved outcomes in patients with coronavirus disease 2019: a retrospective study. *Clin. Microbiol. Infect.* (2020) doi:10.1016/j.cmi.2020.04.026.

150. Wang, X. *et al.* The anti-influenza virus drug, arbidol is an efficient inhibitor of SARS-CoV-2 in vitro. *Cell Discovery* (2020) doi:10.1038/s41421-020-0169-8.
151. Zhu, Z. *et al.* Arbidol monotherapy is superior to lopinavir/ritonavir in treating COVID-19. *J. Infect.* (2020) doi:10.1016/j.jinf.2020.03.060.
152. Li, Y. *et al.* Efficacy and Safety of Lopinavir/Ritonavir or Arbidol in Adult Patients with Mild/Moderate COVID-19: An Exploratory Randomized Controlled Trial. *Med* (2020) doi:10.1016/j.medj.2020.04.001.
153. Wang, M. *et al.* Remdesivir and chloroquine effectively inhibit the recently emerged novel coronavirus (2019-nCoV) in vitro. *Cell Research* (2020) doi:10.1038/s41422-020-0282-0.
154. Yao, X. *et al.* In vitro antiviral activity and projection of optimized dosing design of hydroxychloroquine for the treatment of severe acute respiratory syndrome coronavirus 2 (SARS-CoV-2). *Clin. Infect. Dis.* (2020) doi:10.1093/cid/ciaa237.
155. Geleris, J. *et al.* Observational Study of Hydroxychloroquine in Hospitalized Patients with Covid-19. *N. Engl. J. Med.* (2020) doi:10.1056/nejmoa2012410.
156. Rosenberg, E. S. *et al.* Association of Treatment with Hydroxychloroquine or Azithromycin with In-Hospital Mortality in Patients with COVID-19 in New York State. *JAMA - J. Am. Med. Assoc.* (2020) doi:10.1001/jama.2020.8630.
157. Monteil, V. *et al.* Inhibition of SARS-CoV-2 Infections in Engineered Human Tissues Using Clinical-Grade Soluble Human ACE2. *Cell* (2020) doi:10.1016/j.cell.2020.04.004.
158. Tian, X. *et al.* Potent binding of 2019 novel coronavirus spike protein by a SARS coronavirus-specific human monoclonal antibody. *Emerging Microbes and Infections* (2020) doi:10.1080/22221751.2020.1729069.
159. Xia, S. *et al.* Inhibition of SARS-CoV-2 (previously 2019-nCoV) infection by a highly potent pan-coronavirus fusion inhibitor targeting its spike protein that harbors a high capacity to mediate membrane fusion. *Cell Res.* (2020) doi:10.1038/s41422-020-0305-x.
160. Grein, J. *et al.* Compassionate Use of Remdesivir for Patients with Severe Covid-19. *N. Engl. J. Med.* (2020) doi:10.1056/nejmoa2007016.
161. Beigel, J. H. *et al.* Remdesivir for the Treatment of Covid-19 — Final Report. *N. Engl. J. Med.* (2020) doi:10.1056/nejmoa2007764.
162. Cai, Q. *et al.* Experimental Treatment with Favipiravir for COVID-19: An Open-Label Control Study. *Engineering* (2020) doi:10.1016/j.eng.2020.03.007.
163. Chen, F. *et al.* In vitro susceptibility of 10 clinical isolates of SARS coronavirus to selected antiviral compounds. *J. Clin. Virol.* (2004) doi:10.1016/j.jcv.2004.03.003.
164. De Wilde, A. H. *et al.* Screening of an FDA-approved compound library identifies four small-molecule inhibitors of Middle East respiratory syndrome coronavirus replication in cell culture. *Antimicrob. Agents Chemother.* (2014) doi:10.1128/AAC.03011-14.
165. Mehta, P. *et al.* COVID-19: consider cytokine storm syndromes and immunosuppression. *The Lancet* (2020) doi:10.1016/S0140-6736(20)30628-0.
166. Dexamethasone in Hospitalized Patients with Covid-19 — Preliminary Report. *N.*

- Engl. J. Med.* (2020) doi:10.1056/nejmoa2021436.
167. Xu, X. *et al.* Effective treatment of severe COVID-19 patients with tocilizumab. *Proc. Natl. Acad. Sci. U. S. A.* (2020) doi:10.1073/pnas.2005615117.
 168. Sallard, E., Lescure, F. X., Yazdanpanah, Y., Mentre, F. & Peiffer-Smadja, N. Type 1 interferons as a potential treatment against COVID-19. *Antiviral Res.* (2020) doi:10.1016/j.antiviral.2020.104791.
 169. Shen, C. *et al.* Treatment of 5 Critically Ill Patients with COVID-19 with Convalescent Plasma. *JAMA - J. Am. Med. Assoc.* (2020) doi:10.1001/jama.2020.4783.
 170. Duan, K. *et al.* Effectiveness of convalescent plasma therapy in severe COVID-19 patients. *Proc. Natl. Acad. Sci. U. S. A.* (2020) doi:10.1073/pnas.2004168117.
 171. Wang, C. *et al.* A human monoclonal antibody blocking SARS-CoV-2 infection. *Nat. Commun.* (2020) doi:10.1038/s41467-020-16256-y.
 172. Wu, Y. *et al.* A noncompeting pair of human neutralizing antibodies block COVID-19 virus binding to its receptor ACE2. *Science* (80-.). (2020) doi:10.1126/science.abc2241.
 173. Zost, S. J. *et al.* Potently neutralizing and protective human antibodies against SARS-CoV-2. *Nature* (2020) doi:10.1038/s41586-020-2548-6.
 174. Shi, R. *et al.* A human neutralizing antibody targets the receptor-binding site of SARS-CoV-2. *Nature* (2020) doi:10.1038/s41586-020-2381-y.
 175. Sathish, V., Martin, Y. N. & Prakash, Y. S. Sex steroid signaling: Implications for lung diseases. *Pharmacology and Therapeutics* (2015) doi:10.1016/j.pharmthera.2015.01.007.
 176. Labrie, F. *et al.* Is dehydroepiandrosterone a hormone? *Journal of Endocrinology* (2005) doi:10.1677/joe.1.06264.
 177. RITTENBERG, D. & BLOCH, K. The utilization of acetic acid for the synthesis of fatty acids. *J. Biol. Chem.* (1945).
 178. Bloch, K. & Rittenberg, D. ON THE UTILIZATION OF ACETIC ACID FOR CHOLESTEROL FORMATION. *J. Biol. Chem.* (1942) doi:10.1016/s0021-9258(18)51303-x.
 179. Little, H. N. & Bloch, K. STUDIES ON THE UTILIZATION OF ACETIC ACID FOR THE BIOLOGICAL SYNTHESIS OF CHOLESTEROL. *J. Biol. Chem.* (1950) doi:10.1016/s0021-9258(18)56441-3.
 180. Penning, T. M. Molecular endocrinology of hydroxysteroid dehydrogenases. *Endocrine Reviews* (1997) doi:10.1210/er.18.3.281.
 181. Debes, J. D. & Tindall, D. J. The role of androgens and the androgen receptor in prostate cancer. *Cancer Letters* (2002) doi:10.1016/S0304-3835(02)00413-5.
 182. Nelson, L. R. & Bulun, S. E. Estrogen production and action. *J. Am. Acad. Dermatol.* (2001) doi:10.1067/mjd.2001.117432.
 183. Schiffer, L. *et al.* Human steroid biosynthesis, metabolism and excretion are differentially reflected by serum and urine steroid metabolomes: A comprehensive review. *Journal of Steroid Biochemistry and Molecular Biology* (2019)

- doi:10.1016/j.jsbmb.2019.105439.
184. Klein, S. L. & Huber, S. Sex differences in susceptibility to viral infection. in *Sex Hormones and Immunity to Infection* (2010). doi:10.1007/978-3-642-02155-8_4.
 185. Bouman, A., Schipper, M., Heineman, M. J. & Faas, M. M. Gender difference in the non-specific and specific immune response in humans. *Am. J. Reprod. Immunol.* (2004) doi:10.1111/j.1600-0897.2004.00177.x.
 186. Dao, H. & Kazin, R. A. Gender differences in skin: A review of the literature. *Gend. Med.* (2007) doi:10.1016/S1550-8579(07)80061-1.
 187. Klein, S. L. The effects of hormones on sex differences in infection: From genes to behavior. *Neuroscience and Biobehavioral Reviews* (2000) doi:10.1016/S0149-7634(00)00027-0.
 188. Napravnik, S., Poole, C., Thomas, J. C. & Eron, J. J. Gender difference in HIV RNA levels: A meta-analysis of published studies. *J. Acquir. Immune Defic. Syndr.* (2002) doi:10.1097/00126334-200209010-00002.
 189. Ainbender, E., Weisinger, R. B., Hevizi, M. & Hodes, H. L. Difference in the immunoglobulin class of polioantibody in the serum of men and women. *J. Immunol.* (1968).
 190. Rowley, M. J. & Mackay, I. R. Measurement of antibody-producing capacity in man. I. The normal response to flagellin from *Salmonella adelaide*. *Clin. Exp. Immunol.* (1969).
 191. Farzadegan, H. *et al.* Sex differences in HIV-1 viral load and progression to AIDS. *Lancet* (1998) doi:10.1016/S0140-6736(98)02372-1.
 192. WHO. Sex, gender and influenza. (2010).
 193. Klein, S. L., Hodgson, A. & Robinson, D. P. Mechanisms of sex disparities in influenza pathogenesis. *J. Leukoc. Biol.* (2012) doi:10.1189/jlb.0811427.
 194. Klein, S. L. Sex influences immune responses to viruses, and efficacy of prophylaxis and treatments for viral diseases. *BioEssays* (2012) doi:10.1002/bies.201200099.
 195. Straub, R. H. *et al.* Sex hormone concentrations in patients with rheumatoid arthritis are not normalized during 12 weeks of anti-tumor necrosis factor therapy. *J. Rheumatol.* (2005).
 196. Cunningham, M. & Gilkeson, G. Estrogen receptors in immunity and autoimmunity. *Clin. Rev. Allergy Immunol.* (2011) doi:10.1007/s12016-010-8203-5.
 197. Rochira, V. *et al.* Estrogens in males: What have we learned in the last 10 years? *Asian Journal of Andrology* (2005) doi:10.1111/j.1745-7262.2005.00018.x.
 198. Bouman, A., Jan Heineman, M. & Faas, M. M. Sex hormones and the immune response in humans. *Human Reproduction Update* (2005) doi:10.1093/humupd/dmi008.
 199. Heldring, N. *et al.* Estrogen receptors: How do they signal and what are their targets. *Physiological Reviews* (2007) doi:10.1152/physrev.00026.2006.
 200. Ackerman, L. S. Sex hormones and the genesis of autoimmunity. *Archives of Dermatology* (2006) doi:10.1001/archderm.142.3.371.

201. Filardo, E. J. & Thomas, P. Minireview: G protein-coupled estrogen receptor-1, GPER-1: Its mechanism of action and role in female reproductive cancer, renal and vascular physiology. *Endocrinology* (2012) doi:10.1210/en.2012-1061.
202. Bhatia, A., Sekhon, H. K. & Kaur, G. Sex hormones and immune dimorphism. *Scientific World Journal* (2014) doi:10.1155/2014/159150.
203. Mizushima, T. & Miyamoto, H. The Role of Androgen Receptor Signaling in Ovarian Cancer. *Cells* (2019) doi:10.3390/cells8020176.
204. Bupp, M. R. G. & Jorgensen, T. N. Androgen-induced immunosuppression. *Frontiers in Immunology* (2018) doi:10.3389/fimmu.2018.00794.
205. Mantalaris, A. *et al.* Localization of androgen receptor expression in human bone marrow. *J. Pathol.* (2001) doi:10.1002/1096-9896(0000)9999:9999::AID-PATH803>3.0.CO;2-W.
206. Walecki, M. *et al.* Androgen receptor modulates Foxp3 expression in CD4+CD25+Foxp3+ regulatory T-cells. *Mol. Biol. Cell* (2015) doi:10.1091/mbc.E14-08-1323.
207. Chen, W. C. *et al.* Human mast cells express androgen receptors but treatment with testosterone exerts no influence on IgE-independent mast cell degranulation elicited by neuromuscular blocking agents. *Experimental Dermatology* (2010) doi:10.1111/j.1600-0625.2009.00969.x.
208. Lai, J. J. *et al.* Monocyte/macrophage androgen receptor suppresses cutaneous wound healing in mice by enhancing local TNF- α expression. *J. Clin. Invest.* (2009) doi:10.1172/JCI39335.
209. BENTEN, W. P. M. *et al.* Functional testosterone receptors in plasma membranes of T cells. *FASEB J.* (1999) doi:10.1096/fasebj.13.1.123.
210. Benten, W. P. M., Becker, A., Schmitt-Wrede, H. P. & Wunderlich, F. Developmental regulation of intracellular and surface androgen receptors in T cells. *Steroids* (2002) doi:10.1016/S0039-128X(02)00055-7.
211. Khetawat, G. *et al.* Human megakaryocytes and platelets contain the estrogen receptor β and androgen receptor (AR): Testosterone regulates AR expression. *Blood* (2000) doi:10.1182/blood.v95.7.2289.
212. Viselli, S. M., Reese, K. R., Fan, J., Kovacs, W. J. & Olsen, N. J. Androgens alter B cell development in normal male mice. *Cell. Immunol.* (1997) doi:10.1006/cimm.1997.1227.
213. Berg, A. H., Rice, C. D., Rahman, M. S., Dong, J. & Thomas, P. Identification and characterization of membrane androgen receptors in the ZIP9 zinc transporter subfamily: I. Discovery in female atlantic croaker and evidence ZIP9 mediates testosterone-induced apoptosis of ovarian follicle cells. *Endocrinology* (2014) doi:10.1210/en.2014-1198.
214. Thomas, P., Pang, Y., Dong, J. & Berg, A. H. Identification and characterization of membrane androgen receptors in the ZIP9 zinc transporter subfamily: II. Role of human ZIP9 in testosterone-induced prostate and breast cancer cell apoptosis. *Endocrinology* (2014) doi:10.1210/en.2014-1201.
215. Bulldan, A., Dietze, R., Shihan, M. & Scheiner-Bobis, G. Non-classical testosterone

- signaling mediated through ZIP9 stimulates claudin expression and tight junction formation in Sertoli cells. *Cell. Signal.* (2016) doi:10.1016/j.cellsig.2016.04.015.
216. Mesev, E. V., LeDesma, R. A. & Ploss, A. Decoding type I and III interferon signalling during viral infection. *Nature Microbiology* (2019) doi:10.1038/s41564-019-0421-x.
217. Laffont, S. *et al.* X-Chromosome Complement and Estrogen Receptor Signaling Independently Contribute to the Enhanced TLR7-Mediated IFN- α Production of Plasmacytoid Dendritic Cells from Women. *J. Immunol.* (2014) doi:10.4049/jimmunol.1303400.
218. Seillet, C. *et al.* The TLR-mediated response of plasmacytoid dendritic cells is positively regulated by estradiol in vivo through cell-intrinsic estrogen receptor α signaling. *Blood* (2012) doi:10.1182/blood-2011-08-371831.
219. Berghöfer, B. *et al.* TLR7 Ligands Induce Higher IFN- α Production in Females. *J. Immunol.* (2006) doi:10.4049/jimmunol.177.4.2088.
220. Meier, A. *et al.* Sex differences in the Toll-like receptor-mediated response of plasmacytoid dendritic cells to HIV-1. *Nat. Med.* (2009) doi:10.1038/nm.2004.
221. Trigunaite, A., Dimo, J. & Jørgensen, T. N. Suppressive effects of androgens on the immune system. *Cell. Immunol.* (2015) doi:10.1016/j.cellimm.2015.02.004.
222. Gorski, S. A., Hufford, M. M. & Braciale, T. J. Recent insights into pulmonary repair following virus-induced inflammation of the respiratory tract. *Curr. Opin. Virol.* (2012) doi:10.1016/j.coviro.2012.04.006.
223. Guo, X. zhi J. & Thomas, P. G. New fronts emerge in the influenza cytokine storm. *Seminars in Immunopathology* (2017) doi:10.1007/s00281-017-0636-y.
224. Laura C Miller, Y. S. Macrophage Polarization in Virus-Host Interactions. *J. Clin. Cell. Immunol.* (2015) doi:10.4172/2155-9899.1000311.
225. Keselman, A., Fang, X., White, P. B. & Heller, N. M. Estrogen Signaling Contributes to Sex Differences in Macrophage Polarization during Asthma. *J. Immunol.* (2017) doi:10.4049/jimmunol.1601975.
226. Kumar, A. *et al.* Critically ill patients with 2009 influenza A(H1N1) infection in Canada. *JAMA* **302**, 1872–1879 (2009).
227. Serfung, R. E., Sherman, I. L. & Houseworth, W. J. Excess pneumonia-influenza mortality by age and sex in three major influenza a2 epidemics, United States, 1957-58, 1960 and 1963. *Am. J. Epidemiol.* (1967) doi:10.1093/oxfordjournals.aje.a120753.
228. Eshima, N. *et al.* Sex- and age-related differences in morbidity rates of 2009 pandemic influenza a H1N1 virus of swine origin in japan. *PLoS One* (2011) doi:10.1371/journal.pone.0019409.
229. Hoffmann, J. *et al.* Sex differences in H7N9 influenza A virus pathogenesis. *Vaccine* **33**, 6949–6954 (2015).
230. Satpathy, H. K., Lindsay, M. & Kawwass, J. F. Novel H1N1 virus infection and pregnancy. *Postgraduate Medicine* (2009) doi:10.3810/pgm.2009.11.2080.
231. Louie, J. K., Acosta, M., Jamieson, D. J. & Honein, M. A. Severe 2009 H1N1 Influenza in Pregnant and Postpartum Women in California. *N. Engl. J. Med.* (2010) doi:10.1056/nejmoa0910444.

232. Jamieson, D. J. *et al.* H1N1 2009 influenza virus infection during pregnancy in the USA. *Lancet* (2009) doi:10.1016/S0140-6736(09)61304-0.
233. Robinson, D. P., Lorenzo, M. E., Jian, W. & Klein, S. L. Elevated 17 β -estradiol protects females from influenza a virus pathogenesis by suppressing inflammatory responses. *PLoS Pathog.* (2011) doi:10.1371/journal.ppat.1002149.
234. Tuku, B. *et al.* Testosterone Protects Against Severe Influenza by Reducing the Pro-Inflammatory Cytokine Response in the Murine Lung. *Front. Immunol.* (2020) doi:10.3389/fimmu.2020.00697.
235. Glezen, W. P. *et al.* Epidemiologic patterns of acute lower respiratory disease of children in a pediatric group practice. *J. Pediatr.* (1971) doi:10.1016/S0022-3476(71)80218-4.
236. Simoes, E. A. F. Environmental and demographic risk factors for respiratory syncytial virus lower respiratory tract disease. *J. Pediatr.* (2003) doi:10.1067/s0022-3476(03)00511-0.
237. Karlberg, J., Chong, D. S. Y. & Lai, W. Y. Y. Do Men Have a Higher Case Fatality Rate of Severe Acute Respiratory Syndrome than Women Do? *Am. J. Epidemiol.* (2004) doi:10.1093/aje/kwh056.
238. Alghamdi, I. G. *et al.* The pattern of Middle east respiratory syndrome coronavirus in Saudi Arabia: A descriptive epidemiological analysis of data from the Saudi Ministry of Health. *Int. J. Gen. Med.* (2014) doi:10.2147/IJGM.S67061.
239. Polglase, K., Mezzofiore, G. & Foster, M. Here's why the coronavirus may be killing more men than women. The US should take note. *CNN Heal.* (2020).
240. Zhao, S. *et al.* COVID-19 and gender-specific difference: Analysis of public surveillance data in Hong Kong and Shenzhen, China, from January 10 to February 15, 2020. *Infection Control and Hospital Epidemiology* (2020) doi:10.1017/ice.2020.64.
241. Conti, P. & Younes, A. Coronavirus cov-19/sars-cov-2 affects women less than men: Clinical response to viral infection. *Journal of Biological Regulators and Homeostatic Agents* (2020) doi:10.23812/Editorial-Conti-3.
242. Wenham, C., Smith, J. & Morgan, R. COVID-19: the gendered impacts of the outbreak. *The Lancet* (2020) doi:10.1016/S0140-6736(20)30526-2.
243. Di Stadio, A., Ricci, G., Greco, A., De Vincentiis, M. & Ralli, M. Mortality rate and gender differences in COVID-19 patients dying in Italy: A comparison with other countries. *European Review for Medical and Pharmacological Sciences* (2020) doi:10.26355/eurrev_202004_20980.
244. Borges do Nascimento, I. J. *et al.* Novel Coronavirus Infection (COVID-19) in Humans: A Scoping Review and Meta-Analysis. *J. Clin. Med.* (2020) doi:10.3390/jcm9040941.
245. Richardson, S. *et al.* Presenting Characteristics, Comorbidities, and Outcomes among 5700 Patients Hospitalized with COVID-19 in the New York City Area. *JAMA - J. Am. Med. Assoc.* (2020) doi:10.1001/jama.2020.6775.
246. Channappanavar, R. *et al.* Sex-Based Differences in Susceptibility to Severe Acute Respiratory Syndrome Coronavirus Infection. *J. Immunol.* (2017) doi:10.4049/jimmunol.1601896.

247. Rowland, S. P. & O'Brien Bergin, E. Screening for low testosterone is needed for early identification and treatment of men at high risk of mortality from Covid-19. *Critical Care* (2020) doi:10.1186/s13054-020-03086-z.
248. Iglesias, P. *et al.* Hypogonadism in aged hospitalized male patients: Prevalence and clinical outcome. *J. Endocrinol. Invest.* (2014) doi:10.1007/s40618-013-0009-x.
249. Goodale, T., Sadhu, A., Petak, S. & Robbins, R. Testosterone and the Heart. *Methodist DeBakey cardiovascular journal* (2017) doi:10.14797/mdcj-13-2-68.
250. Gadotti, A. C. *et al.* IFN- γ is an independent risk factor associated with mortality in patients with moderate and severe COVID-19 infection. *Virus Res.* (2020) doi:10.1016/j.virusres.2020.198171.
251. Zhang, F. *et al.* IFN- γ and TNF- α drive a CXCL10⁺ CCL2⁺ macrophage phenotype expanded in severe COVID-19 and other diseases with tissue inflammation. *bioRxiv* (2020).
252. Fox, H. S., Bond, B. L. & Parslow, T. G. Estrogen regulates the IFN-gamma promoter. *J. Immunol.* (1991).
253. Sia, S. F. *et al.* Pathogenesis and transmission of SARS-CoV-2 in golden hamsters. *Nature* (2020) doi:10.1038/s41586-020-2342-5.
254. Imai, M. *et al.* Syrian hamsters as a small animal model for SARS-CoV-2 infection and countermeasure development. *Proc. Natl. Acad. Sci. U. S. A.* (2020) doi:10.1073/pnas.2009799117.
255. Peckham, H. *et al.* Male sex identified by global COVID-19 meta-analysis as a risk factor for death and ICU admission. *Nat. Commun.* (2020) doi:10.1038/s41467-020-19741-6.
256. Ahrenfeldt, L. J., Otavova, M., Christensen, K. & Lindahl-Jacobsen, R. Sex and age differences in COVID-19 mortality in Europe. *Wien. Klin. Wochenschr.* (2020) doi:10.1007/s00508-020-01793-9.
257. Wambier, C. G. & Goren, A. Severe acute respiratory syndrome coronavirus 2 (SARS-CoV-2) infection is likely to be androgen mediated. *J. Am. Acad. Dermatol.* **83**, 308–309 (2020).
258. Shen, L. W., Mao, H. J., Wu, Y. L., Tanaka, Y. & Zhang, W. TMPRSS2: A potential target for treatment of influenza virus and coronavirus infections. *Biochimie* (2017) doi:10.1016/j.biochi.2017.07.016.
259. Lucas, J. M. *et al.* The androgen-regulated protease TMPRSS2 activates a proteolytic cascade involving components of the tumor microenvironment and promotes prostate cancer metastasis. *Cancer Discov.* **4**, 1310–1325 (2014).
260. Stopsack, K. H., Mucci, L. A., Antonarakis, E. S., Nelson, P. S. & Kantoff, P. W. TMPRSS2 and COVID-19: Serendipity or opportunity for intervention? *Cancer Discov.* (2020) doi:10.1158/2159-8290.CD-20-0451.
261. Montopoli, M. *et al.* Androgen-deprivation therapies for prostate cancer and risk of infection by SARS-CoV-2: a population-based study (N = 4532). *Ann. Oncol.* (2020) doi:10.1016/j.annonc.2020.04.479.
262. Smith, J. C. *et al.* Cigarette Smoke Exposure and Inflammatory Signaling Increase the

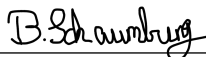
- Expression of the SARS-CoV-2 Receptor ACE2 in the Respiratory Tract. *Dev. Cell* (2020) doi:10.1016/j.devcel.2020.05.012.
263. Rastrelli, G. *et al.* Low testosterone levels predict clinical adverse outcomes in SARS-CoV-2 pneumonia patients. *Andrology* (2020) doi:10.1111/andr.12821.
264. Hussain, A. N., Hussain, F. & Hashmi, S. K. Role of testosterone in COVID-19 patients – A double-edged sword? *Med. Hypotheses* (2020) doi:10.1016/j.mehy.2020.110287.
265. Shores, M. M., Matsumoto, A. M., Sloan, K. L. & Kivlahan, D. R. Low serum testosterone and mortality in male veterans. *Arch. Intern. Med.* (2006) doi:10.1001/archinte.166.15.1660.
266. Rochira, V. & Guaraldi, G. Hypogonadism in the HIV-Infected Man. *Endocrinology and Metabolism Clinics of North America* (2014) doi:10.1016/j.ecl.2014.06.005.
267. Robinson, D. P., Hall, O. J., Nilles, T. L., Bream, J. H. & Klein, S. L. 17 β -Estradiol Protects Females against Influenza by Recruiting Neutrophils and Increasing Virus-Specific CD8 T Cell Responses in the Lungs. *J. Virol.* (2014) doi:10.1128/jvi.02081-13.
268. Larralde, C., Morales, J., Terrazas, I., Govezensky, T. & Romano, M. C. Sex hormone changes induced by the parasite lead to feminization of the male host in murine *Taenia crassiceps* cysticercosis. *J. Steroid Biochem. Mol. Biol.* (1995) doi:10.1016/0960-0760(95)00062-5.
269. Gilliver, S. C. Sex steroids as inflammatory regulators. *Journal of Steroid Biochemistry and Molecular Biology* (2010) doi:10.1016/j.jsbmb.2009.12.015.
270. Zhao, D. *et al.* Endogenous Sex Hormones and Incident Cardiovascular Disease in Post-Menopausal Women. *J. Am. Coll. Cardiol.* (2018) doi:10.1016/j.jacc.2018.01.083.
271. Ruth, K. S. *et al.* Using human genetics to understand the disease impacts of testosterone in men and women. *Nat. Med.* (2020) doi:10.1038/s41591-020-0751-5.
272. Pasquali, R. Obesity and androgens: facts and perspectives. *Fertil. Steril.* (2006) doi:10.1016/j.fertnstert.2005.10.054.
273. Calippe, B. *et al.* 17 β -Estradiol Promotes TLR4-Triggered Proinflammatory Mediator Production through Direct Estrogen Receptor α Signaling in Macrophages In Vivo. *J. Immunol.* (2010) doi:10.4049/jimmunol.0902383.
274. Pratap, U. P. *et al.* Estrogen upregulates inflammatory signals through NF- κ B, IFN- γ , and nitric oxide via Akt/mTOR pathway in the lymph node lymphocytes of middle-aged female rats. *Int. Immunopharmacol.* (2015) doi:10.1016/j.intimp.2015.09.024.
275. Tominaga, K. *et al.* IL-12 synergizes with IL-18 or IL-1 β for IFN- γ production from human T cells. *Int. Immunol.* (2000) doi:10.1093/intimm/12.2.151.
276. Fricke, I. *et al.* Mycobacteria Induce IFN- γ Production in Human Dendritic Cells via Triggering of TLR2. *J. Immunol.* (2006) doi:10.4049/jimmunol.176.9.5173.
277. Darwich, L. *et al.* Secretion of interferon- γ by human macrophages demonstrated at the single-cell level after costimulation with interleukin (IL)-12 plus IL-18. *Immunology* (2009) doi:10.1111/j.1365-2567.2008.02905.x.
278. Mor, G., Amir-Zaltsman, Y., Barnard, G., Ben-Hur, H. & Kohen, F. Evidence for the

- presence of estrogen receptors in monocytes. *Endocrine* (1993).
279. Geraldès, P., Sirois, M. G., Bernatchez, P. N. & Tanguay, J. F. Estrogen regulation of endothelial and smooth muscle cell migration and proliferation: Role of p38 and p42/44 mitogen-activated protein kinase. *Arterioscler. Thromb. Vasc. Biol.* **22**, 1585–1590 (2002).
 280. Nahrendorf, M. & Swirski, F. K. Abandoning M1/M2 for a network model of macrophage function. *Circulation Research* (2016) doi:10.1161/CIRCRESAHA.116.309194.
 281. Hu, G. & Christman, J. W. Editorial: Alveolar macrophages in lung inflammation and resolution. *Frontiers in Immunology* (2019) doi:10.3389/fimmu.2019.02275.
 282. Nikitina, E., Larionova, I., Choinzonov, E. & Kzhyshkowska, J. Monocytes and macrophages as viral targets and reservoirs. *International Journal of Molecular Sciences* (2018) doi:10.3390/ijms19092821.
 283. Yang, Y. *et al.* Exuberant elevation of IP-10, MCP-3 and IL-1ra during SARS-CoV-2 infection is associated with disease severity and fatal outcome. *medRxiv* (2020) doi:10.1101/2020.03.02.20029975.
 284. Vaninov, N. In the eye of the COVID-19 cytokine storm. *Nat. Rev. Immunol.* (2020) doi:10.1038/s41577-020-0305-6.
 285. Kou, X.-X. *et al.* Estradiol Promotes M1-like Macrophage Activation through Cadherin-11 To Aggravate Temporomandibular Joint Inflammation in Rats. *J. Immunol.* (2015) doi:10.4049/jimmunol.1303188.
 286. Fernando, M. R., Reyes, J. L., Iannuzzi, J., Leung, G. & McKay, D. M. The pro-inflammatory cytokine, interleukin-6, enhances the polarization of alternatively activated macrophages. *PLoS One* (2014) doi:10.1371/journal.pone.0094188.
 287. Bhavsar, I., Miller, C. S. & Al-Sabbagh, M. Macrophage Inflammatory Protein-1 Alpha (MIP-1 alpha)/CCL3: As a biomarker. in *General Methods in Biomarker Research and their Applications* (2015). doi:10.1007/978-94-007-7696-8_27.
 288. Lagunas-Rangel, F. A. & Chávez-Valencia, V. High IL-6/IFN- γ ratio could be associated with severe disease in COVID-19 patients. *Journal of Medical Virology* (2020) doi:10.1002/jmv.25900.
 289. Chupp, G. L. *et al.* A Chitinase-like Protein in the Lung and Circulation of Patients with Severe Asthma. *N. Engl. J. Med.* (2007) doi:10.1056/nejmoa073600.
 290. Melgert, B. N. *et al.* More alternative activation of macrophages in lungs of asthmatic patients. *J. Allergy Clin. Immunol.* (2011) doi:10.1016/j.jaci.2010.10.045.
 291. Bobryshev, Y. V., Ivanova, E. A., Chistiakov, D. A., Nikiforov, N. G. & Orekhov, A. N. Macrophages and Their Role in Atherosclerosis: Pathophysiology and Transcriptome Analysis. *Biomed Res. Int.* (2016) doi:10.1155/2016/9582430.
 292. Khan, N. Possible protective role of 17 β -estradiol against COVID-19. doi:10.46439/allergy.1.010.
 293. Assaggaf, H. & Felty, Q. Gender, estrogen, and obliterative lesions in the lung. *International Journal of Endocrinology* vol. 2017 (2017).
 294. Carranza-Lira, S. *et al.* Prolactin secretion in molar and normal pregnancy. *Int. J.*

- Gynecol. Obstet.* **60**, 137–141 (1998).
295. Chen, Y. *et al.* Low testosterone and high cytokine levels correlate with lethal H7N9 infections in men: a retrospective cohort study from 98 H7N9 patients. *medRxiv* (2020).
296. WHO. sex, gender and influenza. *Geneva World Heal. Organ. Press* (2010).
297. Dossett, L. A. *et al.* High levels of endogenous estrogens are associated with death in the critically injured adult. *J. Trauma - Inj. Infect. Crit. Care* (2008) doi:10.1097/TA.0b013e31816543dd.
298. Dong, W. & Willett, K. L. Local expression of CYP19A1 and CYP19A2 in developing and adult killifish (*Fundulus heteroclitus*). *Gen. Comp. Endocrinol.* (2008) doi:10.1016/j.ygcen.2007.05.018.
299. Mahendroo, M. S., Mendelson, C. R. & Simpson, E. R. Tissue-specific and hormonally controlled alternative promoters regulate aromatase cytochrome P450 gene expression in human adipose tissue. *J. Biol. Chem.* (1993) doi:10.1016/s0021-9258(19)36538-x.
300. Evans, C. T., Ledesma, D. B., Schulz, T. Z., Simpson, E. R. & Mendelson, C. R. Isolation and characterization of a complementary DNA specific for human aromatase-system cytochrome P-450 mRNA. *Proc. Natl. Acad. Sci. U. S. A.* (1986) doi:10.1073/pnas.83.17.6387.
301. Honda, S. I., Harada, N. & Takagi, Y. Novel exon 1 of the aromatase gene specific for aromatase transcripts in human brain. *Biochem. Biophys. Res. Commun.* (1994) doi:10.1006/bbrc.1994.1163.
302. Merlotti, D., Gennari, L., Stolakis, K. & Nuti, R. Aromatase Activity and Bone Loss in Men. *J. Osteoporos.* (2011) doi:10.4061/2011/230671.
303. Mah, V. *et al.* Aromatase expression predicts survival in women with early-stage non-small cell lung cancer. *Cancer Res.* **67**, 10484–10490 (2007).
304. Gil, M. *et al.* Macrophages, estrogen and the microenvironment of breast cancer. *J. Steroid Biochem. Mol. Biol.* (1998) doi:10.1016/S0960-0760(98)00143-5.
305. Wright, C. L., Hoffman, J. H. & McCarthy, M. M. Evidence that inflammation promotes estradiol synthesis in human cerebellum during early childhood. *Transl. Psychiatry* (2019) doi:10.1038/s41398-018-0363-8.
306. Ranieri, V. M. *et al.* Acute respiratory distress syndrome: The Berlin definition. *JAMA - J. Am. Med. Assoc.* (2012) doi:10.1001/jama.2012.5669.
307. Shekar, K. *et al.* The combined effects of extracorporeal membrane oxygenation and renal replacement therapy on meropenem pharmacokinetics: A matched cohort study. *Crit. Care* (2014) doi:10.1186/s13054-014-0565-2.
308. Gauth, C. R. & Smith, T. F. Replication and plaque assay of influenza virus in an established line of canine kidney cells. *Appl. Microbiol.* (1968) doi:10.1128/AEM.16.4.588-594.1968.
309. Matrosovich, M., Matrosovich, T., Garten, W. & Klenk, H. D. New low-viscosity overlay medium for viral plaque assays. *Viol. J.* (2006) doi:10.1186/1743-422X-3-63.

9 Eidesstattliche Erklärung

Hiermit versichere ich an Eides statt, die vorliegende Dissertation selbst verfasst und keine anderen als die angegebenen Hilfsmittel benutzt zu haben. Die eingereichte schriftliche Fassung entspricht der auf dem elektronischen Speichermedium. Ich versichere, dass diese Dissertation nicht in einem früheren Promotionsverfahren eingereicht wurde.

15.09.2021 
Datum, Unterschrift

I. Supplements - Hazardous materials

Supplemental Table S1: Hazardous contaminants with applicable P and H phrases

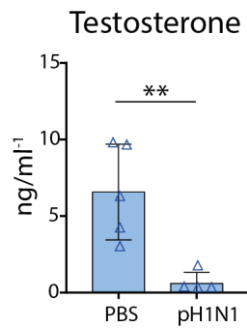
Substance	GHS code	H-phrases	P-phrases
Haematoxylin	GHS07	H302, H315, H319, H335	P261, P305+P351+P338
Hydrochloric acid (37%)	GHS05/07	H290, H314, H335	P280, P303+P361+P353, P304+P340, P305+P31+P338, P310
Ethanol	GHS02	H225	P210, P240,P243,P280,P303+P361+P353
Isoflurane	GHS07	H319, H315, H335, H336	P302+P352, P321, P332+P313, P362, P264, P280, P305+P351+P338, P337+P313, P261, P271, P304+P340, P312, P403+P233, P405, P501
Isopropanol	GHS02/07	H225, H319, H336	P210, P233, P305+P351+P336
Ketamine	GHS07	H302, H332, H335	P261, P264, P301+P312, P304+P340, P330
Methanol	GHS02/06/08	H225, H301, H311, H331, H370	P243, P280, P301+P310, P302+P350, P304+P340, P307+P311
Paraformaldehyde	GHS03/06/07/08	H228, H302+H332, H315, H317, H318, HH335, H341, H350	P202, P210, P270, P280, P305+P351+P338, P308+P313
Penicillin& Streptomycin	GHS07	H302, H317	P280
Pursept-A Xpress	GHS02/07	H225, H319	P210, P271, P305+P351+P338, P337+P313, P403+P233
TPCK-treated trypsin	GHS08	H15, H319, H334, H335	P280, P284, P271, P261, P264, P304+P340, P342+P311, P302+P352, P361+P364, P305+P351+P338, P337+P313, P501
Trypsin-EDTA	GHS07/08	H315, H319, H334	P280, P302+P352, P304+P341, P305+P351+P338, P342+P311



Supplemental Figure 7: GHS codes (pictogrammes)

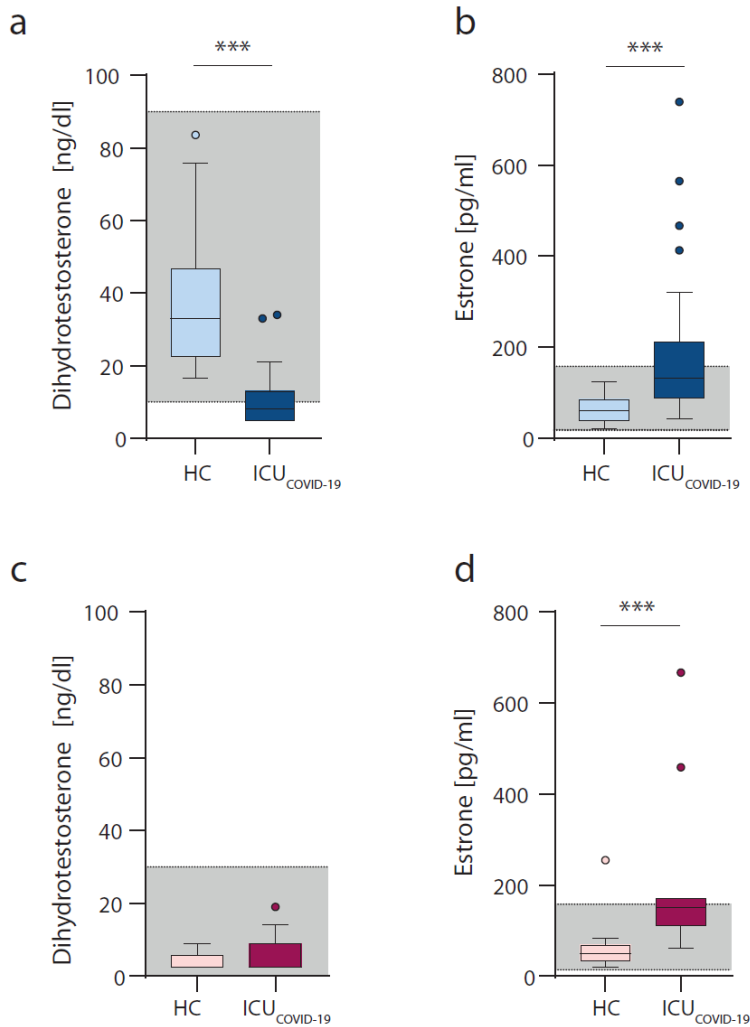
The disposal of waste was carried out according to present guide lines. Before disposal S1- and S2- waste has been autoclaved.

II. Supplements – Figures



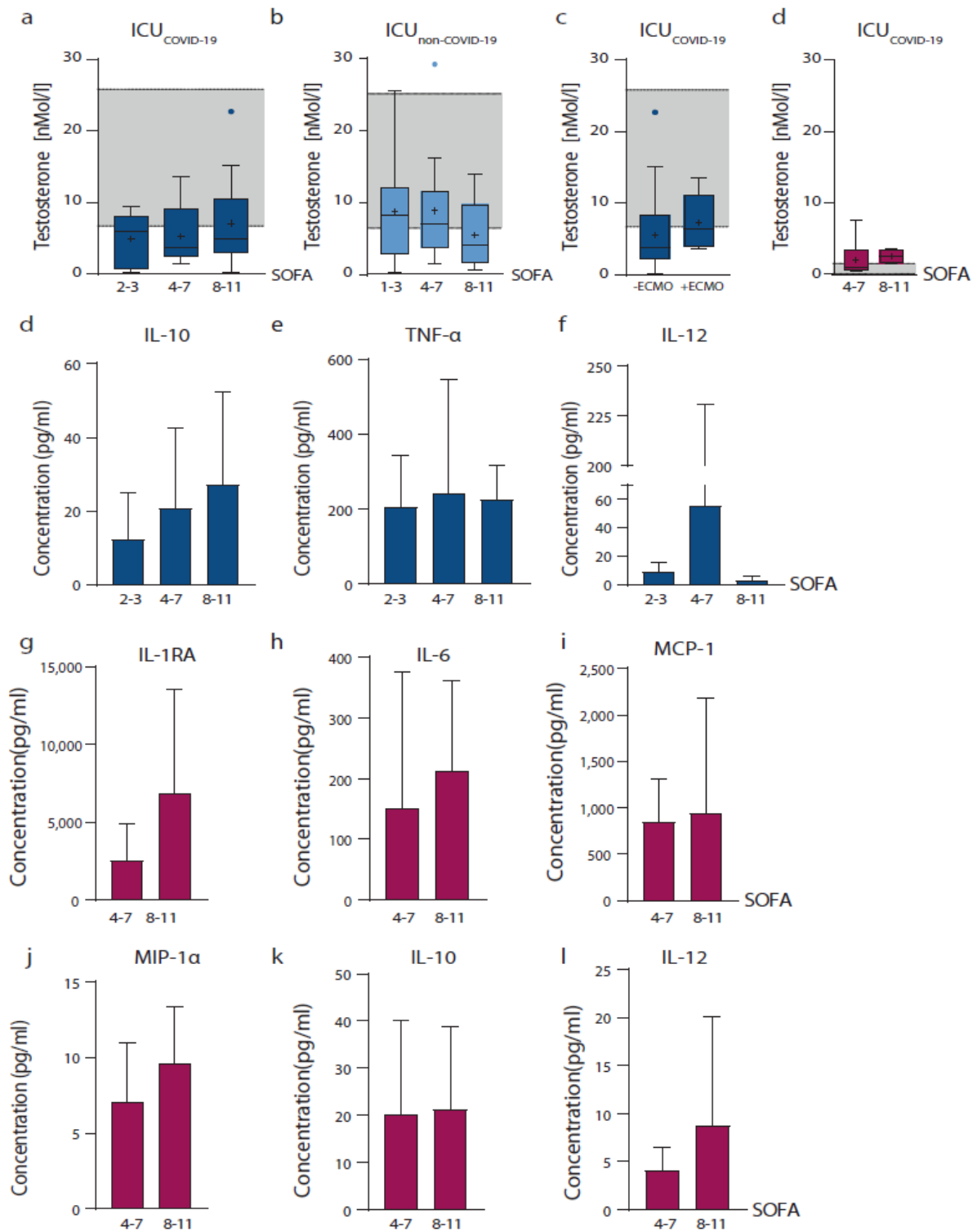
Supplemental Figure 1: Testosterone levels in male mice infected with pH1N1.

Male mice were infected with pH1N1 ($n=4$) or treated with PBS ($n=5$). 3d p.i. testosterone levels in plasma were measured. Values are shown as mean and error bars as SD. Statistical significance was assessed by unpaired Student's t-test. Statistical significance was defined as $P < 0.05$ (** $P < 0.01$).



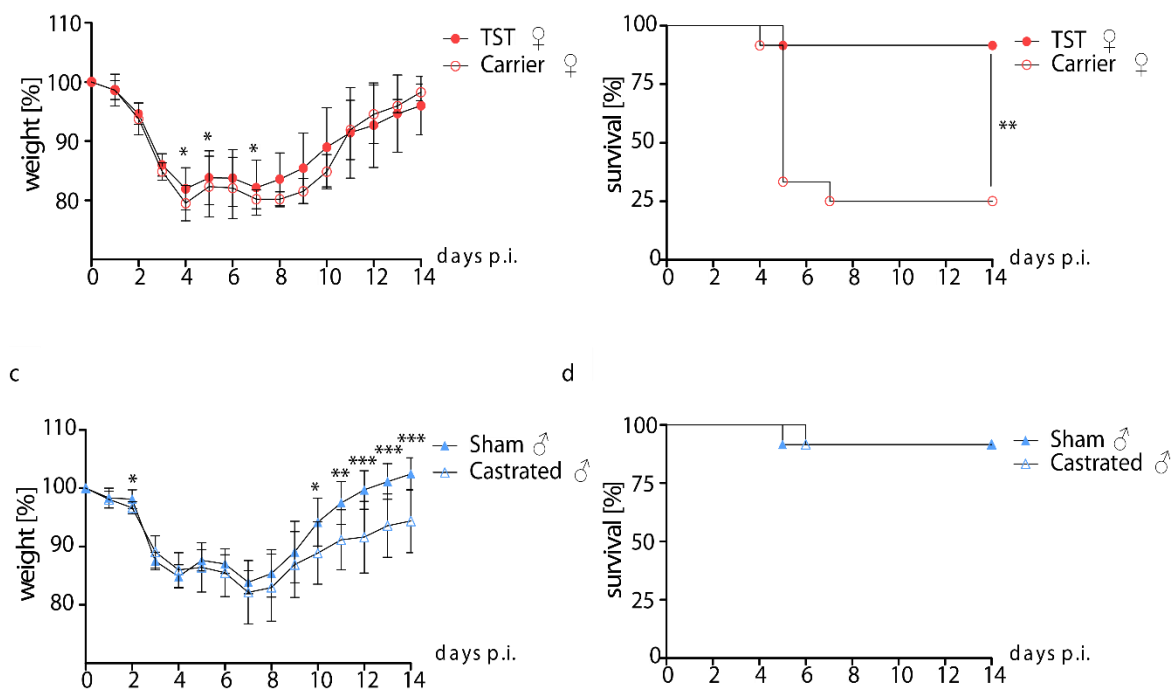
Supplemental Figure 2: Dihydrotestosterone and estrone levels in COVID-19 patients

Dihydrotestosterone (a,c) and dihydrotestosterone (b,c) levels were measured in plasma obtained from COVID-19 patients and healthy donors (HC). Blue graphs represent males (HC, n=30; COVID-19, n=30) and pink graphs represent females (HC, n=20; COVID-19, n=11). Percentile boxplots represent 25-75% of values with the median value indicated by a crossline, and mean values by a plus icon. The laboratory assessed hormone reference ranges are indicated in grey. Statistical significance was assessed via One-Way-ANOVA. Statistical significance was defined as $P < 0.05$ (***) $P < 0.001$.



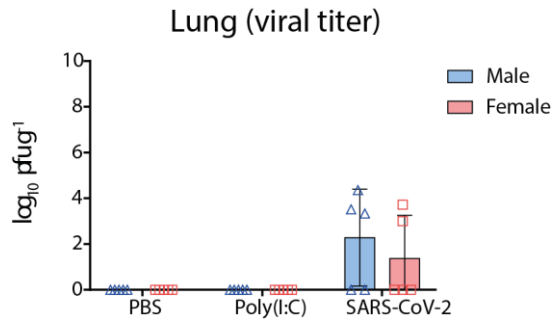
Supplemental Figure 3: Testosterone and cytokine levels in dependency of disease severity.

Testosterone levels were measured in plasma obtained from critically ill male (blue columns) (a-c) and female (pink columns) (d). COVID-19 or non-COVID-19 patients are displayed in dependency of disease severity as assessed by SOFA scores. Male COVID-19 patients were subdivided into patients requiring ECMO therapy (+ECMO) and patients not requiring ECMO therapy (-ECMO) (c). Percentile blots represent 25–75% of values, with the median value indicated by a crossline, and mean values by a plus icon. The laboratory assessed hormone reference ranges are indicated in grey. Values are shown as median and interquartile range. Cytokine levels were measured in males (blue bar graphs) (d-f) and females (pink bar graphs) (g-l) in dependency of the SOFA score. Statistical significance in males was assessed by non-parametric tests (Kruskal-Wallis test and Dunn's test for multiple comparisons). Statistical significance in females was evaluated by unpaired, two-tailed non-parametric Student's t-test (Mann-Whitney test).



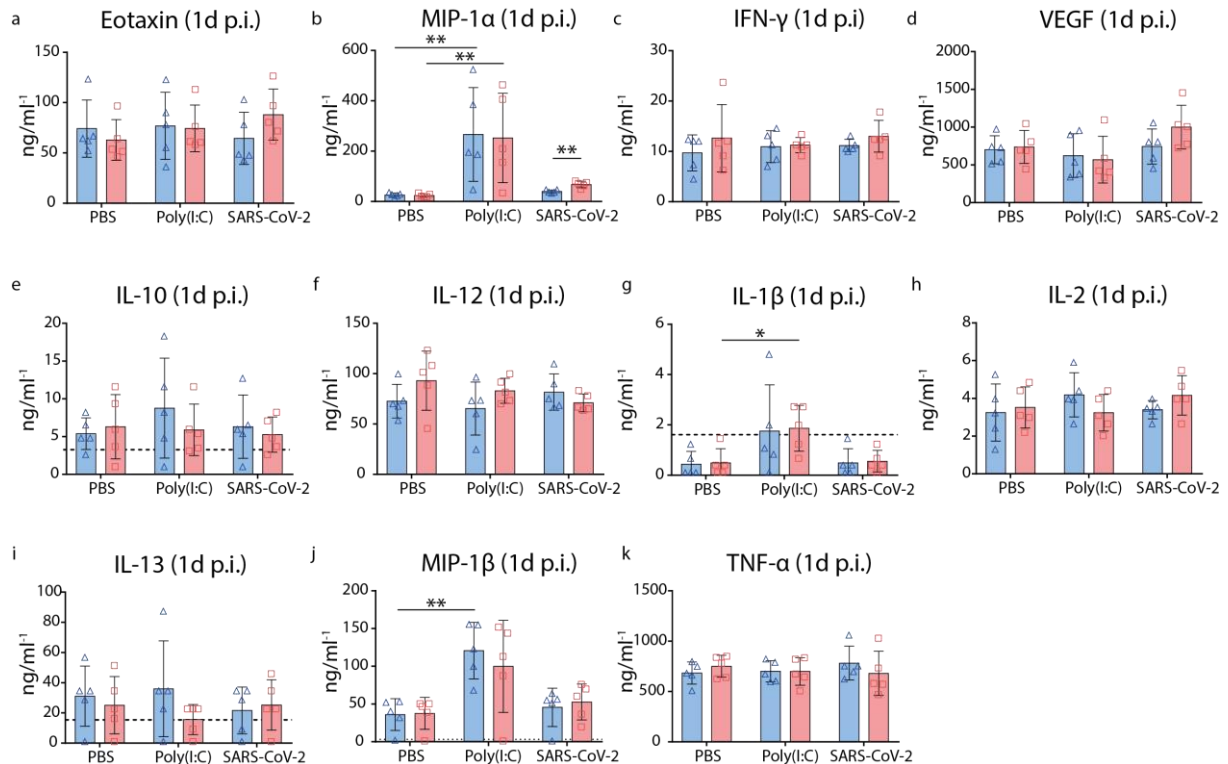
Supplemental Figure 4: Effect of testosterone on weight loss and survival of pH1N1 infected mice.

Female mice with an implanted pump releasing either testosterone (TST) or a carrier substance (a,b) and castrated or sham-operated male mice (c,d) were infected with pH1N1 (10^4 p.f.u./ml) ($n=12$). Weight loss and survival of infected animals was monitored for 14 days. Statistical significance was assessed by Mantel–Cox test for the survival data and Student's t-test for the weight loss data. Statistical significance was defined as $P < 0.05$ (* $P < 0.05$, ** $P < 0.01$, *** $P = 0.001$).



Supplemental Figure 5: Viral lung titers of SARS-CoV-2 infected male and female golden hamsters.

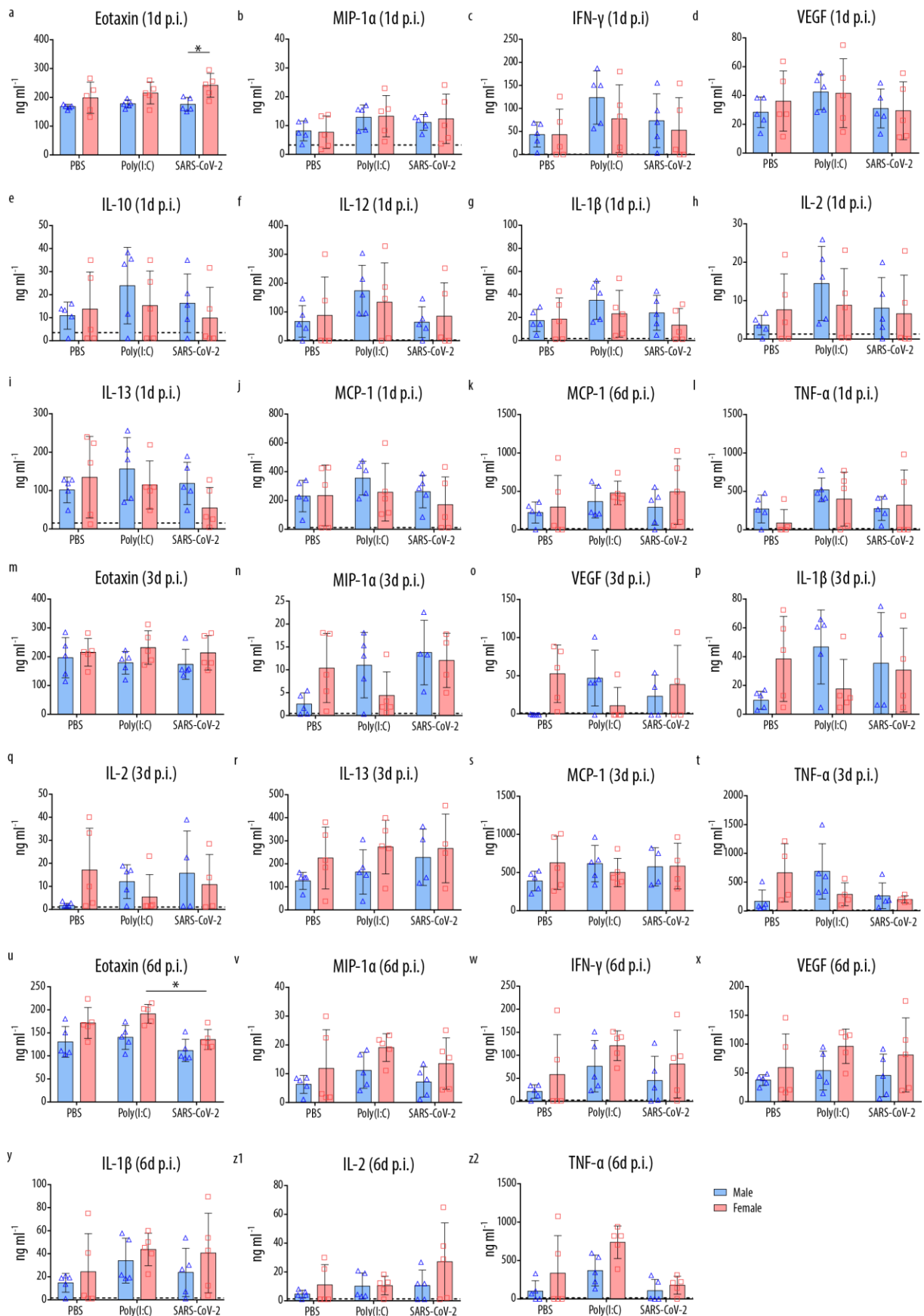
Lungs of SARS-CoV-2 infected male (n=5) and female (n=5) hamsters were harvested 6d p.i. Viral titers were determined by plaque assay. The individual logarithmic virus titers of each lung and their means are shown.



Supplemental Figure 6: Chemokine and cytokine response in male and female Syrian golden hamsters infected with SARS-CoV-2 1 d p.i..

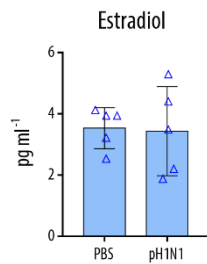
Shown are cytokine and chemokine levels of male and female golden hamsters infected with SARS-CoV-2. Cytokine and chemokines protein levels were measured in lung homogenates obtained from infected hamsters 1 d p.i.. Here: Eotaxin- (a), MIP-1α- (b), IFN-γ- (c), VEGF- (d), IL-10- (e), IL-12- (f), IL-1β- (g), IL-2- (h), IL-13- (i), MIP-1β - (j), and TNF-α (k) protein levels are shown. Statistical significance was evaluated by Kruskal-Wallis one-way ANOVA and by unpaired, two-tailed non-parametric Student's *t*-test. Statistical significance was defined as $P < 0.05$ (* $P < 0.05$, ** $P < 0.01$). Values are shown as median and interquartile range.

Supplements – Figures



Supplemental Figure 7: Chemokine and cytokine responses in plasma of male and female Syrian golden hamsters infected with SARS-CoV-2.

Shown are cytokine and chemokine levels of male and female golden hamsters infected with SARS-CoV-2. Cytokine and chemokines protein levels were measured in plasma obtained from infected hamsters 1,3 and 6d p.i.. Here: Eotaxin- (a,m,u), MIP-1 α - (b,n,v), IFN- γ - (c,w), VEGF- (d,o,x), IL-10- (e), IL-12- (f), IL-1 β - (g,p,y), IL-2- (h,q,z1), IL-13- (i,r), MCP-1 (j,k,s) and TNF- α (l,t,z2) protein levels are shown. Statistical significance was evaluated by Kruskal-Wallis one-way ANOVA and by unpaired, two-tailed non-parametric Student's *t*-test. Statistical significance was defined as $P < 0.05$ (* $P < 0.05$). Values are shown as median and interquartile range.



Supplemental Figure 8: Estradiol levels in male mice infected with pH1N1.

Male mice were infected with pH1N1 or treated with PBS ($n=5$). 3d p.i. estradiol levels in plasma were measured. Values are shown as mean and error bars as SD.

III. Supplements - List of tables and figures

Tables

Table 1: COVID-19 patient comorbidities	27
Table 2: Healthy control, coronary heart disease and COVID-19 patient demographics	28
Table 3: Hormone levels in COVID-19 patients	31

Figures

Figure 1: Coronavirus virion structure.	4
Figure 2: Coronavirus genomic organization.	5
Figure 3: SARS-CoV-2 replication cycle.	8
Figure 4: Interspecies transmission of coronaviruses.	10
Figure 5: Global map of countries with confirmed cases of MERS-CoV.	14
Figure 6: Distribution of COVID-19 related deaths worldwide by continent (as of 9 th December 2020).	16
Figure 7: Potential therapeutic targets in SARS-CoV-2 replication.	19
Figure 8: Biosynthesis of sex hormones in the gonads.	21
Figure 9: Mortality of male and female COVID-19 patients at the intensive care unit.	26
Figure 10: Sex hormone levels in COVID-19 patients, critically-ill non-COVID-19 patients, healthy controls and patients with coronary heart disease.	29
Figure 11: Chemokine and cytokine responses in male COVID-19 patients.	33
Figure 12: Correlation analyzes of plasma IFN- γ levels to testosterone and estradiol levels of COVID-19 patients.	35
Figure 13: Analyzes of sex hormone levels in male and female COVID-19 patients in dependency of disease severity.	37
Figure 14: A schematic of the hypothesized model of estradiol activated macrophages in male COVID-19 patients.	38
Figure 15: Weight loss of SARS-CoV-2 infected male and female golden hamsters.	39
Figure 16: Viral lung and plasma titers of SARS-CoV-2 infected male and female golden hamsters.	40
Figure 17: Viral titers and viral RNA levels of SARS-CoV-2 in the reproductive organs of infected male and female golden hamsters.	41
Figure 18: Chemokine and cytokine responses in male and female Syrian golden hamsters infected with SARS-CoV-2.	43
Figure 19: Hormone levels in male and female Syrian golden hamsters infected with SARS-CoV-2.	45
Figure 20: Aromatase expression levels and endothelial activation in male and female Syrian golden hamsters infected with SARS-CoV-2.	47
Figure 21: Aromatase expression levels in the lungs of male and female Syrian golden hamsters infected with SARS-CoV-2.	50
Figure 22: The role of ACE2 and TMPRSS2 in male COVID-19 susceptibility.	53
Figure 23: Estradiol promotes macrophage secretion of inflammatory cytokines.	57
Figure 24: CYP19A1 promotor binding sites.	59

Supplemental Figures

Supplemental Figure 1: Testosterone levels in male mice infected with pH1N1.....	109
Supplemental Figure 2: Dihydrotestosterone and estrone levels in COVID-19 patients	110
Supplemental Figure 3: Testosterone and cytokine levels in dependency of disease severity.....	112
Supplemental Figure 4: Effect of testosterone on weight loss and survival of pH1N1 infected mice.	112
Supplemental Figure 5: Viral lung titers of SARS-CoV-2 infected male and female golden hamsters.	113
Supplemental Figure 6: Chemokine and cytokine response in male and female Syrian golden hamsters infected with SARS-CoV-2 1 d p.i.....	113
Supplemental Figure 7: Chemokine and cytokine responses in plasma of male and female Syrian golden hamsters infected with SARS-CoV-2.....	115
Supplemental Figure 8: Estradiol levels in male mice infected with pH1N1.....	115

IV. Danksagung

Mein besonderer Dank gilt Prof. Dr. Gülşah Gabriel für die Bereitstellung des überaus interessanten Forschungsprojekts und der außerordentlichen Unterstützung in den letzten Jahren. Insbesondere während des herausfordernden Pandemiejahres habe ich unglaublich viel lernen können und durch deine leitende Expertise und Motivation sehr profitieren können. Die exzellente Förderung als junge Wissenschaftlerin, in Form von Teilnahme an Kongressen und das Ermöglichen von Publikationen, habe ich sehr geschätzt. Vielen Dank für die Zeit, auf die ich immer gerne zurückblicken werde!

Ein großer Dank geht an Dr. Stephanie Stanelle-Bertram, die mich seit meiner Masterarbeit betreut hat. Du hast mir alles beigebracht, was ich für meine Dissertation und darüber hinaus benötigt habe, Steffi. Für meine Fragen hattest du immer ein offenes Ohr und ich konnte immer auf deine Unterstützung vertrauen. Auch für die ausführliche Korrektur meiner Doktorarbeit bedanke ich mich sehr. Ich werde dich immer als herausragende Mentorin in Erinnerung behalten.

Prof. Dr. Gülşah Gabriel und Prof. Dr. Michael Kolbe danke ich herzlich für die Bereitschaft zur schriftlichen Begutachten dieser Arbeit.

Prof. Dr. Hartmut Schlüter, Prof. Dr. Chris Meier und Prof. Dr. Gülşah Gabriel möchte ich herzlich für die Bereitschaft in der Prüfungskommission mitzuwirken danken.

Mein Dank geht ebenfalls an unsere Kooperationspartner. Dr. Kathrin Becker, Dr. Georg Beythien und Prof. Dr. Wolfgang Baumgärtner danke ich für die histologische Aufarbeitung der Hamsterlungen.

Desweiteren möchte ich allen Kollegen, die an meiner Dissertation mitgewirkt haben danken. Insbesondere Zacharias Müller möchte ich für seine exzellente technische Assistenz während der herausfordernden Anfangszeit der Pandemie danken! Ohne deine Unterstützung hätte ich das Projekt nicht stemmen können. Außerdem möchte ich allen Kollegen, namentlich Dr. Stephanie Stanelle-Bertram, Dr. Nancy Mounogou Kouassi, Martin Müller, Martin Zickler, Tian Bai, Dr. Sebastian Beck und Hanna Jania, die in die Hamsterexperimente involviert waren, bedanken. Das war ein sehr herausfordernder Sommer und es war eine großartige Teamarbeit!

Außerdem möchte ich Fabian Stoll und Annika Beyer danken, die mich in den letzten Zügen meiner Doktorarbeit immer motiviert haben!

Danksagung

Annette Gries, Ulla Müller und Sandra Röse möchte ich für die außerordentliche Unterstützung bei meinen Mausexperimenten danken. Eure fröhliche Art, hat die Mausexperimente immer sehr angenehm begleitet.

Außerdem bin ich sehr dankbar, dass aus Arbeitskollegen aufrichtige und lange Freundschaften entstanden sind. Dr. Henning Jacobsen möchte ich für all unsere Stunden, die wir Tränen lachend, egal wo im Institut, verbracht haben, danken. Ein großer Dank geht auch an Dr. Nancy Mounogou Kouassi. Mit dir zusammenzuarbeiten, hat sich immer wie Freizeit angefühlt und ich bin dankbar für all deine Ratschläge ob auf der Arbeit oder im Privaten. Ich hoffe, dass wir uns nicht aus den Augen verlieren!

Am Ende möchte ich mich vor allem bei meinen Eltern, Ali und Perihan Tuku, bedanken, denen ich diese Doktorarbeit widme. Mit eurem Rückhalt und eurer Liebe hatte ich nie Zweifel meine Ziele zu erreichen. Ich bin sehr dankbar dafür immer einen ruhigen Ort bei euch zu finden, bei dem ich mich nach herausfordernden Zeiten während der Dissertation entspannen konnte.

Außerdem danke ich meinem Bruder Medi Tuku. Dein Ehrgeiz war immer ein Vorbild für mich und du hast mir schon damals beigebracht ordentlich zu arbeiten. Auch für die Ratschläge in unseren langen Telefonaten von London nach Hamburg danke ich dir sehr. Vielen Dank auch an meine Schwägerin Linna Ai, die immer großes Interesse an meinem Projekt gezeigt hat!

Desweiteren danke ich meiner Familie aus Köln, Rojin, Mase und Emer Tuku. Auch wenn wir uns leider viel zu selten gesehen haben, seit ich meine Dissertation begonnen habe, habe ich immer um eure Unterstützung und euren Rückhalt gewusst.

Zuletzt möchte ich mich aus ganzem Herzen bei meinem Ehemann, Aljoscha Schaumburg, bedanken. Wir gehen schon seit meinem Bachelorstudium einen gemeinsamen Weg und ich bin dir sehr dankbar für deine bedingungslose Unterstützung, sowie die Liebe, Geduld und Ruhe, die du aufgebracht hast, auch zu Zeiten, in denen wir beide viel zu tun haben. Es ist immer wieder schön, nach der Arbeit nachhause zukommen. Du bist mein Hafen.